JOURNAL OF FOOD PROCESS ENGINEERING

D.R. HELDMAN
and
R.P. SINGH
COEDITORS

FOOD & NUTRITION PRESS, INC.

OLUME 17, NUMBER 2 MAY 1994

JOURNAL OF FOOD PROCESS ENGINEERING

All articles for publication and inquiries regarding publication should be sent to DR. D.R. HELDMAN, COEDITOR, *Journal of Food Process Engineering*, Food Science/Engineering Unit, University of Missouri-Columbia, 235 Agricultural/Engineering Bldg., Columbia, MO 65211 USA; or DR. R.P. SINGH, COEDITOR, *Journal of Food Process Engineering*, University of California, Davis, Department of Agricultural Engineering, Davis, CA 95616 USA.

All subscriptions and inquiries regarding subscriptions should be sent to Food & Nutrition Press, Inc., 2 Corporate Drive, P.O. Box 374, Trumbull, CT 06611 USA.

One volume of four issues will be published annually. The price for Volume 17 is $132.00, which includes postage to U.S., Canada, and Mexico. Subscriptions to other countries are $152.00 per year via surface mail, and $161 per year via airmail.

Subscriptions for individuals for their own personal use are $102.00 for Volume 17, which includes postage to U.S., Canada, and Mexico. Personal subscriptions to other countries are $122.00 per year via surface mail, and $131.00 per year via airmail. Subscriptions for individuals should be sent directly to the publisher and marked for personal use.

The *Journal of Food Process Engineering* (ISSN:0145-8876) is published quarterly (March, June, September and December) by Food & Nutrition Press, Inc.—Office of Publication is 2 Corporate Drive, P.O. Box 374, Trumbull, Connecticut 06611 USA.

Second class postage paid at Bridgeport, CT 06602.

POSTMASTER: Send address changes to Food & Nutrition Press, Inc., 2 Corporate Drive, P.O. Box 374, Trumbull, Connecticut 06611 USA.

JOURNAL OF FOOD PROCESS ENGINEERING

JOURNAL OF FOOD PROCESS ENGINEERING

Journal of FOOD PROCESS ENGINEERING

VOLUME 17
NUMBER 2

Coeditors: D.R. HELDMAN
R.P. SINGH

FOOD & NUTRITION PRESS, INC.
TRUMBULL, CONNECTICUT 06611 USA

ISSN 0145-8876

Printed in the United States of America

CONTENTS

DENSITY OF FRESH AND FROZEN SEAFOOD

MD. SHAFIUR RAHMAN and R.H. DRISCOLL

Department of Food Science and Technology
University of New South Wales
P.O. Box 1, Kensington, NSW 2033
Australia

Accepted for Publication August 3, 1993

ABSTRACT

The apparent density varied from 1042 to 1093 kg/m^3 and 972 to 1017 kg/m^3 for fresh seafood at 20C and frozen seafood at −30C, respectively. The apparent density of frozen squid mantle meat decreased from 1062 to 990 kg/m^3 when temperature varied from −1.5 to −40C.

INTRODUCTION

Density is one of the most important transport properties and so is widely used in process calculations. Density has a direct effect on the other thermophysical properties of materials. Hence, in most cases, density is a variable in the prediction equation. Density data for food materials are scarce in the literature. Sanz *et al.* (1987) compiled the thermophysical properties of meat products and concluded that there is a need to acquire experimental values of density. Meffert (1983) also mentioned that incorporation of simple physical data, such as density and initial freezing point in the existing tables of basic constituents of food-stuffs, would provide enough data for the prediction of thermophysical properties. Lozano *et al.* (1983) mentioned that there is little published data on porosity, apparent density and shrinkage of food materials as a function of moisture content. There are a number of compilations of the thermophysical properties of food materials by Woodams and Nowrey (1968), Dickerson (1968), Polley *et al.* (1980), ASHRAE (1981) and Sanz *et al.* (1987). These compilations indicated that some information is available in the literature about the density of meat and fish, but it is difficult to find the density data of fresh and frozen seafood. The objective of this study was to measure the density of fresh and frozen seafood, and present them in terms of models.

Most of the density prediction models are based on empirical correlations. Theoretical models exist that are based on the conservation of both mass and

Journal of Food Process Engineering **17** (1994) 121-140.

volume. A number of authors proposed models on the above basis. But there are negligible data available in the literature to justify the validity of the model, as was mentioned by Heldman (1982). Mannapperuma and Singh (1989) also noted that when food is treated as an ideal mixture (the mixing process conserves both mass and volume), then the density of food after freezing can also be predicted by a theoretical model, but again this was not experimentally verified by the above authors. In this paper a density prediction model is developed using mass and volume conservation, and new terms are introduced to account for interaction of the phases and formation of air phase during processing.

Recently in the case of organic liquid-liquid mixtures, a number of authors confirmed that there was a deviation in total volume, which might be positive or negative (Bravo *et al.* 1991; Ortega *et al.* 1991; Arimoto *et al.* 1990). Positive means increase and negative means decrease in net volume. In the literature, excess volume and excess enthalpy of binary mixture are also called excess property of mixture. The excess volume of binary mixtures showed a range of behaviors: in some cases there was a single or double peak in the plot, and in some cases there were positive and negative lobes in the plots. Bravo *et al.* (1991) studied the excess volume of binary mixture of decanol and n-alkenes (n-heptane, n-octane, n-nonane and n-decane). n-heptane gave a maximum decrease in excess volume of $\epsilon_{ex} = -0.055$. The excess properties were usually not easy to correlate. The most widely used equation was given by Redlich and Kister (1948) to correlate the excess volume and can be written as:

$$V_{ex} = X_1 X_2 \sum_{j=1}^{N} A_{ij}(X_1 - X_2)^{j-1} \tag{1}$$

where X_1 and X_2 are the mass fraction of component 1 and 2, and A_{ij} is the coefficient of correlation. Bravo *et al.* (1991) and Arimoto *et al.* (1990) used the above equation with N = 4 to correlate excess volume. Actually the above equation can be transformed into a polynomial of X_1 by expanding series terms. For this reason polynomial forms of the equation (linear and quadratic forms) are used.

MATERIALS AND METHODS

Apparent Density of Fresh Sample

The procedure for apparent density measurement was that of Lozano *et al.* (1980). In this procedure, the sample was weighed in both air and water.

$$\rho_{ap} = \rho_w(W/B) \tag{2}$$

where W is the weight of sample in air (kg) and B is the buoyant force (kg), ρ_{ap} and ρ_w are the apparent density of sample and water (kg/m^3).

Apparent Density of Frozen Sample

Apparent density of frozen seafoods at −30C was measured as per Keppeler and Boose (1970). The density determination consisted of finding the weight of frozen seafoods with known volume. Fresh seafoods were chopped and placed in a stainless steel cylinder (inner diameter = 2.2 cm; depth = 4.7 cm; thickness = 3 mm) wrapped with electric tape. The sample in the cylinder was frozen at −30C, then the excess frozen sample was removed with a sharp knife. The cylinder and frozen sample were immediately weighed. Knowing the mass of the sample and volume of the cylinder the density was estimated.

Apparent density of frozen samples was measured at different temperatures as follows: eight cylindrical glass bottles of diameter 2 cm with small necks filled three fourths (20 g) with chopped seafoods and the rest with toluene were frozen at −40C. After freezing, the bottles were immediately placed inside glass wool insulation columns of inner and outer diameter 2 and 7 cm, respectively. The temperature was then recorded from one bottle by a thermocouple placed inside the center of the bottle. At different temperatures, the bottles were taken out, one at a time, from the glass wool insulation and toluene (at the same temperature of the sample) was added to completely fill the bottle. The bottle was closed immediately and weight was determined. From the mass and volume of the sample, which was estimated by subtracting the volume of toluene from the volume of bottle, the density was calculated. The volume of toluene was estimated from the mass and density at the respective temperatures. The detail descriptions of the proximate analysis of seafood are given in Rahman and Driscoll (1991) and Rahman (1991).

Terminology

True Density. The density of a pure substance or a material calculated from its components (ρ_t).

Substance or Solid Density. The density measured when the substance has been thoroughly broken into pieces small enough to guarantee that no pores remain (ρ_s).

Apparent Density. The density of the substance including all pores remaining in the materials (ρ_{ap}).

Proposed Model

Food materials can be considered as multiphase systems. When the mixing process conserves both mass and volume, then the density of the multiphase system can be written as:

$$\frac{1}{\rho_t} = \sum_{i=1}^{m} \frac{X_i}{\rho_{ti}} \tag{3}$$

where ρ_{ti} and ρ_t are the true density of component i and composite mixture respectively, and X_i is the mass fraction of the ith component.

Miles *et al.* (1983), and Choi and Okos (1985) proposed the above equation for predicting the density of food materials. But the above equation has limited cases where there is no air phase present and no interaction between the phases (for example, swelling or shrinkage). Rahman (1991) extended the theoretical model introducing the pore volume and interaction term in the above equation. The apparent density of a composite mixture can be divided into three components based on conservation of mass and volume:

Apparent volume	=	Actual volume of the component phases	+	Volume of pore or air	+	Excess volume due to the interaction of phases

The excess volume can be positive or negative depending on the process, whereas porosity is always positive. The above equation can be written as:

$$\frac{1}{\rho_{ap}} = \sum_{i=1}^{m} \frac{X_i}{\rho_{ti}} + V_a + V_{ex} \tag{4}$$

where V_a is the volume of air (m^3/kg), V_{ex} is the excess volume (m^3/kg).

Define:

Porosity, $$\epsilon_{ap} = V_a/V_{ap} \tag{5}$$

Excess volume fraction, $$\epsilon_{ex} = V_{ex}/V_{ap} \tag{6}$$

$$V_{ap} = 1/\rho_{ap} \tag{7}$$

The Eq. (4) can be transformed as:

$$\frac{1}{\rho_{ap}} = \sum_{i=1}^{m} \frac{X_i}{\rho_{ti}} + \epsilon_{ap}\ V_{ap} + \epsilon_{ex}\ V_{ap} \tag{8}$$

$$or\ \frac{1}{\rho_{ap}} = \frac{1}{(1 - \epsilon_{ex} - \epsilon_{ap})} [\sum_{i=1}^{m} \frac{X_i}{\rho_{ti}}] \tag{9}$$

When porosity and excess volume fraction are negligible, then Eq. (9) can be transformed to:

$$\frac{1}{\rho_{ap}} = \frac{1}{\rho_t} = \sum_{i=1}^{m} \frac{X_i}{\rho_{ti}} \tag{10}$$

Porosity (or air volume fraction) and excess volume fraction can be calculated by:

$$\epsilon_{ap} = 1 - \rho_{ap} / \rho_s \tag{11}$$

$$\epsilon_{ex} = 1 - \rho_s / \rho_t \tag{12}$$

where ρ_s is the substance density (i.e., excluding air phase) (kg/m^3).

The validity of the model was tested by F-ratio analysis and mean percent deviation.

RESULTS AND DISCUSSION

Apparent Density of Fresh Seafood

The apparent density of fresh seafood varied from 1042 to 1093 kg/m^3 (Table 1), while the density of meat and fish varied from 901 to 1100 kg/m^3 (Rahman 1991). The apparent density of fresh seafood decreased with increase in moisture content (Fig.1). The experimental data were fitted to the proposed models as shown in Table 2.

TABLE 1.
APPARENT DENSITY OF FRESH SEAFOOD AT 20 ± 3C

Seafoods	*Water*[a]	*Protein*[a]	*Fat*[a]	*Ash*[a]	*Apparent density*[a] (kg/m^3)
Squid	82.60	15.46	0.18	1.06	1058
(mantle)	(0.32)	(0.89)	(0.05)	(0.10)	(3)
Squid	83.90	13.08	0.84	1.47	1055
(mantle)	(0.08)	(0.76)	(0.13)	(0.06)	(2)
Squid	83.77	14.07	0.26	1.19	1059
(mantle)	(0.34)	(0.82)	(0.06)	(0.03)	(4)
Squid	81.91	14.96	1.09	1.13	1064
(mantle)	(0.23)	(0.67)	(0.10)	(0.08)	(4)
Squid	79.28	16.75	2.34	1.34	1066
(mantle)	(0.14)	(0.24)	(0.31)	(0.04)	(3)
Squid	82.07	13.03	3.33	1.19	1061
(mantle)	(0.16)	(0.37)	(0.11)	(0.05)	(3)
Squid	81.53	13.59	2.99	1.31	1062
(mantle)	(0.05)	(1.55)	(0.53)	(0.02)	(4)
Squid	78.59	16.59	3.44	1.20	1067
(tentacle)	(0.09)	(0.88)	(0.46)	(0.06)	(3)
Squid	81.27	14.46	3.03	1.09	1055
(tail)	(0.31)	(0.68)	(0.23)	(0.02)	(2)
Squid	84.66	11.02	3.13	1.08	1048
(tail)	(0.31)	(0.90)	(0.23)	(0.10)	(3)
Scallop	85.63	10.57	1.33	0.87	1069
	(0.34)	(0.87)	(0.09)	(0.12)	(4)
Mussel	77.44	18.69	0.97	1.50	1086
	(0.19)	(0.56)	(0.32)	(0.10)	(2)
king prawn	76.52	12.89	2.74	1.83	1077
(green)	(0.20)	(1.02)	(0.34)	(0.05)	(3)
king prawn	75.68	17.52	1.55	2.19	1085
(green)	(0.15)	(1.25)	(0.23)	(0.07)	(3)
king prawn	73.90	19.21	1.30	2.03	1093
(green)	(0.24)	(0.96)	(0.13)	(0.04)	(3)

TABLE 1. *(Continued)*

king prawn	77.32	18.75	1.75	1.89	1072
(green)	(0.14)	(0.31)	(0.09)	(0.17)	(4)
king prawn	75.33	18.22	1.23	1.84	1082
(green)	(0.23)	(0.13)	(0.20)	(0.02)	(3)
king prawn	75.23	19.48	2.92	1.82	1088
(green)	(0.39)	(1.13)	(0.45)	(0.03)	(3)
king prawn	75.69	18.95	3.40	1.57	1081
(tiger)	(0.11)	(0.29)	(0.46)	(0.02)	(2)
Calamari	79.44	12.22	3.96	1.29	1066
(mantle)	(0.69)	(1.60)	(0.05)	(0.22)	(5)
Calamari	81.63	11.19	2.63	1.19	1062
(mantle)	(0.09)	(1.31)	(0.16)	(0.03)	(4)
Calamari	80.13	16.21	1.10	1.23	1064
(mantle)	(0.13)	(0.85)	(0.22)	(0.06)	(2)
Calamari	79.95	16.37	0.65	1.45	1060
(mantle)	(0.25)	(0.56)	(0.09)	(0.02)	(3)
Calamari	80.34	16.37	0.95	1.22	1055
(mantle)	(0.80)	(0.67)	(0.13)	(0.07)	(4)
Calamari	79.70	15.65	2.18	1.28	1063
(mantle)	(0.43)	(0.98)	(0.12)	(0.10)	(4)
Calamari	80.15	15.99	2.38	1.34	1063
(mantle)	(0.29)	(0.57)	(0.24)	(0.01)	(4)
Calamari	82.74	13.16	1.56	1.01	1049
(wing)	(0.13)	(0.66)	(0.13)	(0.04)	(3)
Calamari	82.65	12.25	1.65	0.82	1050
(wing)	(0.31)	(0.74)	(0.09)	(0.01)	(2)
Calamari	83.40	11.39	3.87	0.96	1047
(wing)	(0.12)	(0.17)	(0.77)	(0.03)	(3)
Calamari	83.67	11.60	1.30	0.79	1048
(tentacle)	(0.22)	(0.45)	(0.23)	(0.04)	(3)
Calamari	82.88	10.68	2.10	0.80	1049
(tentacle)	(0.30)	(0.15)	(0.10)	(0.03)	(2)

TABLE 1. *(Continued)*

Calamari	84.53	11.51	2.24	0.59	1050
(tentacle)	(0.57)	(0.30)	(0.08)	(0.17)	(3)
Octopus	80.61	12.43	2.65	1.69	1069
(mantle)	(0.08)	(1.57)	(0.10)	(0.28)	(2)
Octopus	84.11	11.56	2.25	2.26	1056
(mantle)	(0.16)	(0.48)	(0.13)	(0.09)	(2)
Octopus	77.44	18.06	1.89	2.23	1074
(mantle)	(0.53)	(0.56)	(0.23)	(0.12)	(4)
Octopus	79.18	16.54	2.70	1.68	1075
(mantle)	(0.95)	(0.29)	(0.19)	(0.22)	(4)
Octopus	85.31	9.63	2.16	1.47	1042
(tentacle)	(0.10)	(1.04)	(0.39)	(0.05)	(9)
Octopus	80.32	10.97	2.76	1.27	1065
(tentacle)	(0.07)	(1.46)	(0.38)	(0.05)	(5)
Octopus	82.05	14.09	0.75	1.87	1061
(tentacle)	(0.76)	(0.32)	(0.12)	(0.10)	(3)
Octopus	82.23	13.60	1.25	1.89	1058
(tentacle)	(0.32)	(0.87)	(0.14)	(0.07)	(2)
Octopus	78.63	17.04	2.29	1.89	1071
(tentacle)	(0.43)	(0.76)	(0.14)	(0.08)	(2)
Octopus	80.71	13.58	3.30	2.30	1067
(tentacle)	(0.19)	(0.20)	(0.58)	(0.03)	(4)
Cuttle	81.31	15.71	1.30	1.07	1059
(mantle)	(0.16)	(0.32)	(0.14)	(0.00)	(1)
Cuttle	81.44	14.01	2.41	0.97	1064
(mantle)	(0.27)	(0.40)	(0.14)	(0.00)	(4)

[a] Average of 3 samples

[b] Values in parentheses are standard deviations

[c] Proximate compositions are in % wet basis

[d] Carbohydrate can be calculated by difference

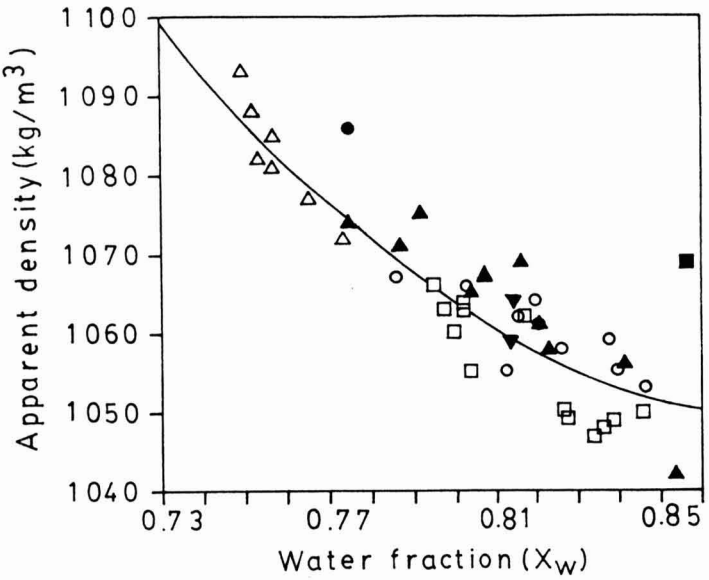

FIG. 1. APPARENT DENSITY OF FRESH SEAFOODS AS A FUNCTION OF WATER MASS FRACTION
○ Squid; ■ scallop; ● mussel; △ king prawn; □ calamari; ▲ octopus; ▼ cuttle. (Model 2)

F-ratio were calculated to test the validity of the models. All models differed significantly from the experimental data ($p < 0.05$). Hence none of the models was a good explanation of the physical processes occurring, but from the F-ratio it was possible to chose the best model. The quadratic model (model 2) was thus chosen to predict the apparent density of fresh seafood (Table 2). There was no significant difference between the empirical and semi-empirical models. Hence, empirical or semi-empirical models should be recommended for prediction of apparent density of fresh seafood.

The experimentally measured apparent density can be considered as substance density because fresh seafood meat does not contain air phase. In fitting the theoretical model the density of the components were taken from Choi and Okos (1985). For all experimental data points, the theoretical model gave lower values than the measured values. This indicated that there must be an excess volume.

After modifying the theoretical model to include excess volume, there was an improvement in the model prediction. The significant improvement of the theoretical model indicated that the excess volume fraction can be correlated with initial water or component mass fraction. Excess volume fractions of fresh

TABLE 2.
DIFFERENT MODELS USED FOR ANALYZING DENSITY OF FRESH SEAFOOD

Model	*Equation*
(Empirical)	
Model 1	$\rho_{ap} = 1351 - 357X_w$
Model 2	$\rho_{ap} = 2684 - 3693X_w + 2085{X_w}^2$
(theoretical)	
Model 3	$\frac{1}{\rho_{ap}} = \frac{1}{\rho_t} = \sum_{i=1}^{m} \frac{X_i}{\rho_{ti}}$
(Semi-empirical)	
Model 4	$\frac{1}{\rho_{ap}} = \frac{1}{1-\epsilon_{ex}} \sum_{i=1}^{m} \frac{X_i}{\rho_{ti}}$ where $-\epsilon_{ex} = 0.038 - 0.025X_w$
Model 5	$\frac{1}{\rho_{ap}} = \frac{1}{1-\epsilon_{ex}} \sum_{i=1}^{m} \frac{X_i}{\rho_{ti}}$ where $-\epsilon_{ex} = 0.787 - 1.900X_w + 1.17{X_w}^2$
Model 6	$\frac{1}{\rho_{ap}} = \frac{1}{1-\epsilon_{ex}} \sum_{i=1}^{m} \frac{X_i}{\rho_{ti}}$ where $-\epsilon_{ex} = (93.24X_{wo} + 42.97X_{po} + 2640X_{fo} - 4256X_{ao} - 1086X_{co})\ 10^{-4}$

[a] X_{wo}, X_{po}, X_{fo}, X_{ao} and X_{co} are the mass fraction of water, protein, fat, ash and carbohydrate of fresh seafood

seafood are shown in Fig. 2. The semi-empirical model 6 was significantly improved from the other semi-empirical models. Hence excess volume can also be correlated with the proximate composition.

The mean percent deviation of the models varied from 0.43 to 1.75%. Although the σ values of semi-empirical and empirical models were nearly identical, semi-empirical models are preferred because they have some theoretical basis and so are more likely to be applicable outside the experimentally tested range.

Apparent Density of Frozen Seafood at −30C

Simple prediction equations, for example Plank's equation for the prediction of freezing time, required a constant density of frozen foods. Hence, density of frozen seafood at −30C was measured and modeled. The apparent density of

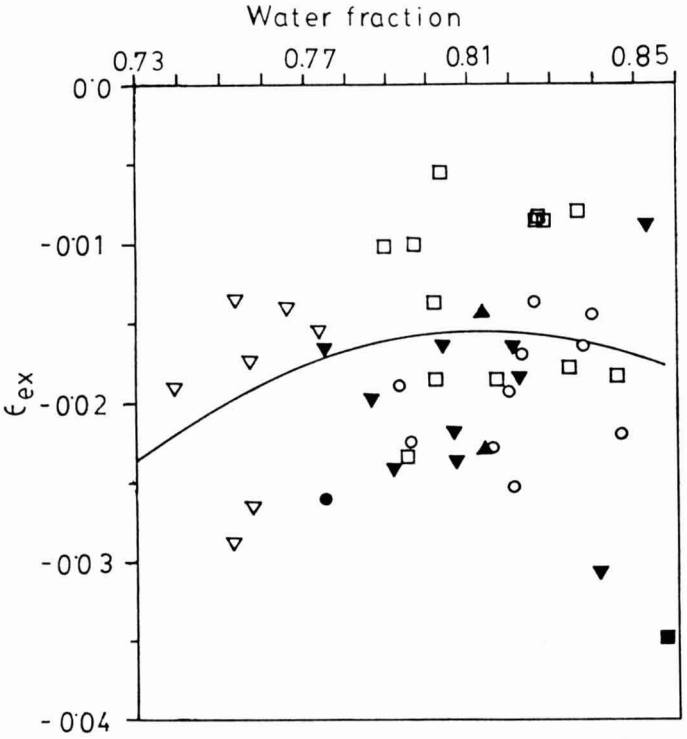

FIG. 2. EXCESS VOLUME FRACTION OF SEAFOODS AS A FUNCTION OF WATER MASS FRACTION
○ Squid; ■ scallop; ● mussel; ▽ king prawn; □ calamari; ▼ octopus; ▲ cuttle. (Quadratic model)

frozen seafood varied from 972 to 1017 at −30C (Table 3), and decreased with increase in initial water content (Fig. 3). The experimental data were fitted to the model as shown in Table 4.

Models 2, 5 and 7 were not significantly different from the experimental data ($p < 0.05$) and hence can explain the physical process occurring. The semi-empirical model (model 5) gave the best prediction for the apparent density of frozen seafood at −30C on the basis of F-ratio. The component densities were taken from Choi and Okos (1985) at −30C for theoretical models. The fraction of ice content was calculated from the equation given by Nakaide (1968):

$$X_I = X_{wo}[1 - T_f / T] \tag{13}$$

where X_{wo} is the initial water mass fraction before freezing, and T_f and T are the freezing point and process temperature, respectively.

TABLE 3.
APPARENT DENSITY OF FRESH (20 ± 3C) AND FROZEN (−30C) SEAFOODS

Materials	Proximate composition[a] (% wet basis)				Apparent density[a] (kg/m^3)	
	Water[a]	*Protein*[a]	*Fat*[a]	*Ash*[a]	*Fresh*	*Frozen*
Water					1000	921
Cuttle	81.44	14.01	2.41	0.97	1064	990
(mantle)	(0.27)	(0.40)	(0.14)	(0.00)	(4)	(5)
Squid	84.66	11.02	3.13	1.08	1048	975
(tail)	(0.31)	(0.90)	(0.22)	(0.10)	(3)	(4)
Prawn	75.23	19.48	2.92	1.82	1088	1017
(abdomen)	(0.39)	(2.13)	(0.75)	(0.03)	(3)	(6)
Calamari	84.53	11.31	3.24	0.59	1050	972
(tentacle)	(0.57)	(0.30)	(0.08)	(0.17)	(3)	(4)
Squid	82.07	13.03	3.33	1.19	1061	981
(mantle)	(0.16)	(0.37)	(0.11)	(0.05)	(3)	(5)
Squid	81.53	13.59	2.99	1.31	1062	982
(mantle)	(0.05)	(1.55)	(0.53)	(0.02)	(4)	(6)

[a] Average of 3 samples

[b] Values in parentheses are standard deviations

[c] Proximate compositions are in % wet basis

[d] Carbohydrate can be calculated by difference

TABLE 4.
DIFFERENT MODELS USED FOR ANALYZING DENSITY OF FROZEN SEAFOOD AT −30C

Model	*Equation*
(Empirical)	
Model 1	$\rho_{ap} = 1370 - 469X_{wo}$
Model 2	$\rho_{ap} = 1390 - 520X_{wo} + 31.56X_{wo}^{2}$
(Theoretical)	
Model 3	$\frac{1}{\rho_{ap}} = \frac{1}{\rho_t} = \sum_{i=1}^{m} \frac{X_i}{\rho_{ti}}$ (*assume all water as ice*)
Model 4[a]	$\frac{1}{\rho_{ap}} = \frac{1}{\rho_t} = \sum_{i=1}^{m} \frac{X_i}{\rho_{ti}}$
(Semi-empirical)	
Model 5[a]	$\frac{1}{\rho_{ap}} = \frac{1}{1 - \epsilon_{ex}} \sum_{i=1}^{m} \frac{X_i}{\rho_{ti}}$ where $-\epsilon_{ex} = 0.069 - 0.071X_{wo}$
Model 6[a]	$\frac{1}{\rho_{ap}} = \frac{1}{1 - \epsilon_{ex}} \sum_{i=1}^{m} \frac{X_i}{\rho_{ti}}$ where $-\epsilon_{ex} = 0.559 - 1.29X_{wo} + 0.768X_{wo}^{2}$
Model 7[a]	$\frac{1}{\rho_{ap}} = \frac{1}{1 - \epsilon_{ex}} \sum_{i=1}^{m} \frac{X_i}{\rho_{ti}}$ where $-\epsilon_{ex} = 0.021X_{wo} + 0.061X_{po} - 0.534X_{fo} + 0.205X_{ao} - 0.043X_{co})$

TABLE 4. *(Continued)*

[1] $\epsilon_{ex} = [\rho_{ap,exp}/\rho_{ti}] - 1$

[2] Component data from Choi and Okos (1985) at -30 C

[a] $T_f = -62.97 + 145.08X_{wo} - 84.82X_{wo}^2$ (Rahman 1991)
$X_I = X_{wo}[1 - T_f/T]$
$X_w = X_{wo} - X_I$

[b] X_{wo}, X_{po}, X_{fo}, X_{ao} and X_{co} are the mass fraction of water, protein, fat, ash and carbohydrate of fresh seafood

[c] X_w and X_I are the mass fraction of water and ice during freezing

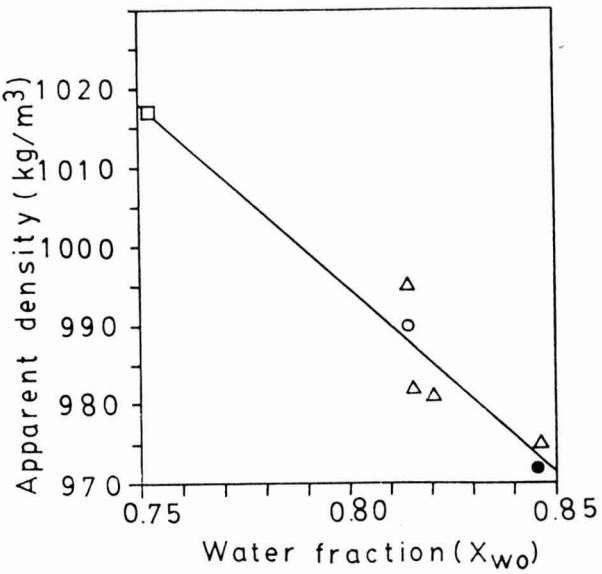

FIG. 3. APPARENT DENSITY OF FROZEN SEAFOODS AS A FUNCTION OF INITIAL WATER MASS FRACTION AT −30C
□ King prawn; ○ cuttle; △ squid; ● calamari.
(Model 1)

The prediction of the theoretical model was significantly different from the empirical and semi-empirical models. The deviation of the experimental data from the theoretical model might be due to the inaccurate prediction of the ice content, and/or the excess volume due to the interaction of the phases, and/or the thermal stress due to ice formation. Miles and Morley (1977) studied the internal pressure and tension on meat during freezing and found a maximum of 60 bars. The excess volume fraction was calculated assuming that the ice prediction was accurate, so that these three factors are interrelated (Fig. 4). The significant improvement in the predictions of the semi-empirical models indicated that the excess volume fraction can be correlated with the initial water content.

The mean percent deviation of the models varied from 0.4 to 1.4%. The empirical and semi-empirical models resulted in similar mean percent deviations.

Temperature Effect on Apparent Density Below 0C

The density of frozen food materials depends on the amount of ice formation, and the rate of formation of ice depends on the temperature below 0C. Hence the apparent density of frozen squid mantle meat was measured from −1.5 to −40C. The apparent density of frozen squid mantle meat varied from 1062 to 990 kg/m^3 (Table 5) and decreased with decrease in temperature (Fig. 5). The main reason for the decreasing density is the formation of ice below the freezing point. The experimental data were fitted to the models shown in Table 6.

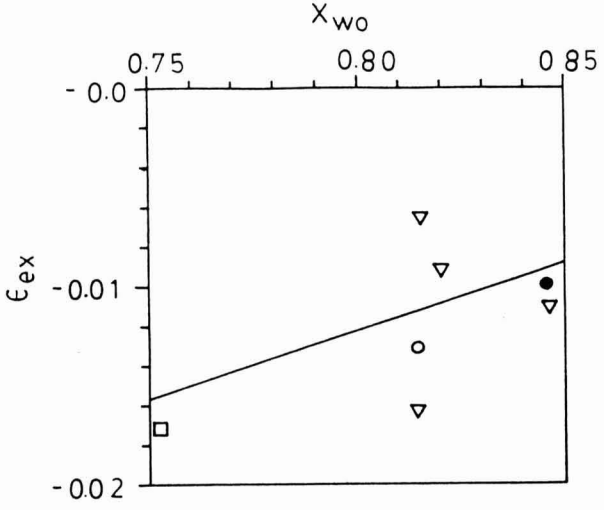

FIG. 4. EXCESS VOLUME FRACTION OF FROZEN SEAFOOD AT −30C
□ King prawn; ○ cuttle; ▽ squid; ● calamari. (Linear model)

TABLE 5.
APPARENT DENSITY OF FROZEN SQUID MANTLE MEAT AT DIFFERENT TEMPERATURES

T (C)	Apparent density[a]		
	Fresh	Frozen	Water
-40.0		990 (4)	922
-30.0		995 (5)	921
-20.0		1004 (5)	920
-15.0		1010 (3)	919
-10.0		1006 (6)	918
-6.0		1019 (10)	918
-5.0		1023 (7)	918
-4.0		1025 (9)	917
-3.5		1039 (11)	917
-3.0		1030 (10)	917
-2.5		1038 (3)	917
-2.0		1042 (5)	917
-1.5		1062 (4)	917
20.0	1059 (3)		-

[a] Average of 3 samples

[b] Values in parentheses are standard deviations

[c] $T_f = -62.97 + 145.08X_{wo} - 84.82X_{wo}^2$ (Rahman 1991)

[d] X_{wo}=0.8143; X_p=0.1335; X_f=0.0260; X_{as}=0.0135; X_p=0.0127

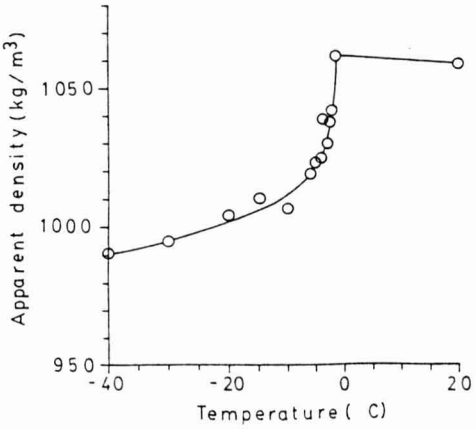

FIG. 5. APPARENT DENSITY OF FROZEN SQUID MANTLE AS A FUNCTION OF TEMPERATURE
(Model 5)

TABLE 6.
DIFFERENT MODELS USED FOR ANALYZING DENSITY OF FROZEN SQUID MANTLE MEAT AT DIFFERENT TEMPERATURES

Model	*Equation*
(Empirical)	
Model 1	$\rho_{ap} = 1037 + 1.429T$
Model 2	$\rho_{ap} = 1047 + 3.603T + 0.0573T^2$
(Theoretical)	
Model 3	$\frac{1}{\rho_{ap}} = \frac{1}{\rho_t} = \sum_{i=1}^{m} \frac{X_i}{\rho_{ti}}$
(Semi-empirical)	
Model 4	$\frac{1}{\rho_{ap}} = \frac{1}{1-\epsilon_{ex}} \sum_{i=1}^{m} \frac{X_i}{\rho_{ti}}$ where $-\epsilon_{ex} = (397 + 7.051T)10^{-4}$
Model 5[a]	$\frac{1}{\rho_{ap}} = \frac{1}{1-\epsilon_{ex}} \sum_{i=1}^{m} \frac{X_i}{\rho_{ti}}$ where $-\epsilon_{ex} = (393 + 5.877T - 0.0309T^2)10^{-4}$

[1] $\epsilon_{ex} = [\rho_{ap,exp}/\rho_{ti}] - 1$

[2] Component data from Choi and Okos (1985)

[a] $T_f = -62.97 + 145.08X_{wo} - 84.82X_{wo}^2$ (Rahman 1991)
$X_I = X_{wo}[1 - T_f/T]$
$X_w = X_{wo} - X_I$

[b] X_{wo}, X_{po}, X_{fo}, X_{ao} and X_{co} are the mass fraction of water, protein, fat, ash and carbohydrate of fresh seafood

[c] X_w and X_I are the mass fraction of water and ice during freezing

The semi-empirical models (models 4 and 5) were not significantly different from the experimental data ($p < 0.05$) because model F-ratio was lower than tabulated F-ratio and hence are sufficient to explain the physical processes occurring. Model 4 gave the best prediction for the frozen squid meat on the basis of lowest F-ratio value. The theoretical model was again significantly different in its predictions from the empirical and semi-empirical models. The excess volume is given in Fig. 6 as a function of temperature.

The mean percent deviation of the models varied from 0.5 to 3% for squid mantle meat. The mean percent deviation of the density prediction for fresh and frozen seafood by theoretical model was lower than 3%. Although empirical or semi-empirical models gave better predictions, the empirical parameters must be known. Since the parameters will vary for different materials and are not always available in the literature, theoretical model should be used in general for fresh and frozen seafood. An error of less than 3% is normally tolerable for design and process calculations.

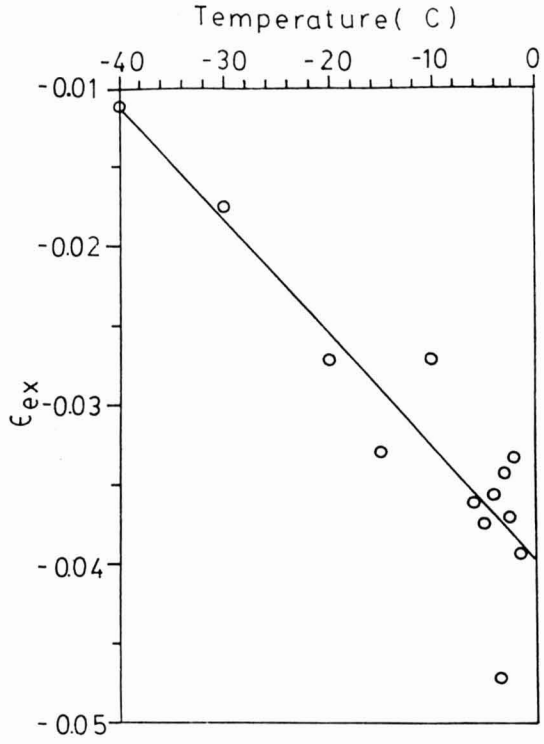

FIG. 6. EXCESS VOLUME FRACTION OF FROZEN SQUID MANTLE MEAT AS A FUNCTION OF TEMPERATURE
(Linear model)

REFERENCES

ARIMOTO, A., OGAWA, H. and MURAKAMI, S. 1990. Temperature dependence of molar excess volumes and excess thermal expansion coefficients for binary mixtures of cyclohexane with some hydrocarbons between 298.15 and 313.15 K. Thermochim. Acta *163*, 191–202.

ASHRAE. 1981. Thermal properties of foods. In *Fundamentals Handbook*, American Society of Heating, Refrigeration and Air Conditioning Engineers, New York.

BRAVO, R., PINTOS, M., AMIGO, A. and GARCIA, M. 1991. Densities and viscosities of binary mixtures decanol + some n-alkanes at 298.15 K. Phys. Chem. Liq. *22*(4), 245–253.

CHOI, Y. and OKOS, M.R. 1985. Effects of temperature and composition on the thermal properties of foods. In *Food Engineering and Process Applications*. Vol. 1. *Transport Phenomena*, (M.L. Maguer and P. Jelen, eds.).

DICKERSON, R.W. 1968. Thermal properties of foods. In *The Freezing Preservation of Food*, (D.K. Tressler, W.B. Van Arsdel and M.R. Copley, eds.) pp. 26–51, Van Nostrand Reinhold/AVI, New York.

HELDMAN, D.R. 1982. Food properties during freezing. Food Technol. *36* (Feb.), 92–96.

KEPPELER, R.H. and BOOSE, T.R. 1970. Thermal properties of frozen sucrose solutions. Trans. ASAE *13*, (3) 335–339.

LOZANO, J.E., ROTSTEIN, E. and URBICAIN, M.J. 1980. Total porosity and open-pore porosity in the drying of fruits. J. Food Sci. *45*, 1403–1407.

LOZANO, J.E., ROTSTEIN, E. and URBICAIN, M.J. 1983. Shrinkage, porosity and bulk density of foodstuffs at changing moisture contents. J. Food Sci. *48*, 1497–1553.

MANNAPPERUMA, J.D. and SINGH, R.P. 1989. A computer-aided method for the prediction of properties and freezing/thawing times of foods. J. Food Eng. *9* (4), 275–304.

MEFFERT, H.F.T. 1983. History, aims, results and future of thermophysical properties work within COST 90. In *Thermophysical Properties of Foods*, (R. Jowitt, F. Escher, B. Hallstrom, H.F.T. Meffert, W.E.L. Spiess and G. Vos, eds.) pp. 229–267, Applied Science Publishers/Elsevier, New York.

MILES, C.A., BEEK, G.V. and VEERKAMP, C.H. 1983. Calculation of thermophysical properties of foods. In *Thermophysical Properties of Foods* (R. Jowitt, F. Escher, B. Hallstrom, H.F.T. Meffert, W.E.L. Spiess and G. Vos, eds.) pp. 229–267, Applied Science Publishers/Elsevier, New York.

MILES, J. and MORELEY, M.J. 1977. Measurement of internal pressures and tensions in meat during freezing, frozen storage and thawing. J. Food Technol. *12*, 387–402.

NAKAIDE, M. 1968. Shokuhinkoogyo-no-reitoo (*Refrigeration in Food Engineering*), pp. 16–33, Koorin Shoin., Tokyo.

ORTEGA, J., MATOS, J. S. and PEREZ, E. 1991. Volumetric behavior of binary systems cyclohexane with the hexanol isomers at 298.15 K. Thermochim. Acta *180*, 1–8.

POLLEY, S.L., SNYDER, O.P. and KOTNOUR, P. 1980. A compilation of thermal properties of foods. Food Technol. *34* (11), 76.

RAHMAN, M.S. 1991. Thermophysical properties of seafoods. Ph. D. thesis. University of New South Wales, Australia.

RAHMAN, M.S. and DRISCOLL, R.H. 1991. Thermal conductivity of seafoods: calamari, octopus and prawn. Food Aust. *43* (8), 356.

RAHMAN, M.S., POTLURI, P.L. and VARAMIT, A. 1991. Thermal conductivities of fresh and dried seafood powders. Trans. ASAE *34* (1), 217.

REDLICH, O. and KISTER, A.T. 1948. Algebraic representation of thermodynamic properties and the classification of solution. Ind. Eng. Chem. *40*, 341 (cited by Bravo *et al.* 1991).

SANZ, P.D., ALONSO, M.D. and MASCHERONI, R.H. 1987. Thermophysical properties of meat products: General bibliography and experimental values. Trans. ASAE *30* (1), 283.

WOODAMS, E.E. and NOWREY, J.H. 1968. Literature values of thermal conductivities of foods. Food Technol. *22* (Apr.), 494–502.

ABSORPTION OF WATER IN LONG-GRAIN ROUGH RICE DURING SOAKING[1]

RENFU LU, TERRY J. SIEBENMORGEN[2] and TRACY R. ARCHER

Biological and Agricultural Engineering Department
University of Arkansas
Fayetteville, AR 72701

Accepted for Publication August 3, 1993

ABSTRACT

Soaking tests were conducted to determine the rate of water absorption in Newbonnet long-grain rough rice ranging from 14 to 30% initial moisture content (dry basis) at 11, 20, 30, 40, and 50C. Four rewetting models were compared, and the following model by Becker (1959) was found to best fit the experimental data, while the rice moisture content during soaking was lower than about 40% (dry basis):

$$M(t) = M_o + \Delta M_o + \alpha^* \sqrt{t}$$

(see a list of symbols at the end of the article). The absorption rate, dM/dt, increased with temperature and decreased with initial moisture content. A regression equation was obtained to relate the parameter α to temperature and initial rice moisture content. The initial moisture gain was not significantly affected by temperature and initial rice moisture content. The average initial moisture gain over the test temperature range was 0.75 percentage points.

INTRODUCTION

During the harvest season, rain and nocturnal dew incidence often cause an increase in rice moisture content and may lead to kernel fissuring. Studies have shown that absorption of liquid water is the major cause of rice kernel fissuring in the field (e.g., Craufurd 1962; Srinivas *et al.* 1978; Siebenmorgen *et al.* 1992). Hence, it is important to understand the water absorption in rice kernels

[1] Published with the approval of the Associate Vice President of Agriculture/Research, Agricultural Experiment Station, University of Arkansas, Fayetteville, AR. Mention of a commercial product name does not imply endorsement by the University of Arkansas.

[2] To whom correspondence should be sent.

Journal of Food Process Engineering **17** (1994) 141-154.

during rain or dew periods and the resulting effects on rice milling quality so that proper management of harvesting schedules can be established. Srinivas *et al.* (1978) studied the fissuring of rough rice during soaking. They reported that the proportion of fissured kernels was related to initial moisture content, soak temperature, and time. Siebenmorgen and Jindal (1986) developed an equation for predicting head rice yield reduction for long-grain rough rice exposed to the four different absorptive conditions, including soaking. However, they did not determine the effects of soak temperatures and times on head rice yield reduction.

Although the effects of rain or dew on head rice yield have been reported by many researchers, the extent to which they affect head rice yield has not been quantified. This is perhaps because it is difficult to simulate actual rain or dew formation conditions. Lu *et al.* (1992) developed mathematical models for predicting the changes in rice milling quality, including head rice yield and total milled rice yield, and field yield during a harvest season. They used an equation developed by Siebenmorgen and Jindal (1986) for predicting head rice yield reduction during water soaking to predict the head rice yield reduction caused by rain in the field, and reasonable prediction results were obtained when compared with the experimental data. This suggests that the rewetting of rice by rain or dew is similar to the soaking of rice in water. Hence, information on moisture absorption behavior of rice during soaking at temperatures representative of field conditions would help determine the rain or dew effects on head rice yield. Such information is also vital for developing a model for predicting changes in rice field moisture content during the harvest season (Lu and Siebenmorgen 1992b).

Therefore, the objectives of this study were to measure the water absorption in long-grain rough rice during soaking as affected by temperature (ranging from 11 to 50C) and initial moisture content (ranging from 14 to 30%) and to develop a rewetting model to predict the water absorption in long-grain rough rice during soaking.

MATERIALS AND METHODS

Experimental Procedure

A long-grain rice variety, 'Newbonnet', was used in the soaking tests. The rice was harvested at approximately 23% moisture content[3] from a commercial field in Keiser, Arkansas. Blank kernels and foreign material were removed with

[3]Unless otherwise specified, all moisture contents mentioned herein are on a dry basis.

a Carter Dockage Tester. The cleaned rice was placed in burlap bags and stored at 1C until testing. The rice moisture content at the time of removal from the cold storage for testing was about 18%.

Soaking tests were conducted over a range of initial moisture contents. The samples lower than 18% moisture content were obtained by drying the rice on wire-mesh trays at room temperature (approximately 24C). To attain higher moisture content samples, the rice was first remoistened to about 22% moisture content using a conditioning chamber with air supplied by a temperature and relative humidity control unit (Parameter Generation and Control 300 CFM Climate Lab-AA, PGC Inc.). The conditioning chamber was set at 25C and 85% relative humidity. After removal from the conditioning chamber, the samples were misted using a plant misting bottle for approximately one minute to attain moisture contents greater than 22%. The purpose of using the two-step remoistening procedure was to minimize fissuring of the rice kernels. After the desired moisture contents were obtained, all samples were bagged in plastic bags and placed in cold storage for about one week to allow equilibration of moisture within kernels. Six moisture content levels were obtained ranging from 14 to 34%. This represents the range typically encountered during the harvest season. However, the samples at 34% moisture content molded after about one week in the cold storage. Hence, only five moisture content levels were used in the soaking tests. The initial sample moisture contents used in the experiments are shown in Table 1.

Soaking tests were conducted at 11, 20, 30, 40, and 50C. Those kernels with damaged or split hulls were removed prior to testing. Samples, 4 g each, were placed in wire-mesh baskets (approximately 7 × 7 cm). There were approximately 170 kernels in each of the samples at 14% initial moisture content, and fewer kernels were in the other samples, depending on the sample initial moisture content. The amount of rice for each sample was determined based on the studies of Engels *et al.* (1986) and Lu and Siebenmorgen (1992a). Each sample was weighed to an accuracy of ± 0.1 mg using an analytical balance. The baskets were then submersed in a constant temperature water pan (± 0.5C) that had been equilibrated to the required temperature. The pan, which could accommodate about 40 baskets, was placed inside a conditioning chamber. The water depth in the pan was maintained at about 2.5 cm for the entire test period. The baskets were removed from the water pan at time intervals of 0.25, 0.50, 0.75, 1.0, 1.5, 2.0, 3.0, 4.0, 5.0, 6.0, 8.0, 12.0, 24.0 36.0, 48.0, and 72.0 h. The soaked rice was emptied onto two layers of paper towels. The kernels were quickly blotted with the paper towels 4–5 times to remove the surface water. This blotting procedure was established based on the preliminary test results and other reported studies (e.g., Becker 1960; Fan *et al.* 1963). After blotting, the sample was transferred to a metal cup for weight measurement. The test duration was 72 h for temperatures less than or equal to 30C, 48 h for 40C,

TABLE 1.
INITIAL AND FINAL RICE MOISTURE CONTENT (M_o and M_f) USED IN FITTING THE ABSORPTION CURVE, INITIAL MOISTURE GAIN (ΔM_o), α, R^2, AND RMSE* FROM THE REGRESSION ANALYSIS FOR EQ. (1)

Temp (C)	M_o (%)	M_f (%)	ΔM_o (%)	α^{**} ($x10^2$, $h^{-0.5}$)	R^2	RMSE
11.0	14.2	41.0	1.13	3.039	0.995	0.52
	17.8	41.5	0.06	2.778	0.995	0.51
	22.7	42.6	0.91	2.321	0.995	0.42
	26.9	44.4	1.23	2.106	0.975	0.82
	29.2	45.8	1.26	1.978	0.975	0.78
20.0	14.4	42.3	0.69	3.865	0.997	0.40
	18.0	42.0	-0.07	3.568	0.995	0.50
	21.2	43.1	0.52	3.219	0.994	0.51
	26.3	45.3	0.71	2.857	0.987	0.65
	28.6	47.8	0.72	2.842	0.983	0.76
30.0	14.4	40.2	1.33	5.322	0.988	0.76
	18.0	41.4	0.22	4.893	0.996	0.42
	22.9	44.2	0.21	4.264	0.997	0.32
	26.9	46.2	0.91	3.846	0.992	0.44
	29.0	46.6	0.98	3.477	0.987	0.52
40.0	14.1	38.9	1.10	7.169	0.993	0.65
	17.6	39.4	0.58	6.316	0.996	0.41
	22.6	40.3	0.26	5.172	0.995	0.38
	26.8	43.5	0.61	4.880	0.991	0.47
	29.1	44.7	0.48	4.574	0.990	0.46
50.0	14.3	38.2	1.44	8.325	0.989	0.74
	16.8	38.4	0.97	7.591	0.994	0.52
	22.7	39.3	0.43	5.924	0.992	0.46
	26.9	42.2	1.08	5.256	0.987	0.53
	28.9	43.6	0.97	5.172	0.984	0.55

* Root mean square error between the experimental data and the model fitted values (% kg/kg).

** The regression analysis results were based on the soaking data obtained within 72 h for 11 C, 48 h for 20 C, 24 h for 30 C, 12 h for 40 C, and 8 h for 50 C.

and 24 h for 50C. Relatively short time periods were chosen for the 40 and 50C treatments because the absorption rates at these two temperatures were faster than those at the lower temperatures. Germination of rice kernels was noticed after 48 and 24 h of soaking in water at the respective temperatures of 20 and

30C. No germination was found at 11, 40, and 50C. The data obtained after germination were not used in the analysis. Some solids losses (less than 2.5% of the original kernel dry matter weight) were also noticed for the samples soaked for extended time periods. However, such losses had negligible effects on the final moisture content determinations. The sample moisture contents were determined by oven drying for 24 h at 130C (Jindal and Siebenmorgen 1987). All experiments were duplicated.

Rewetting Models

Several rewetting models have been used by researchers to describe water absorption in cereal grains and legumes. Becker (1959) derived an equation for predicting average moisture content change in solids of arbitrary shape from Fick's law of diffusion. For a short time period, Becker's equation has the following form:

$$M(t) = M_o + \Delta M_o + \alpha * \sqrt{t} \tag{1}$$

where α is the lumped parameter, which has the following expression:

$$\alpha = \frac{2}{\sqrt{\pi}} * (M_s - M_o) * \frac{S}{V} * \sqrt{D} \tag{2}$$

Becker (1960) pointed out that the initial moisture gain, ΔM_o, is primarily due to rapid capillary action. Equation (1) has been successfully used to model water absorption in wheat (Becker 1960), corn and sorghum (Fan *et al.* 1963), and rice during parboiling (Bandopadhyay and Ghose 1965; Bandyopadhyay and Roy 1976, 1977, and 1978).

Singh and Kulshrestha (1987) and Peleg (1988) proposed the following empirical model to describe water absorption in cereal grains and legumes:

$$M(t) = M_o + \frac{t}{k_1 + k_2 * t} \tag{3}$$

Equation (3) was later derived by Singh (1990) based on the assumption that hydration of the substance of the solid rather than diffusion of water is the rate controlling step during absorption process. Sopade and Obekpa (1990) and Sopade *et al.* (1992) used Eq. (3) to model water absorption in soybeans, cowpeas, peanuts, corn, millet, and sorghum.

The following two models have also been used to describe the moisture absorption behavior of rice and other cereal grains (e.g., Misra and Brooker 1980; Banaszek and Siebenmorgen 1990):

$$M(t) = M_e + (M_o - M_e) * \exp(-k * t) \quad (4)$$

$$M(t) = M_e + (M_o - M_e) * \exp(-k * t^n) \quad (5)$$

Equations (1), (3), (4), and (5) were used to fit the soaking data. The equilibrium moisture content M_e in Eq. (4) and (5) was treated as an unknown parameter because it could not be obtained directly from the soaking data. The parameters in Eq. (1), (4), and (5) were determined using a nonlinear regression method (SAS 1988). In performing the regression analysis, Eq. (3) was transformed to the linear form as shown by Peleg (1988) so that linear regression could be applied to determine the two parameters.

RESULTS AND DISCUSSION

Absorption Data

The experimental data on the absorption of water in the Newbonnet rough rice with the three selected initial moisture contents at 11, 30, and 50C are shown in Fig. 1–3. The moisture absorption rate was affected by soak temperature. The kernels absorbed water at a slower rate at 11C than at 30 or 50C. It appeared that after 72 h of soaking in water at 11C, the kernels would continue to gain moisture at a fairly steady rate (Fig. 1). Figure 2 shows that during the 24 h soaking in water at 30C, the rice kernels gained moisture progressively. The equilibrium moisture content could not be obtained because the rice started to germinate after 24 h of soaking in water. Similar absorption curves were also obtained for 20C, but the germination started after 48 h. At 40 and 50C, the rice moisture content increased rapidly during the first 12 h of soaking. Thereafter, the rice gradually approached the equilibrium moisture content (Fig. 3).

Figures 1–3 further show that the absorption rate appeared to decrease with initial rice moisture content. This is consistent with the results reported by Banaszek and Siebenmorgen (1990) for rice exposed to high relative humidity air, in which the increasing initial moisture content level decreased the absorption rate and increased the equilibrium moisture content.

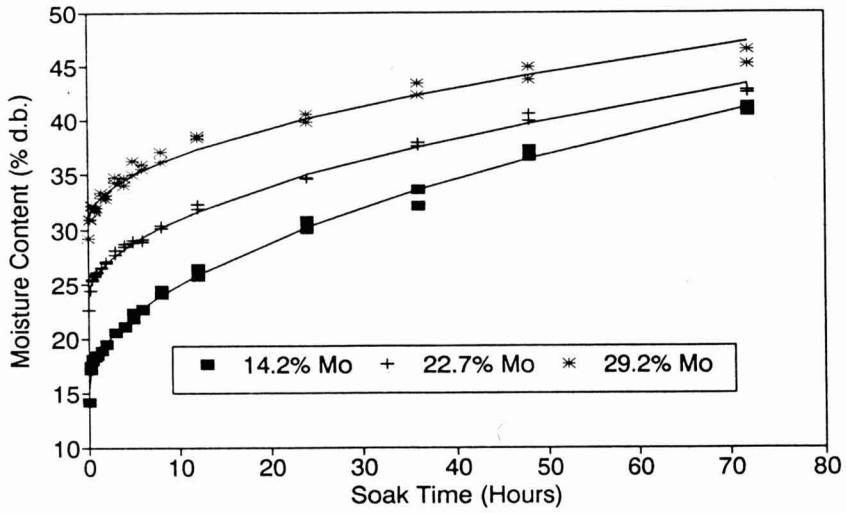

FIG. 1. EXPERIMENTAL DATA AND THE FITTED ABSORPTION CURVES [EQ. (1)] FOR NEWBONNET ROUGH RICE AT THREE INITIAL MOISTURE CONTENTS (M_os) SOAKED AT 11.0C

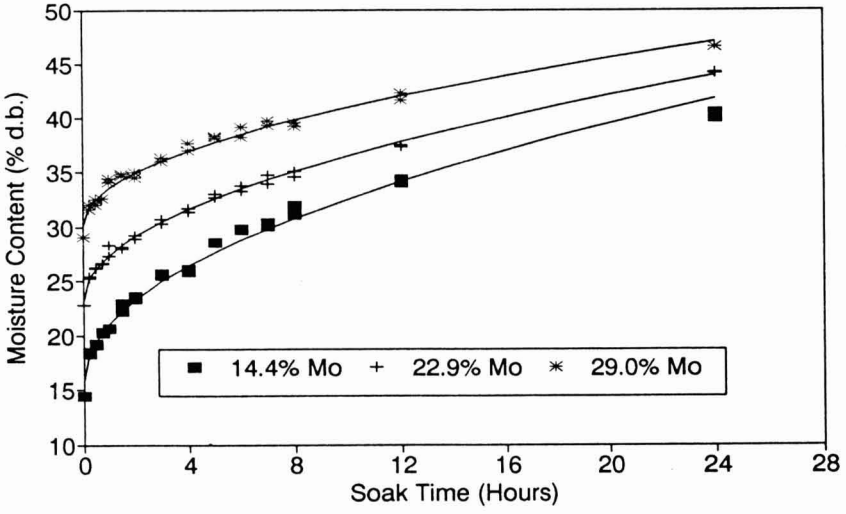

FIG. 2. EXPERIMENTAL DATA AND THE FITTED ABSORPTION CURVES [EQ. (1)] FOR NEWBONNET ROUGH RICE AT THREE INITIAL MOISTURE CONTENTS (M_os) SOAKED AT 30.0C

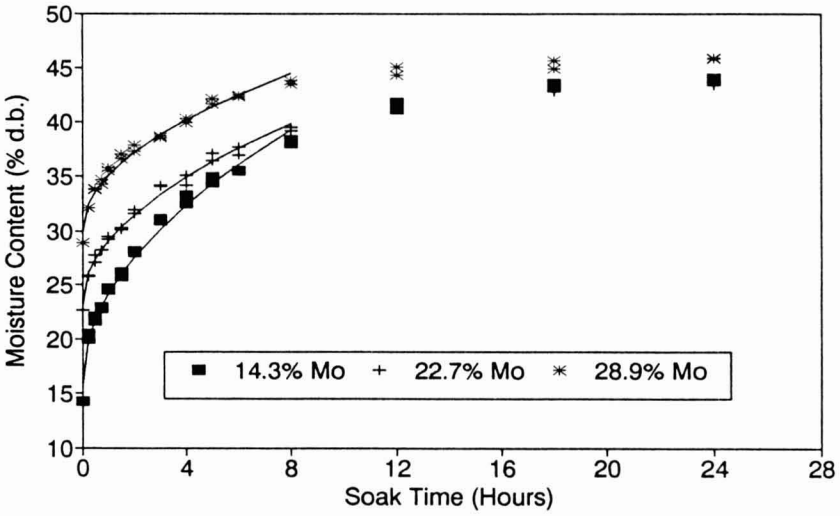

FIG. 3. EXPERIMENTAL DATA AND THE FITTED ABSORPTION CURVES [EQ. (1)] FOR NEWBONNET ROUGH RICE AT THREE INITIAL MOISTURE CONTENTS (M_os) SOAKED AT 50.0C

Comparison of Rewetting Models

Figure 4 shows a comparison of the regression curves from Eq. (1), (3), (4), and (5) with the absorption data for the 14.4% initial moisture content rice soaked at 20C for 48 h. The root mean square errors (RMSEs) between the experimental data and the fitted values were 0.40, 1.93, 1.85, and 0.54 (% kg/kg) for Eq. (1), (3), (4), and (5), respectively. Equation (1) gave the best fit to the experimental data. Equations (3) and (4) did not fit the experimental data well and underpredicted the experimental data for the first 2–5 h soaking period and the last 12-h soaking period and overpredicted the experimental data for the intermediate soaking period. This trend prevailed for the higher moisture content rice. The relative performances of Eq. (1), (3), (4), and (5) for 11 and 30C were the same as those for 20C.

However, for 40 and 50C, Eq. (5) was the best model to fit the experimental data with the RMSEs ranging from 0.38 to 0.53 (% kg/kg) for the five initial moisture contents. The RMSEs for Eq. (3) and (4) ranged from 0.72 to 1.40 and from 1.18 to 2.13 (% kg/kg), respectively. Equation (1) gave the worst fit for the experimental data among the four rewetting models in this case [the RMSEs ranged from 1.55 to 3.02 (% kg/kg)].

The poor performances of Eq. (1) for 40 and 50C were attributed to the fact that it is only applicable for a certain range of moisture content and is not valid when the rice approaches its equilibrium moisture content. The experimental

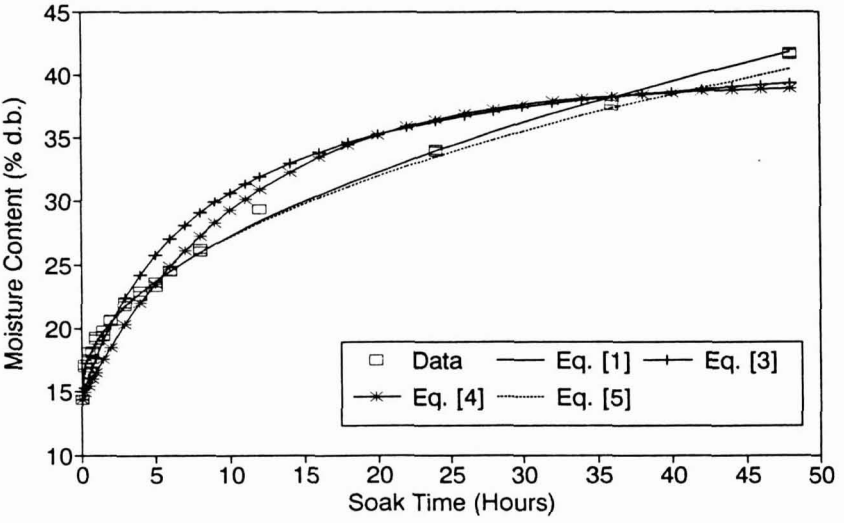

FIG. 4. COMPARISON OF EXPERIMENTAL DATA AND THE FITTED ABSORPTION CURVES FROM THE FOUR REWETTING MODELS FOR NEWBONNET ROUGH RICE AT AN INITIAL MOISTURE CONTENT OF 14.4% SOAKED AT 20.0C

data showed that the moisture content of rice increased very slowly and gradually approached equilibrium after about 8–12 h of soaking at 40 and 50C. Hence, further analysis was performed to fit the experimental data for the first 12 h at 40C and 8 h at 50C with Eq. (1), (3), (4), and (5). In this case, the relative performances of the four rewetting models were the same as those for temperatures lower than or equal to 30C. Since most rice kernel fissuring occurs during the initial few hours of soaking (Srinivas *et al.* 1978), it is imperative that the selected model accurately predict the water absorption in rice during this time period. Compared to the other three models, Eq. (1) gave a better prediction of the water absorption in rice for the initial soaking period. Hence, Eq. (1) was chosen as the best model to describe water absorption in long-grain rice. The limitations of Eq. (1) are discussed further in the next subsection.

Equation (5), which fits the data reasonably well, was not chosen since it requires knowledge of the equilibrium moisture content, which could not be obtained from the experimental data. The regression analyses often failed to converge for temperatures lower than or equal to 30C, which was, in part, attributed to the relatively large number of unknown parameters. The equilibrium moisture contents determined from the nonlinear regression analyses varied widely from one set of data to another and, in some cases, was unrealistically high. Further, Eq. (5) is an empirical model and is more complex than Eq. (1) in terms of the regression analysis.

Determination of the Model Parameters for Equation (1)

If water absorption in rice is a diffusion process, then Eq. (1) suggests that the moisture content will be a linear function of the square root of soak time. Figure 5 shows the moisture content change with the square root of soak time for rice with an initial moisture content of approximately 14.3% at the five soak temperatures. A linear relationship between the measured moisture content and $t^{0.5}$ existed when soak temperature was less than or equal to 30C. At 40 and 50C, the rice moisture content increased linearly with $t^{0.5}$ until about 3.5 $h^{0.5}$ (12 h) and 2.8 $h^{0.5}$ (8 h), respectively. Thereafter, the absorption curve conspicuously deviated from the straight line. Figure 5 further shows that regardless of the soak temperature, moisture content varied linearly with $t^{0.5}$ until it reached about 40%, above which Eq. (1) would no longer give an accurate prediction. This critical moisture content level appeared to increase slightly with initial rice moisture content and was approximately between 40 and 46% for the higher initial moisture content rice. Hence, it was concluded that Eq. (1) is adequate for describing water absorption in long-grain rice during soaking while the rice moisture content is lower than about 40%.

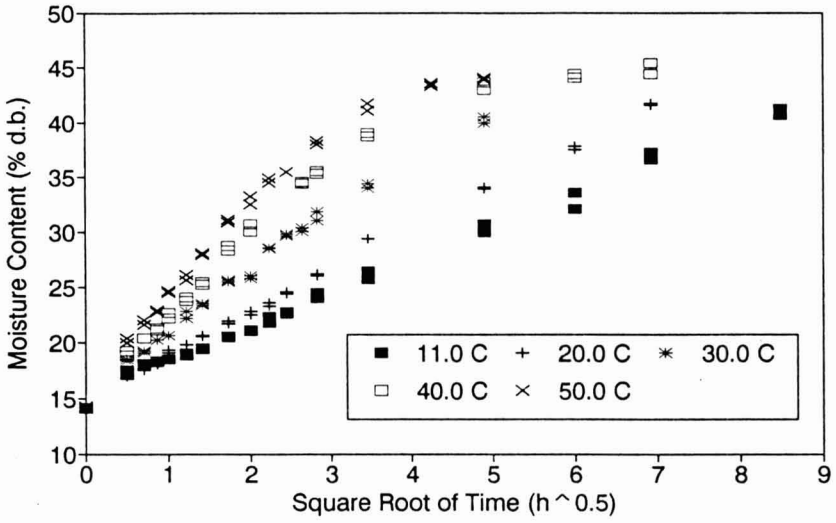

FIG. 5. CHANGE OF THE RICE MOISTURE CONTENT WITH THE SQUARE ROOT OF ABSORPTION TIME FOR NEWBONNET ROUGH RICE AT AN INITIAL MOISTURE CONTENT OF ABOUT 14%

Figures 1–3 show that the fitted regression curves by Eq. (1) compared very well with the experimental data at 11, 30, and 50C for the soaking time periods of 72, 24, and 8 h, respectively. Similar results were also obtained for 20 and 40C. Table 1 summarizes the values of M_o, M_f, ΔM_o, α, and pertinent statistics. The high R^2 values and the small RMSEs indicate that Eq. (1) adequately predicted water absorption in long-grain rice during soaking. However, it should be noted that the regression analysis results in Table 1 were obtained based on the soaking data obtained within 72 h for 11C, 48 h for 20C, 24 h for 30C, 12 h for 40C, and 8 h for 50C. The rice moisture contents at the end of these soaking time periods ranged from 38 to 48%.

The α value increased with temperature and decreased with initial moisture content (Table 1). A stepwise regression analysis (SAS 1988) was performed to relate the parameter α to the temperature and initial moisture content. The following regression equation was obtained for the parameter α:

$$\alpha = a + b * T + c * T * M_o \tag{6}$$

The regression coefficients and associated statistics are presented in Table 2. Soak temperature alone accounted for about 76% of the change in the parameter α while the interaction effect of initial moisture content and soak temperature accounted for a 23% change. Hence, temperature had a more pronounced effect on the parameter α than the initial rice moisture content.

Once the α value is determined, the moisture diffusivity, D, can be, in principle, calculated from Eq. (2) when the surface moisture content, M_s, and the volume and surface area of the solid are known. Becker (1960) and Fan *et al.* (1963) provided a method for calculating the M_s value from absorption data.

TABLE 2.
COEFFICIENTS AND STATISTICS OF THE REGRESSION EQUATION FOR THE PARAMETER α [EQ. (6)]

	Parameter	STD*	Partial R^2	MSE**
a	1.239306	0.094787	---	
b	0.201220	0.005497	0.761	0.039089
c	-0.004343	0.000214	0.227	

* Standard deviation.
** Mean square error for the regression equation.

However, the method was found not adequate for calculating the M_s value from the data obtained in this study. Therefore, no further effort was made in calculating M_s.

Table 1 also shows that the initial moisture gains over all five soak temperatures were less than 1.5 percentage points. The statistical analysis indicated that the effect of soak temperature and the initial rice moisture content on the ΔM_0 value was not significant at the 0.05 level. Hence ΔM_0 was chosen to be 0.75 percentage points, the average value over all initial moisture gain data.

Becker (1960) reported that the initial moisture gain ΔM_0 in wheat was a function of soak temperature. Bandyopadhyay and Roy (1978) also reported that ΔM_0 in rice during parboiling was affected by soak temperature. But Fan *et al.* (1963) found that ΔM_0 for corn and sorghum was constant over the test temperature range. The differences in the reported results between this study and those by Becker (1960) and Bandyopadhyay and Roy (1978) are speculated to be due to different test conditions and varietal differences.

CONCLUSIONS

(1) The absorption of water in long-grain rough rice was best described by the diffusion model derived by Becker (1959) when the rice moisture content during soaking was below about 40% for temperatures ranging from 11 to 50C.

(2) The absorption rate increased with temperature and decreased with initial rice moisture content. The rewetting parameter α in Eq. (1) was determined as a function of temperature and initial rice moisture content.

(3) The initial moisture gain ΔM_0 was not significantly affected by temperature and initial rice moisture content at the 0.05 level. The average initial moisture gain for the long-grain rough rice soaked at temperatures of 11 to 50C was 0.75 percentage points.

NOMENCLATURE

Symbol	Description	Unit
a, b, c	Regression coefficients in Eq. (6)	—
D	Moisture diffusivity of the solid	m^2/h
k	Parameter in Eq. (4) and (5)	—
k_1, k_2	Parameters in Eq. (3)	—
M(t)	Moisture content after soaking in water for time t	% dry basis
M_e	Equilibrium moisture content	% dry basis
M_f	Final moisture content used in fitting the absorption curve	% dry basis

M_0	Initial moisture content	% dry basis
ΔM_0	Initial moisture gain at the instant of soaking (i.e., $t = 0^+$)	% dry basis
M_s	Surface moisture content	% dry basis
n	Parameter in Eq. (5)	—
S	Surface area of the solid	m^2
t	Time	h
T	Soak temperature	C
V	Volume of the solid	m^3
α	Lumped parameter in Eq. (1)	$h^{-0.5}$

REFERENCES

BANASZEK, M.M. and SIEBENMORGEN, T.J. 1990. Moisture adsorption rates of rough rice. Trans. ASAE *33* (4), 1257–1262.

BANDOPADHYAY, B. and GHOSE, T.K. 1965. Studies on the hydration of Indian paddy. Part I. A rate equation for the soaking operation. Indian J. Technol. *3*, 360–365.

BANDYOPADHYAY, S. and ROY, N.C. 1976. Kinetics of absorption of liquid water by paddy grains during soaking. Indian J. Technol. *14*, 27–30.

BANDYOPADHYAY, S. and ROY, N.C. 1977. Studies on swelling and hydration of paddy by hot soaking. J. Food Sci. Technol. *14* (3), 95–98.

BANDYOPADHYAY, S. and ROY, N.C. 1978. A semi-empirical correlation for prediction of hydration characteristics of paddy during parboiling. J. Food Technol. *13*, 91–98.

BECKER, H.A. 1959. A study of diffusion in solids of arbitrary shape, with application to the drying of the wheat kernel. J. Appl. Polymer Sci. *1* (2), 212–226.

BECKER, H.A. 1960. On the absorption of liquid water by the wheat kernel. Cereal Chem. *37*, 309–323.

CRAUFURD, R.Q. 1962. Moisture changes in raw and parboiled paddy in west Africa and their influence upon milling quality. I. Moisture changes in the ripening crop. Empire. J. Exper. Agric. *20* (120), 315–320.

ENGELS, C., HENDRICKX, M., DE SAMBLANX, S., DE GRYZE, I. and TOBBACK, P. 1986. Modeling water diffusion during long-grain rice soaking. J. Food Eng. *5*, 55–73.

FAN, L., CHU, P. and SHELLENBERGER, J.A. 1963. Diffusion of water in kernels of corn and sorghum. Cereal Chem. *40*, 303–313.

JINDAL, V. K and SIEBENMORGEN, T.J. 1987. Effects of oven drying temperature and drying time on rough rice moisture content determination. Trans. ASAE *30* (4), 1185–1192.

LU, R. and SIEBENMORGEN, T.J. 1992a. Moisture diffusivity of long grain rough rice components. Trans. ASAE *35* (6), 1955–1961.

LU, R. and SIEBENMORGEN, T.J. 1992b. Modeling rice field moisture content during the harvest season. ASAE Paper 92-6520, ASAE, St. Joseph, MI.

LU, R., SIEBENMORGEN, T.J., DILDAY, R.H. and COSTELLO, T.A. 1992. Modeling long-grain rice milling quality and yield during the harvest season. Trans. ASAE *35* (6), 1905–1913.

MISRA, M.K and BROOKER, D.B. 1980. Thin layer drying and rewetting equations for shelled yellow corn. Trans. ASAE *23* (5), 1254–1260.

PELEG, M. 1988. An empirical model for the description of moisture sorption curves. J. Food Sci. *53* (4), 1216–1217, 1219.

SAS. 1988. SAS/STAT User's Guide, Release 6.03. ed., SAS Institute, Cary, NC.

SIEBENMORGEN, T.J., COUNCE, P.A., LU, R. and KOCHER, M.F. 1992. Correlation of head rice yield with individual kernel moisture content distribution at harvest. Trans. ASAE *35* (6), 1879–1884.

SIEBENMORGEN, T.J. and JINDAL, V.K. 1986. Effects of moisture adsorption on the head rice yields of long-grain rice. Trans. ASAE *29* (6), 1767–1771.

SINGH, B.P.N. 1990. Model for absorption of liquid water by grains. Trans. ASAE *32* (6), 2067–2072.

SINGH, B.P.N. and KULSHRESTHA, S.P. 1987. Kinetics of water sorption by soybean and pigeonpea grains. J. Food Sci. *52* (6), 1538–1541, 1544.

SOPADE, P.A., AJISEGIRI, E.S. and BADAU, M.H. 1992. The use of Peleg's equation to model water absorption in some cereal grains during soaking. J. Food Eng. *15*, 269–283.

SOPADE, P.A. and OBEKPA, J.A. 1990. Modelling water absorption in soybean, cowpea and peanuts at three temperatures using Peleg's equation. J. Food Sci. *55* (4), 1084–1087.

SRINIVAS, T., BHASHYAM, M.K, MUNE GOWDA, M.K. and DESIKACHAR, H.S.R. 1978. Factors affecting crack formation in rice varieties during wetting and field stresses. Indian J. Agric. Sci. *48* (7), 424–432.

OPTIMUM STERILIZATION: A COMPARATIVE STUDY BETWEEN AVERAGE AND SURFACE QUALITY

C.L.M. SILVA, F.A.R. OLIVEIRA[1], and P.A.M. PEREIRA

Escola Superior de Biotecnologia - UCP
Rua Dr. António Bernardino de Almeida
4200 Porto, Portugal

and

M. HENDRICKX

Katholieke Universiteit Leuven
Laboratory of Food Technology
Kardinaal Mercierlaan 92
3001 Heverlee, Belgium

Accepted for Publication August 3, 1993

ABSTRACT

Sterilization temperatures to maximize volume average or surface quality retention were calculated for one-dimensional conduction heating foods as a function of (1) Food Properties, (2) Processing Conditions and (3) Processing Criteria. A target lethality at the least-lethality point was used as a constraint, and optimal temperatures were qualitatively and quantitatively compared for equal design variables.

Average quality optimum conditions depend linearly on the inverse square of the D_{refq}-value for the quality factor. These conditions do not vary linearly with all the other influential variables, opposite to what had been observed for surface quality. Optimum temperature for maximum average quality is always higher than the corresponding one for surface quality, but the difference is not constant. A systematic approach to the dependence of average quality optimal conditions on all the relevant parameters was carried out and quantitative relations were obtained. Optimum average quality retention is independent of surface heat transfer resistance.

[1]Author to whom correspondence should be addressed.

Journal of Food Process Engineering **17** (1994) 155-176.

INTRODUCTION

The mathematical description of microorganisms thermal degradation kinetics together with an accurate model of heat flow into a conduction heating product allows the theoretical assessment of the sterilization process (Teixeira *et al.* 1969a). If an objective function is specified, it is possible to optimize the sterilization conditions (Teixeira *et al.* 1969b). Holdsworth (1985) and Silva *et al.* (1993) have presented extensive critical reviews on the modelling of optimal processing conditions for sterilized prepackaged foods.

Several objective functions, such as minimization of energy consumption and economic costs (Barreiro *et al.* 1984) and formation of toxic compounds (Lund 1982), can be considered. However, regarding consumers interests, the maximization of nutrients and quality-attributes retention is usually the most important goal (Silva *et al.* 1992b; Ridgway and Brimelow 1990).

Depending on the quality parameter to optimize two options can be considered (Ohlsson 1980a): maximizing quality retention in terms of (1) surface (Ohlsson 1980a,b,c; Hendrickx *et al.* 1990, 1992a,b, 1993; Silva *et al.* 1992b) or (2) volume average (Ohlsson 1980a,b,c; Teixeira *et al.* 1969b, 1975; Thijssen *et al.* 1978; Saguy and Karel 1979; Thijssen and Kochen 1980; Martens 1980; Nadkarni and Hatton 1985; Tucker and Holdsworth 1990, 1991; Banga *et al.* 1991).

Although in this research field several works have been published, few attempted to develop a consistent relationship between optimal conditions and all influential variables. Hendrickx *et al.* (1990, 1992a,b, 1993) and Silva *et al.* (1992a) developed generalized semi-empirical formulae to calculate optimal temperatures for maximum surface quality as a function of all relevant variables: target sterility value at the least-lethality point, reduced Fourier number or heat penetration parameter, z-value for quality factor thermal degradation kinetics, Biot number, geometry and initial product temperature. These equations are multilinear regressions and have also been applied to case studies such as finite cylindrical can (Hendrickx *et al.* 1992b). However, for average quality optimization a similar work is lacking. Ohlsson (1980a,b,c) detected a linear relationship between optimal temperatures to minimize volume average cook-value and the heat penetration parameter, f_h, for infinite slab and finite cylinder conduction heating foods. However, the range of values simulated for f_h was narrow. Furthermore, when the average cook-value is used as objective function, the influence of the reference D-value for the quality attribute kinetics on optimal conditions was disregarded (Silva *et al.* 1992a).

With the exception of Ohlsson (1980a,b,c) and Banga *et al.* (1991), few authors compared average and surface quality optimum conditions. Ohlsson (1980a,b) stated that for infinite slab and finite cylinder geometries optimum temperatures for minimum average cook-value were approximately 7.5–10C and

2.5C above the ones for minimum surface quality degradation, respectively. However, the range of cases studies carried out was very limited and as referred above the objective function used to maximize the average quality retention was not the most suitable (Silva *et al.* 1992a). Banga *et al.* (1991) studied the influence of optimum variable retort temperature profile on average quality and concluded that this policy does not offer significant advantages over constant retort temperature. On the contrary, when an optimized variable retort temperature is applied the surface quality can be significantly improved.

Therefore, the main objectives of this work were (1) the development of a relationship between optimal constant temperatures to maximize average quality retention and all the influential variables (2) to study the effect of the sterilization conditions on the final product quality, and (3) a comparative study between average and surface quality optimal constant temperatures for equal relevant variables.

MATERIALS AND METHODS

Optimal sterilization temperatures to minimize average quality degradation of conduction heating foods were calculated as a function of all relevant variables. A calculation approach similar to the one presented by Silva *et al.* (1992b) was applied.

A first order inactivation kinetics (both for microorganisms and quality factors) was assumed, and described with a decimal reduction time (D_{ref}) and a z-value. The z-value for thermal death of microorganisms (z_m) was set equal to 10C (Pflug and Odlaug 1978) and optimal conditions were determined for a range of D_{refq} and z_q values, including all the available data for quality attribute kinetics of thermal destruction (Lund 1975, 1977) (Table 1).

An explicit finite-difference numerical method, with a noncapacitance surface node (Chau and Gaffney 1990), was used to simulate the heat transfer into the food. One-dimensional geometries only were considered, i.e., infinite slab, infinite cylinder and sphere. A constant and uniform overall heat transfer coefficient at the product surface accounted for the packaging material and heating medium thermal resistance. The food was assumed as homogeneous, isotropic and with uniform initial temperature (T_o). The heating medium time-temperature profile was a step function with a cooling temperature of 20C. The initial product temperature and heating medium come-up-time were set equal to 10C and zero, respectively, since these parameters are not expected to affect optimal temperatures (Silva *et al.* 1992a).

The optimization procedure used a target F_o-value (F_t) at the slowest product heating point as a *constraint*

$$F_o = \int_0^t 10^{(T_c - T_{refm})/z_m} dt \qquad (1)$$

TABLE 1.
RANGE OF VARIABLE VALUES USED TO CALCULATE OPTIMAL STERILIZATION TEMPERATURES

Variable	minimum value	maximum value
D_{refq} (min)	5	905
z_q (C)	15	45
RF (s^{-1})	2.844×10^{-5}	6.400×10^{-3}
f_h (min) *sphere*	0.608	596.3
inf. *cyl.*	1.036	527.6
inf. *slab*	2.430	1163.8
Bi	0.9	∞
F_t (min)	3	15

and the *objective function* was the volume average quality retention,

$$(N / No)_{ave} = \frac{1}{V} \int_0^V 10^{-\frac{1}{D_{refq}} \int_0^{t'} 10^{(T - T_{refq}) / z_q} dt} dV' \qquad (2)$$

This is the most adequate function when the average quality is to be maximized (Silva *et al.* 1992a).

The range of influential variable values used to determine optimal conditions included a wide range of practical sterilization processes (Silva *et al.* 1992b) (Table 1). Case studies for which optimum holding temperature (*design variable*) was over 160C, or final average retention was less than 10%, were considered out of practical interest.

Considering an infinite surface heat transfer coefficient, the effect of the D_{ref}-value for the quality factor on optimal conditions was studied; 7680 optimization case-studies were calculated, resultant from the combination of 3 geometries, 5 values for F_t, 8 values for **RF**, 4 values for z_q, and 16 values for D_{refq}. To study the influence of surface resistance to heat transfer, a second

database of 6048 case studies (7 D_{refq}, 3 F_t, 4 **RF**, 4 z_q, 6 Bi and 3 geometries) was generated. The selection of the different number of levels for each of the relevant variables was based on previous authors' experience (Hendrickx *et al.* 1990, 1993; Silva *et al.* 1992b). Biot numbers higher than 0.9 only were used, because at lower values the optimal temperature tends to infinity.

Optimal holding temperatures to maximize surface quality were also calculated using generalized regression equations presented by Hendrickx *et al.* (1993) and Silva *et al.* (1992b) (Table 2).

TABLE 2.
GENERALIZED (SEMI)-EMPIRICAL EQUATIONS OF OPTIMAL STERILIZATION TEMPERATURES, *TO MAXIMIZE SURFACE QUALITY*, AS A FUNCTION OF RELEVANT VARIABLES

Equation No.

Infinite surface heat transfer coefficient

$$T_{op} = 86.68 + 9.73 * \log(F_t/f_h) + 10.46 * \ln(z_q) + 0.025 * T_o \quad (1)$$

Finite surface heat transfer coefficient

$$T_{op} = \mathbf{a} + \mathbf{b} * \log(F_t/f_h) + \mathbf{c} * \ln(z_q) + \mathbf{d}/Bi + \mathbf{e} * z_q/Bi$$

Geometry	a	b	c	d	e	
Inf. slab	91.37	9.71	9.32	-6.58	1.15	2
Inf. cyl.	90.96	9.83	9.34	-4.73	1.20	3
Sphere	90.79	9.72	9.30	-3.72	1.24	4

All geometries, finite surface heat transfer coefficient

$$T_{op} = 124.18 + 9.70 * \log(F_t * \mathbf{RF}) + 9.57 * \ln(z_q) - 9.22 / Bi + 1.15 * z_q/Bi - 8.61 * 2^{(V/A_M)} \quad (5)$$

RESULTS AND DISCUSSION

Effect of D_{refq}-Value

Typical results for the dependence of optimal temperature for volume average quality on D_{refq}-value are illustrated in Fig. 1 and 2. For D_{refq}-values smaller than approximately 300 min, $(T_{op})^{ave}$ is very sensitive to small variations of this parameter (Fig. 1). This range of degradation rates corresponds to texture and color kinetics, which are not so resistant to thermal treatment (Lund 1975, 1977). For this type of products the sterilization must be processed at higher temperatures and shorter processing times. This effect depends on geometry, being minimal for spheres and maximal for infinite slab containers (Fig. 2). The heat transfer into an infinite slab package is slower, therefore to minimize the volume average quality degradation in this type of containers the sterilization must be accelerated. Furthermore, the volume integrated quality retention approaches more the quality at the surface for a spherical geometry. For D_{refq}-values larger than 300 min (e.g., vitamins), the optimum holding temperature is not affected by this variable.

The dependence of optimal temperature on D_{refq} can be expressed by a linear relation between $(T_{op})^{ave}$ and $1/D_{refq}^2$. The parameters of this relation are a function of the F_t-value (Fig. 1), Reduced Fourier number (**RF**) or heat penetration parameter (f_h), z_q-value and geometry (Fig. 2). Optimal temperature is higher and more sensitive to the D_{refq}-value for sterilizations with long processing times (i.e., process with larger F_t-value and heat penetration parameter f_h or for infinite slab containers).

Effect of Product Heating Rate, z_q-Value and F_t-Value

The influence of **RF** or f_h, F_t-value and z_q-value on optimum processing temperature, to minimize volume average quality degradation for constant D_{refq}-value, can be concluded from Fig. 3, 4 and 5.

If the heating rate is not too slow, optimum holding temperature decreases with increasing heat penetration parameter f_h. Products with low thermal diffusivity or large heat transfer length must be processed with smoother conditions. However, when the heating rate is very small (e.g., big containers) optimum temperature increases because an increase of the surface quality thermal degradation guarantees an higher volume average quality retention. This effect is more evident when the quality attribute kinetics is less sensitive to temperature variations (i.e., higher z_q-values) (Fig. 3).

For low values of the heat penetration parameter f_h (or large values of **RF**) optimal temperature to maximize average retention is log-linear with f_h or **RF**, where for slow heating rate foods (large f_h or small **RF**) an inversion is observed and optimum tends to increase (Fig. 3). This effect is more important

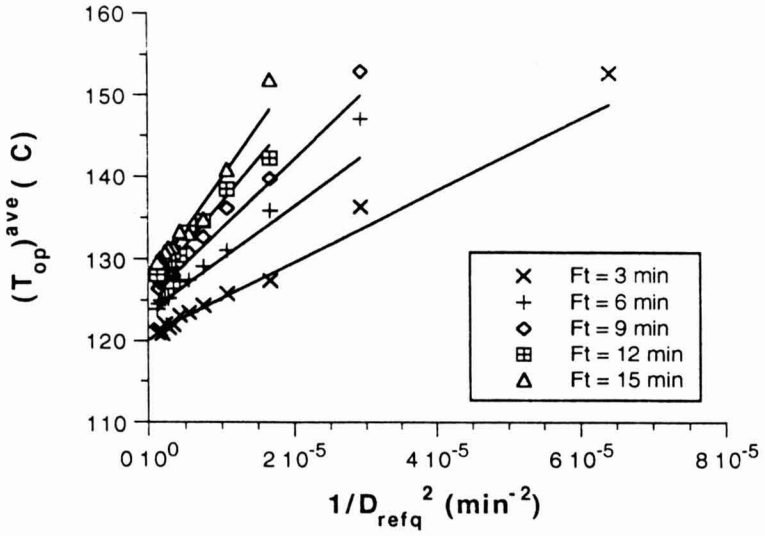

FIG. 1. OPTIMAL PROCESSING TEMPERATURE TO MAXIMIZE AVERAGE QUALITY RETENTION, FOR AN INFINITE SLAB PRODUCT, AS A FUNCTION OF D_{refq}-VALUE FOR z_q = 35C, **RF** = 6.17E − 5 s^{-1} AND Bi = ∞
Lines represent results predicted by regression equations in Table 3.

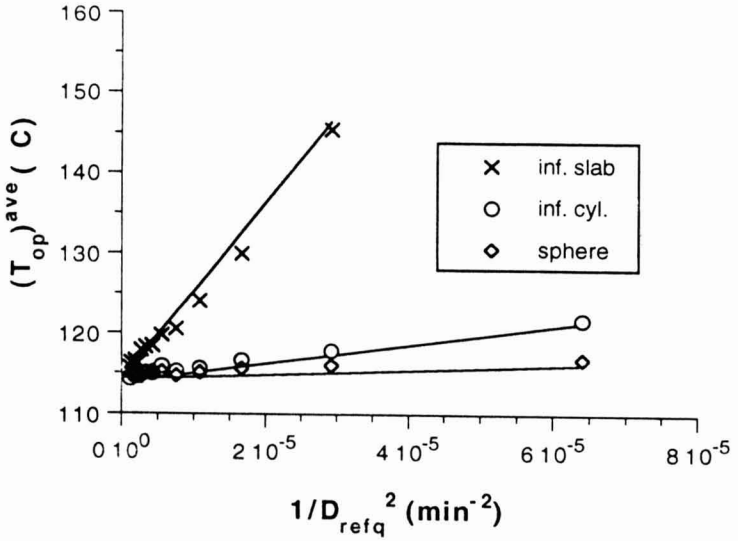

FIG. 2. OPTIMAL PROCESSING TEMPERATURE TO MAXIMIZE AVERAGE QUALITY RETENTION, AS A FUNCTION OF D_{refq}-VALUE FOR F_t = 9 MIN, z_q = 25C AND **RF** = 2.84E − 5 s^{-1} AND Bi = ∞
Continuous lines represent results predicted by regression equations in Table 3.

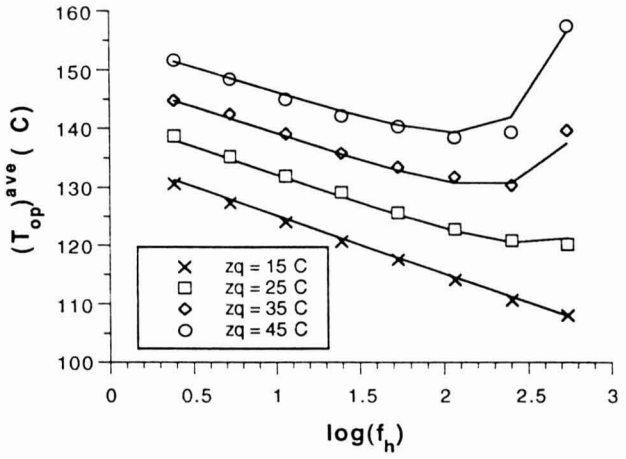

FIG. 3. OPTIMAL PROCESSING TEMPERATURE TO MAXIMIZE AVERAGE QUALITY RETENTION, FOR AN INFINITE SLAB PRODUCT, AS A FUNCTION OF f_h FOR D_{refq} = 485 MIN, F_t = 12 MIN AND Bi = ∞
Continuous lines represent results predicted by regression equations in Table 3.

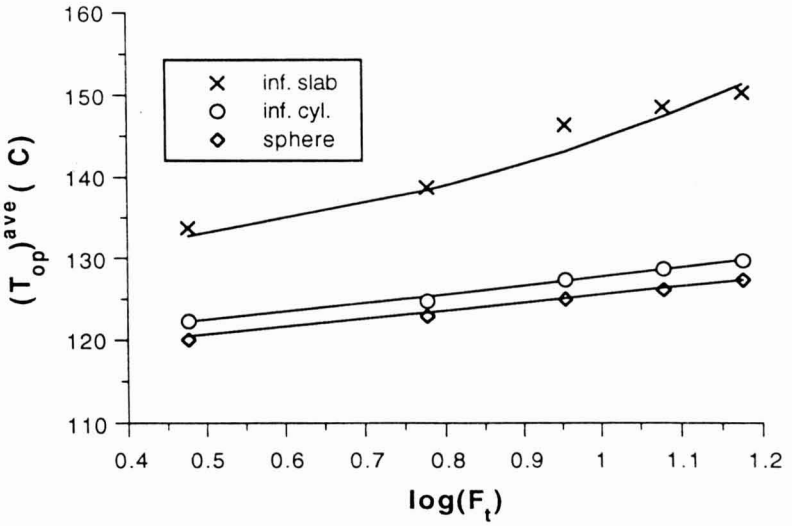

FIG. 4. OPTIMAL PROCESSING TEMPERATURE TO MAXIMIZE AVERAGE QUALITY RETENTION AS A FUNCTION OF F_t-VALUE FOR D_{refq} = 605 MIN, z_q = 45C, **RF** = 2.84E − 5 s^{-1} AND Bi = ∞
Continuous lines represent results predicted by regression equations in Table 3.

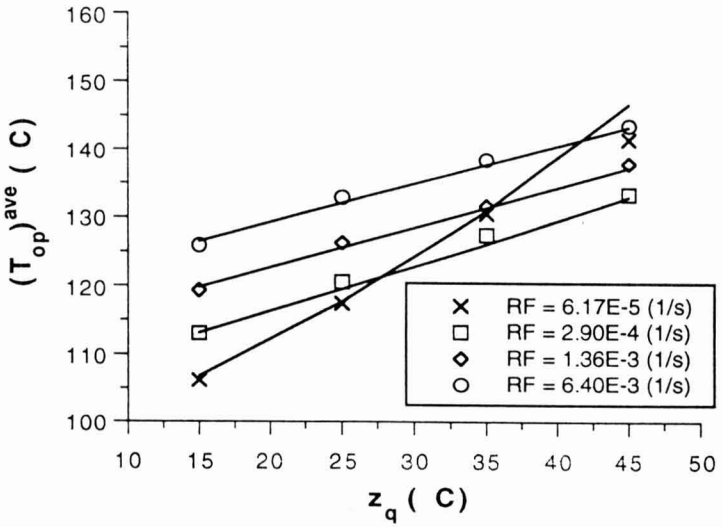

FIG. 5. OPTIMAL PROCESSING TEMPERATURE TO MAXIMIZE AVERAGE QUALITY RETENTION, FOR AN INFINITE CYLINDER PRODUCT, AS A FUNCTION OF z_q-VALUE FOR D_{refq} = 65 MIN, F_t = 3 MIN AND Bi = ∞
Continuous lines represent results predicted by regression equations in Table 3.

for larger z_q-values, and infinite slab geometries. A log-linear relation had already been observed between optimum temperature to minimize surface quality degradation, although for the whole range of f_h values (Hendrickx *et al.* 1990, 1993; Silva *et al.* 1992b).

Optimum temperatures to minimize average quality degradation increase with increasing target F_o-value (Fig. 4). For some conditions this relation is linear, but this may not be taken as a general rule. For instance, in the case of an infinite slab, optimal temperature is more sensitive to increases in the target F_o-value for products that require an high F_t-value.

Higher z_q-values correspond to higher $(T_{op})^{ave}$ temperatures (Fig. 5). This should be expected, since a higher z_q-value represents a more thermal-resistant quality factor. It can be noticed once more that the product heat transfer rate has an important role: for low **RF** values (slow heating rate) the influence of z_q on optimal temperatures is very significant (Fig. 5).

It can be observed that the total processing time (t′), corresponding to the optimum holding temperature, when the resistance to heat transfer at the surface is neglectable is insensitive to the F_t-value (Fig. 6). This is an important rule of thumb, already reported for optimum surface quality conditions (Silva *et al.* 1992b). This means that if an optimized process for a given product with a given F_t is known, the optimal process for another F_t requirement will have the same processing time. The optimal processing temperature for this case can then be easily obtained. Furthermore, as it should be expected, optimum total

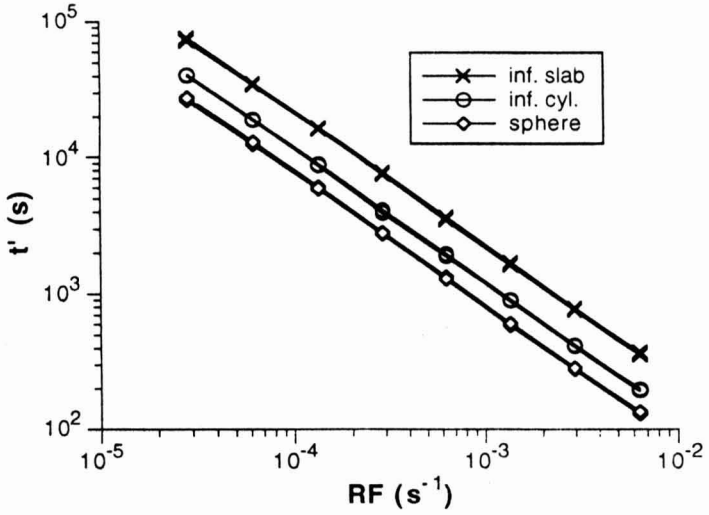

FIG. 6. OPTIMAL TOTAL PROCESSING TIME AS A FUNCTION OF **RF** FOR TARGET F_o-VALUE = 3, 6, 9, 12 AND 15 MIN, D_{refq} = 905 MIN, z_q = 15C AND Bi = ∞

processing time (t') decreases for faster heating foods containers [i.e., higher Reduced Fourier number (**RF**) and spherical products].

It is also very important to note that average quality retention does not change linearly with optimum temperature. This implies that for some conditions there is a wide range of temperatures that can produce quite acceptable products, while for others, meeting the optimum temperature is very important. Particularly average quality retention decreases or increases with the z_q-value depending on the value of the Reduced Fourier number (**RF**) (Fig. 7). When the heating rate is high (large **RF** value) optimum temperatures are high (Fig. 3) and the retention increases with the z-value for the quality attribute. On the contrary, if the product heats very slowly, optimal temperature increases if the z_q-value is large, but the average quality retention decreases.

Effect of Surface Resistance to Heat Transfer

It was concluded that optimal average quality temperatures decrease for smaller surface heat transfer resistance (large Biot numbers) conditions (Fig. 8). Small Bi numbers imply slower heat transfer rate to the least-lethality point and the sterilization must be accelerated using higher temperatures. A linear relation was observed for $(T_{op})^{ave}$ as a function of $c_1/Bi+c_2*z_q/Bi$, where c_1 and c_2 are constants dependent on the geometry. This type of relation had also been detected for optimal temperature to maximize surface quality (Silva *et al.* 1992a) (Table 2).

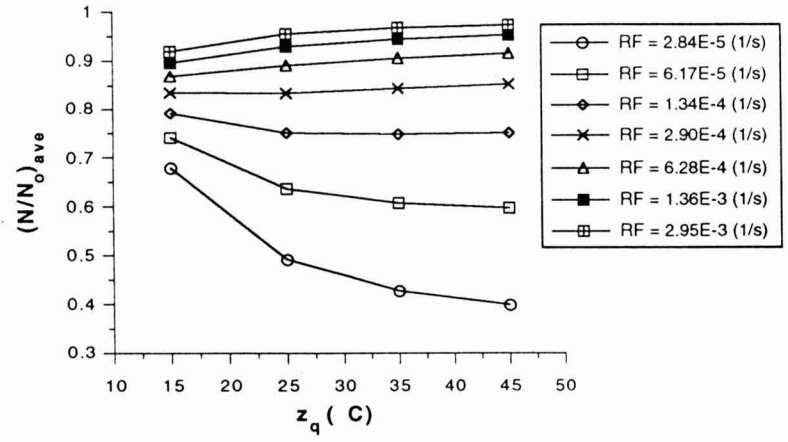

FIG. 7. AVERAGE QUALITY RETENTION, FOR A SPHERICAL PRODUCT, AS A FUNCTION OF z_q-VALUE FOR D_{refq} = 305 MIN, F_t = 15 MIN AND Bi = ∞

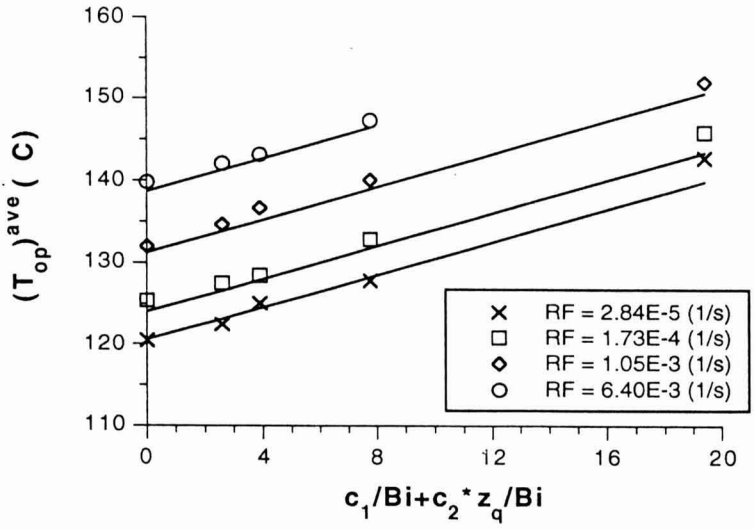

FIG. 8. OPTIMAL PROCESSING TEMPERATURE TO MAXIMIZE AVERAGE QUALITY RETENTION, FOR AN INFINITE SLAB PRODUCT, AS A FUNCTION OF $c_1/Bi+c_2*z_q/Bi$ (c_1 AND c_2 ARE CONSTANTS) FOR D_{refq} = 605 MIN, F_t = 15 MIN AND z_q = 25C
Continuous lines represent results predicted by regression equations in Table 3.

Optimum average quality retention is insensitive to the surface Biot number (Fig. 9). Therefore, although different surface resistances to heat transfer lead to different optimal temperature, working at optimal conditions allows the same optimum average retention. This means that a conduction heating food packed in metal or plastic containers, sterilized in static or agitated retorts operated by steam or pressurized water do not have different volume average quality retention, if processed at optimal conditions. This has obviously implications in terms of costs. However, plastic containers, agitated and pressurized water retorts may offer significant advantages in terms of the final uniformity in quality retention distribution. These statements need experimental verification.

A Systematic Approach

For each geometry, it was possible to express the influence of all the variables (D_{refq}, f_h or **RF**, F_t, z_q and Bi) on $(T_{op})^{ave}$ as a multilinear relationship (STATA, 1990). Multiple linear regressions were performed (Table 3), using the heat penetration parameter (f_h) or the Reduced Fourier number (**RF**) and considering separately infinite and finite surface heat transfer coefficients. Continuous lines in Fig. 1, 2, 3, 4, 5 and 8 were calculated using the formulae presented in Table 3. Using these expressions for $(T_{op})^{ave}$, a formula method may then be used to evaluate the corresponding processing time.

Silva *et al.* (1992a) introducing the ratio: $V/(A^*l)$ were able to develop a regression equation for $(T_{op})^{surf}$ valid for the three one-dimensional geometries.

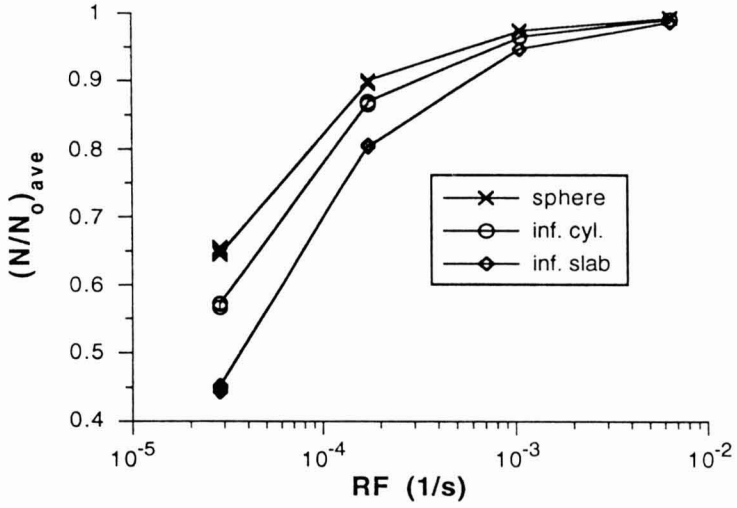

FIG. 9. AVERAGE QUALITY RETENTION AS A FUNCTION OF **RF** FOR Bi = 0.9 , 2, 5, 10, 15 AND ∞, D_{refq} = 455 MIN, F_t = 3 MIN AND z_q = 45C

TABLE 3.
GENERALIZED (SEMI)-EMPIRICAL EQUATIONS OF OPTIMAL STERILIZATION TEMPERATURES, *TO MAXIMIZE AVERAGE QUALITY*, AS A FUNCTION OF RELEVANT VARIABLES

$$T_{op} = \mathbf{a} + \mathbf{b} \cdot z_q + \log(F_t/f_h) \cdot (\mathbf{c} + \mathbf{d} \cdot z_q) + 1/D_{refq}^2 \cdot [\mathbf{e} \cdot F_t^2 + f_h^{3/2} \cdot (\mathbf{f} + \mathbf{h} \cdot F_t + z_q^2 \cdot (\mathbf{g} + \mathbf{i} \cdot F_t))] + \mathbf{j} / Bi + \mathbf{k} \cdot z_q/Bi$$

T_{op} (C), z_q (C), F_t (min), f_h (min), D_{refq} (min)

Geometry		a	b	c	d	e	f	g	h	i	j	k	corr. coef.
Inf. slab	h_∞	113.9	0.701	10.75	-0.047	45.02	-16.21	0.061	-3.10	0.016			0.992
	h_{finite}	113.9	0.707	10.82	-0.061	38.87	-10.18	0.029	-2.00	0.010	-7.47	1.98	0.987
Inf. cyl.	h_∞	113.4	0.571	10.38	-0.024	0.730	-6.04	0.031	-0.799	0.005			0.993
	h_{finite}	113.8	0.552	10.40	-0.027	0.809	-5.22	0.019	-1.03	0.004	-7.74	1.87	0.993
Sphere	h_∞	112.9	0.515	10.20	-0.015	0.273	-2.74	0.019	-0.156	0.002			0.996
	h_{finite}	113.4	0.478	9.97	-0.011	0.335	-1.91	0.011	-0.239	0.002	-9.41	1.94	0.993

$$T_{op} = \mathbf{a} + \mathbf{b} \cdot z_q + \log(F_t \cdot \mathbf{RF}) \cdot (\mathbf{c} + \mathbf{d} \cdot z_q) + 1/D_{refq}^2 \cdot [\mathbf{e} \cdot F_t^2 + (1/\mathbf{RF})^{3/2} \cdot (\mathbf{f} + \mathbf{h} \cdot F_t + z_q^2 \cdot (\mathbf{g} + \mathbf{i} \cdot F_t))] + \mathbf{j} / Bi + \mathbf{k} \cdot z_q/Bi$$

T_{op} (C), z_q (C), F_t (min), **RF** (s^{-1}), D_{refq} (min)

Geometry		a	b	c	d	e	f	g	h	i	j	k	corr. coef.
Inf. slab	h_∞	133.3	0.617	10.75	-0.047	45.02	-0.031	1.18E-3	-0.006	3.16E-5			0.992
	h_{finite}	132.6	0.628	10.37	-0.034	36.52	-0.042	1.30E-4	-0.005	2.94E-5	-17.35	2.25	0.993
Inf. cyl.	h_∞	136.0	0.518	10.38	-0.024	0.730	-0.003	1.68E-5	-4.32E-4	2.58E-6			0.993
	h_{finite}	136.5	0.484	10.47	-0.027	0.742	-0.003	1.80E-5	-1.61E-4	2.26E-6	-16.56	2.00	0.994
Sphere	h_∞	137.5	0.478	10.20	-0.015	0.273	-6.64E-4	4.50E-6	-3.78E-4	5.01E-7			0.996
	h_{finite}	137.1	0.457	9.97	-0.011	0.296	0.001	2.53E-6	-7.34E-4	6.81E-7	-14.78	1.92	0.992

The same approach was tried, and two equations (in terms of f_h or **RF**) were obtained:

$$(T_{op})^{ave} = \mathbf{a} + z_q * (\mathbf{b} + \mathbf{c} * V/(A.l)) + \log(F_t/f_h) * (\mathbf{d} + \mathbf{e} * V/(A.l) + \mathbf{f} * z_q) + 1/D_{refq}^2 * [F_t^2 * (\mathbf{g} + \mathbf{h} * V/(A.l)) + f_h^{3/2} * (\mathbf{i} + \mathbf{j} * z_q^2 + F_t * (\mathbf{k} + \mathbf{l} * V/(A.l) + z_q^2 * (\mathbf{m} + \mathbf{n} * V/(A.l))))] + \mathbf{o} / Bi + \mathbf{p} * z_q/Bi$$

$$(T_{op})^{ave} (C); z_q (C); F_t (min); f_h (min); D_{refq} (min) \quad (3)$$

and

$$(T_{op})^{ave} = \mathbf{a} + z_q * (\mathbf{b} + \mathbf{c} * V/(A.l)) + \log(F_t * \mathbf{RF}) * (\mathbf{d} + \mathbf{e} * V/(A.l) + \mathbf{f} * z_q) + 1/D_{refq}^2 * [F_t^2 * (\mathbf{g} + \mathbf{h} * V/(A.l)) + (1/\mathbf{RF})^{3/2} * (\mathbf{i} + \mathbf{j} * z_q^2 + F_t * (\mathbf{k} + \mathbf{l} * V/(A.l) + z_q^2 * (\mathbf{m} + \mathbf{n} * V/(A.l))))] + \mathbf{o} / Bi + \mathbf{p} * z_q/Bi$$

$$(T_{op})^{ave} (C); z_q (C); F_t (min); \mathbf{RF} (s^{-1}); D_{refq} (min) \quad (4)$$

where the values for the constants are shown in Table 4.

Equations (3) and (4) and equations in Table 3 allow calculation of optimal temperatures without the need of computer modelling. However, the user must be aware of the assumptions used in its development in order to avoid misuse. Equations (3) and (4) may be applicable to any finite geometry, however validation is required (Silva *et al.* 1994).

Comparative Study Between Average and Surface Quality

In order to compare optimal conditions for maximum volume average quality with the corresponding for maximum surface quality, plots of $(T_{op})^{ave} - (T_{op})^{surf}$ as a function of D_{refq}, f_h, F_t, z_q and Bi (Fig. 10, 11 12, 13 and 14) were generated. Average quality optimal temperatures are always higher than optimal temperatures for surface quality, but this difference depends on the values of all the influential variables. Ohlsson (1980a,b) stated that this difference for an infinite slab product was from 7.5 to 10C and 2.5C for a finite cylinder container. However, the case-studies carried out in their work did not include all the range of practical interest. Furthermore, the objective function was not adequate and the influence of the D_{refq}-value on $(T_{op})^{ave}$ was not considered (Silva *et al.* 1992a). To maximize quality in terms of volume average quality, the sterilization conditions must be more rigorous in order to accelerate the heat transfer into the product and decrease the difference of lag heating times through the whole container.

TABLE 4.
VALUES FOR THE CONSTANTS IN EQ. (3) AND (4)

Equation	a	b	c	d	e	f	g	h	i	j	k	l	m	n	o	p	corr. coef.
3	113.8	0.343	0.389	10.85	-0.725	-0.032	-1.52	5.22	-3.03	0.015	1.05	-3.86	-0.0044	0.017	-9.10	1.94	0.988
4	135.9	0.359	0.234	10.11	0.715	-0.040	-0.018	1.60	0.0024	5.93e-6	0.0027	-0.0074	-1.22E-5	3.41E-5	-14.35	1.95	0.980

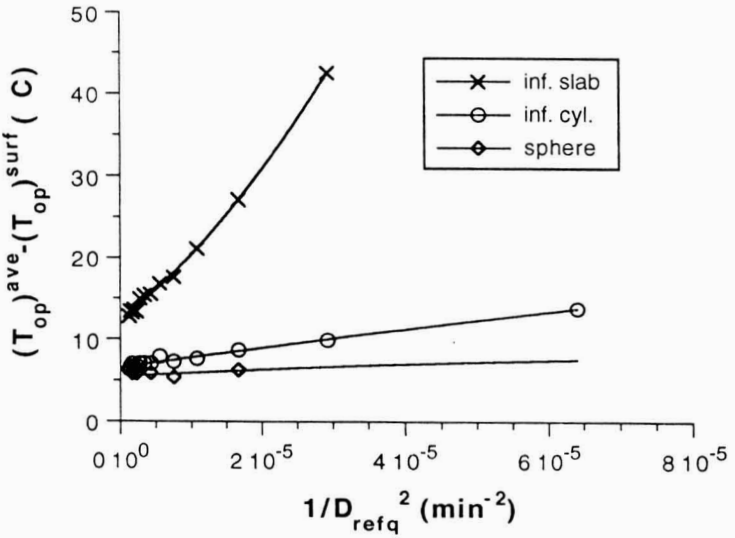

FIG. 10. DIFFERENCE BETWEEN $(T_{op})^{ave}$ AND $(T_{op})^{surf}$, AS A FUNCTION OF D_{refq}-VALUE FOR F_t = 9 MIN, z_q = 25C AND **RF** = 2.84E−5 s^{-1} AND Bi = ∞

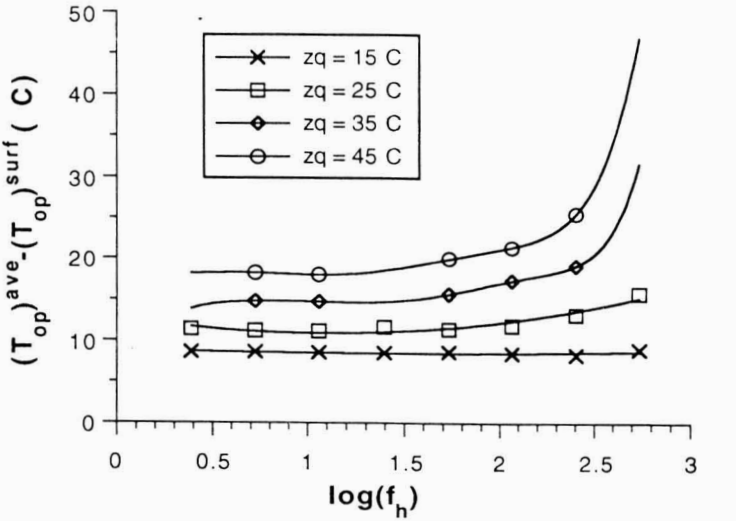

FIG. 11. DIFFERENCE BETWEEN $(T_{op})^{ave}$ AND $(T_{op})^{surf}$, FOR AN INFINITE SLAB PRODUCT, AS A FUNCTION OF f_h FOR D_{refq} = 485 MIN, F_t = 12 MIN AND Bi = ∞

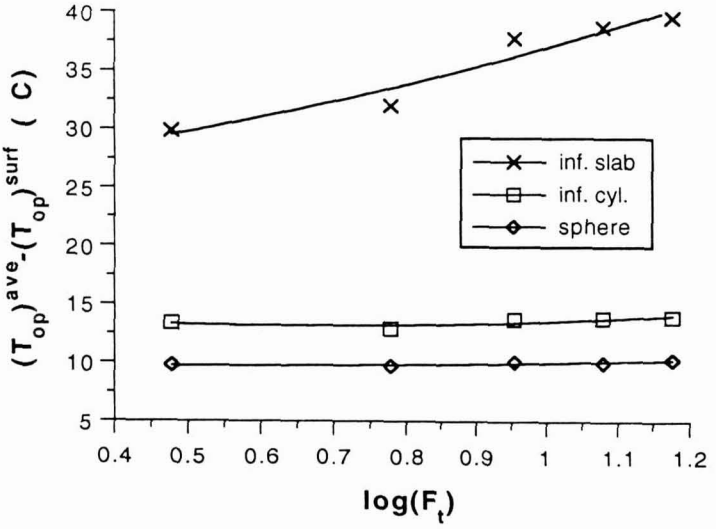

FIG. 12. DIFFERENCE BETWEEN $(T_{op})^{ave}$ AND $(T_{op})^{surf}$, AS A FUNCTION OF F_t-VALUE FOR D_{refq} = 605 MIN, z_q = 45C, **RF** = 2.84E−5 s^{-1} AND Bi = ∞

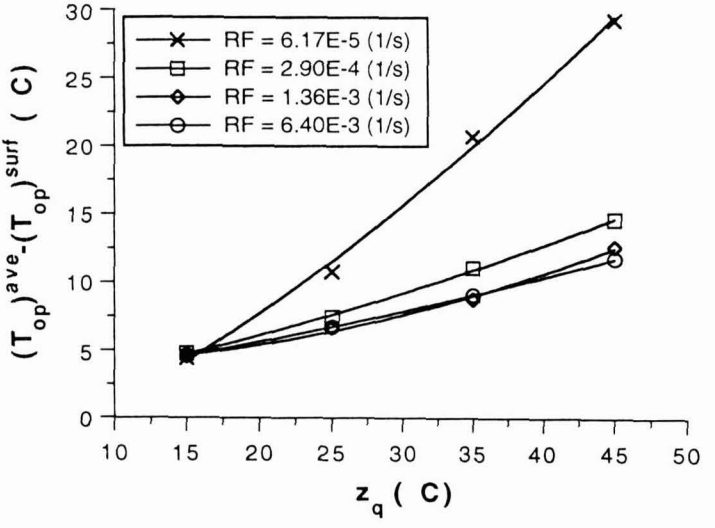

FIG. 13. DIFFERENCE BETWEEN $(T_{op})^{ave}$ AND $(T_{op})^{surf}$, FOR AN INFINITE CYLINDER PRODUCT, AS A FUNCTION OF z_q-VALUE FOR D_{refq} = 65 MIN, F_t = 3 MIN AND Bi = ∞

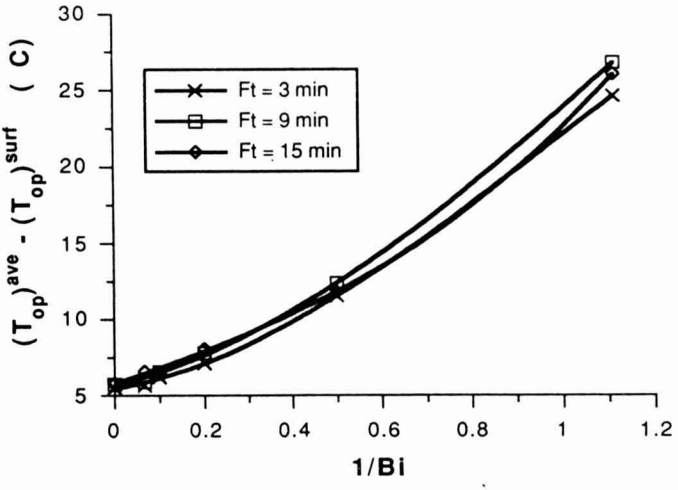

FIG. 14. DIFFERENCE BETWEEN $(T_{op})^{ave}$ AND $(T_{op})^{surf}$, FOR AN INFINITE SLAB PRODUCT, AS A FUNCTION OF Bi for D_{refq} = 605 MIN, F_t = 15 MIN AND z_q = 25C

$(T_{op})^{ave} - (T_{op})^{surf}$ decreases with the D_{refq}-value (Fig. 10) and Biot number (Fig. 14), and increases with the heat penetration parameter f_h (Fig. 11), z_q-value (Fig. 11 and 13), and F_t-value (Fig. 12). The geometry is also a parameter to consider, the difference between optimal temperatures increases from a spherical to an infinite slab shape container (Fig. 10 and 12). The selection of the optimum sterilization temperature to minimize volume average quality degradation is more important for food products that heat up slowly (this means products with low thermal diffusivities, large containers and heating medium conditions were the heat transfer coefficient is finite), which need to be sterilized more intensively (larger F_t-value), and with high rates of quality factor thermal degradation. These case studies are also the ones for which bigger differences between $(T_{op})^{ave}$ and $(T_{op})^{surf}$ are observed and where the optimum final retention is low.

Optimum surface quality temperatures are a linear function of: $\log(F_t/f_h)$ or $\log(F_t*\mathbf{RF})$, $\ln(z_q)$, 1/Bi, z_q/Bi and $2^{(V/(A.l))}$ (Table 2), and do not depend on the D_{refq}-value (Silva *et al.* 1992a). These linear relationships are not observed for optimum average quality temperatures [Table 3, Eq. (3) and (4)].

The conclusions that have been drawn are based on the assumption that the volume average or surface quality retentions to be optimized are for quality factors having the same degradation kinetics. However, this assumption may not be always true. The degradation rate of quality factors normally optimized at the surface (e.g., color) is usually faster than the kinetics for quality factors optimized in volume average terms (e.g., vitamins). A further extended study is needed to conclude about the validity of the above results for such a situation.

CONCLUSIONS

The influence of D_{refq}, z_q, f_h or **RF**, F_t and Bi on optimal conditions to maximize average quality retention was analyzed. A general relationship between optimal temperatures and all the relevant parameters was developed. The applicability of these formulae to two or three-dimensional food geometries has to be assessed.

Optimal temperatures to minimize surface quality degradation were compared with the corresponding ones for average quality. The selection of the optimum sterilization temperature to minimize volume average quality degradation is more important for foods that heat up slowly, need to be sterilized more intensively and with high rate of thermal degradation for the quality factor. In these situations differences between optimal temperature to maximize volume average quality and holding temperature to maximize surface quality are also more significant, and quality retention is low.

There is a need to study how optimal conditions for average quality affect surface quality and vice-versa. A new objective function might be considered.

NOMENCLATURE

A	Area (m^2)
Bi	Biot number (= h*l/k) (dimensionless)
dV′	Volume element (m^3)
D	Decimal reduction time (time required for the number or concentration of spores, microorganisms or quality factor to be reduced by a factor of 10 at a given temperature) (min)
D_{ref}	Decimal reduction time at the reference temperature (min)
D_{refq}	Decimal reduction time at the reference temperature, T_{refq}, for the nutrient or quality factor (min)
f_h	Heat penetration parameter—slope factor of a heating curve (time required for the difference between heating medium temperature and food temperature to decrease by a factor of 10) (min)
F_o	Sterility value at reference temperature 121.15C and z_m = 10C (equivalent exposure time at reference temperature received by the slowest-heating zone in the container with regard to the destruction of a microorganism whose thermal resistance is characterized by z_m = 10C) (min)
F_t	Target sterilizing value at reference temperature 121.15C and z_m = 10C (min)
h	Surface heat transfer coefficient ($W/(m^2K)$)
h_{finite}	Finite surface heat transfer coefficient ($W/(m^2K)$)
$h\infty$	Infinite surface heat transfer coefficient ($W/(m^2K)$)
k	Thermal conductivity (W/(m K))

l	Characteristic length (radius of an infinite cylinder or a sphere and half thickness of an infinite slab) (m)
N	Level of nutrients or quality factor at time t
N_o	Initial level of nutrients or quality factor
$(N/N_o)_{ave}$	Volume average quality retention
RF	Reduced Fourier number ($= \alpha/l^2$) (s^{-1})
t	Time (s)
t'	Total processing time (s)
T	Temperature (C)
T_c	Temperature in the least-lethality spot (C)
T_o	Initial temperature of the food (C)
T_{op}	Optimum processing temperature (C)
$(T_{op})^{ave}$	Optimum processing temperature to maximize volume average quality retention (C)
$(T_{op})^{surf}$	Optimum processing temperature to maximize surface quality retention (C)
T_{ref}	Reference temperature (C)
T_{refm}	Reference temperature for the microorganism (121.1 C)
T_{refq}	Reference temperature for the quality factor (121.1 C)
V	Volume (m^3)
z	z-Value (number of degrees Celsius required to reduce the D-value by a factor of ten) (C)
z_m	z-Value for the microorganism (C)
z_q	z-Value for the nutrient or quality factor (C)
α	Thermal diffusivity (m^2/s)

ACKNOWLEDGMENTS

Authors C.L.M. Silva, F.A.R. Oliveira and P.A.M. Pereira acknowledge JNICT (Junta Nacional de Investigação Científica e Tecnológica).

REFERENCES

BANGA, J.R., PEREZ-MARTIN, R.I., GALLARDO, J.M. and CASARES, J.J. 1991. Optimization of the thermal processing of conduction-heated canned foods: study of several objective functions. J. Food Eng. *14*, 25–51.

BARREIRO, J.A., PEREZ, C.R. and GUARIGUATA, C. 1984. Optimization of energy consumption during the heat processing of canned foods. J. Food Eng. *3*, 27–37.

CHAU, K.V. and GAFFNEY, J.J. 1990. A finite-difference model for heat and mass transfer in products with internal heat generation and transpiration. J. Food Sci. *55*, 484–487.

HENDRICKX, M., SILVA, C., OLIVEIRA, F. and TOBBACK, P. 1992a. Optimization of heat transfer in thermal processing of conduction heated foods. In *Advances in Food Engineering*, (R.P. Singh and M.A. Wirakartakusumah, eds.) pp. 221–235, CRC Press, London.

HENDRICKX, M., SILVA, C., OLIVEIRA, F. and TOBBACK, P. 1992b. Optimizing thermal processes of conduction heated foods: generalized equations for optimal processing temperatures. In *Food Engineering in a Computer Climate*, St John's College, Cambridge, Mar. 30–Apr. 1, pp. 271–276.

HENDRICKX, M., SILVA, C., OLIVEIRA, F. and TOBBACK, P. 1993. Generalized (semi)-empirical formulas for optimal sterilization temperatures of conduction heated foods with infinite surface heat transfer coefficients. J. Food Eng. *19*, 141–158.

HENDRICKX, M., VAN GENECHTEN, K. and TOBBACK, P. 1990. Optimizing quality attributes of conduction heated foods, a simulation approach. In *Engineering and Food: Preservation Processes and Related Techniques*, Vol. 2, (W.E.L. Spiess and H. Shubert, eds.) pp. 167–176. Elsevier Applied Science, London.

HOLDSWORTH, S.D. 1985. Optimisation of thermal processing — a review. J. Food Eng. *4*, 89–116.

LUND, D.B. 1975. Effects of blanching, pasteurization and sterilization on nutrients. In *Nutritional Evaluation of Food Processing*, (R.S. Harris and E. Karmas, eds.) pp. 205–240, Van Nostrand Reinhold/AVI, New York.

LUND, D.B. 1977. Design of thermal processes for maximizing nutrient retention. Food Technol. *2*, 71–78

LUND, D.B. 1982. Applications of optimization in heat processing. Food Technol. *2*, 97–100.

MARTENS, T. 1980. Mathematical Model of Heat Processing in Flat Containers. Ph.D thesis, Katholieke Universiteit Leuven, Belgium.

NADKARNI, M.M. and HATTON, T.A. 1985. Optimal nutrient retention during the thermal processing of conduction-heated canned foods: application of the distributed minimum principle. J. Food Sci *50*, 1312–1321.

OHLSSON, T. 1980a. Optimal sterilization temperatures for flat containers. J. Food Sci. *45*, 848-852.

OHLSSON, T. 1980b. Optimal sterilization temperatures for sensory quality in cylindrical containers J. Food Sci. *45*, 1517–1521.

OHLSSON, T. 1980c. Optimization of heat sterilization using C-values. In *Food Process Engineering*, pp. 137–145, Applied Science Publishers, U.K.

PFLUG, I.J. and ODLAUG, T.E. 1978. A review of z and F values used to ensure the safety of low-acid canned foods. Food Technol. *6*, 63–70.

RIDGWAY, G. and BRIMELOW, C.J.B. 1990. Optimal food process design and control. Food Control *1*, 4–5.

SAGUY, I. and KAREL, M. 1979. Optimal retort temperature profile in

optimizing thiamin retention in conduction-type heating of canned foods. J. Food Sci. *44*, 1485–1490.

SILVA, C., HENDRICKX, M., OLIVEIRA, F. and TOBBACK, P. 1992a. Critical evaluation of commonly used objective functions to optimize overall quality and nutrient retention of heat preserved foods. J. Food Eng. *17*, 241–258.

SILVA, C.L.M, HENDRICKX, M., OLIVEIRA, F. and TOBBACK, P. 1992b. Optimal sterilization temperatures for conduction heating foods considering finite surface heat transfer coefficients. J Food Sci. *57* (3), 743–748.

SILVA, C.L.M, OLIVEIRA, F.A.R. and HENDRICKX, M. 1993. Modelling optimum processing conditions for the sterilization of prepackaged foods: a review. Food Control *4* (2), 67–78.

SILVA, C.L.M., OLIVEIRA, F.A.R. and HENDRICKX, M. 1994. Quality optimization of conduction heating foods sterilized in different packages. Int. J. Food Sci. Technol. (In Press).

STATA. 1990. *STATA — Reference Manual*, Computing Resource Center, 1640 Fifth Street, Santa Monica, CA 90401.

TEIXEIRA, A.A., DIXON, J.R., ZAHRADNIK, J.W. and ZINSMEISTER, G.E. 1969a. Computer determination of spore survival distributions in thermally-processed conduction-heated foods. Food Technol. *23* (3), 78–80.

TEIXEIRA, A.A., DIXON, J.R., ZAHRADNIK, J.W. and ZINSMEISTER, G.E. 1969b. Computer optimization of nutrient retention in the thermal processing of conduction-heated foods. Food Technol. *23* (6), 137–142.

TEIXEIRA, A.A., ZINSMEISTER, G.E. and ZAHRADNIK, J.W. 1975. Computer simulation of variable retort control and container geometry as a possible means of improving thiamine retention in thermally processed foods. J. Food Sci. *40*, 656–659.

THIJSSEN, H.A.C., KERKHOF, P.J.A.M. and LIEFKENS, A.A.A. 1978. Short-cut method for the calculation of sterilization conditions yielding optimum quality retention for conduction-type heating of packaged foods. J. Food Sci. *43*, 1096–1101.

THIJSSEN, H.A.C. and KOCHEN, L.H.P. 1980. Calculation of optimum sterilization conditions for packed conduction-type foods. J. Food Sci. *45*, 1267–1272.

TUCKER, G. and HOLDSWORTH, D. 1990. Optimisation of quality factors for foods thermally processed in rectangular containers. In *Process Engineering in the Food Industry. 2. Convenience Foods and Quality Assurance*, (R.N Field and J.A. Howell, eds.) pp. 59–74, Elsevier Applied Science, London.

TUCKER, G.S. and HOLDSWORTH, S.D. 1991. Mathematical modelling of sterilization and cooking processes for heat preserved foods — applications of a new heat transfer model. Trans I ChemE *69*, part C, 5–12.

ELECTRODIALYSIS OF WHEY PERMEATES AND RETENTATES OBTAINED BY ULTRAFILTRATION

A. PÉREZ[1], L.J. ANDRÉS, R. ÁLVAREZ and J. COCA[2]

Department of Chemical Engineering
University of Oviedo
33071 Oviedo, Spain

and

C.G. HILL, JR.

Department of Chemical Engineering
University of Wisconsin
Madison, WI 53706

Accepted for Publication August 7, 1993

ABSTRACT

Demineralization of a synthetic UF-whey permeate and a reconstituted UF-whey retentate was studied in a laboratory electrodialysis (ED) unit.

Data on conductivity, ionic concentration, ash removal, electrical efficiency and energy consumption are reported at three temperatures (20, 35 and 45C) and three flow rates (100, 160 and 230 l/h). The extent of deashing is lower for the UF-whey retentate than for the UF-whey permeate as a result of concentration polarization, which results in an increase of the boundary layer thickness, due to deposition of proteins and salts on the membranes.

INTRODUCTION

Whey disposal is a major problem for manufacturers of cheese and casein. Whey contains approximately 50% of the solids present in whole milk, most of the water, soluble vitamins and minerals. Typically, the total solids content of sweet whey is 6 wt%. Of these solids, the major constituents are protein (12 wt%), ash (7 wt%) and lactose (71 wt%) on a dry basis.

[1]Present address:INTEQUI.Universidad de San Luis, Argentina.
[2]To whom correspondence should be addressed.

Journal of Food Process Engineering **17** (1994) 177-190.

The recovery of proteins from whey is usually carried out by ultrafiltration (UF). UF membranes used for whey processing typically retain 95–99% of the protein in the retentate while allowing the lactose and ash to pass through the membrane.

The UF retentate is enriched in the milk protein α-lactalbumin, β-lactoglobulin and immunoglobulin. Most whey protein concentrates (WPC) contain either 35 wt% or 50 wt%/protein. On a dry basis these retentates are characterized by a high level of minerals. In order to use whey as an ingredient in infant formulations, a high level (26–65%) of demineralization is required. Removal of residual salts in the retentate can be accomplished by electrodialysis (ED) or ion exchange. In the WPC 60 and 80%, the mineral content is low and occasionally has to be supplemented with other minerals. Use of ED to demineralize high concentrated WPC can be justified if separation of the individual proteins is intended. The protein concentrates are potentially a high value product, providing that removal of the salts can be achieved (Batchelder 1987; Ryder 1980).

The UF permeate contains approximately 5.7% total solids (TS), of which some 85% is lactose and salts. The permeate cannot be disposed of as such because of its high BOD-value of 25000–40000 mg oxygen per liter. The permeate can be further processed by reverse osmosis (RO) to yield a concentrate rich in lactose and a permeate characterized by a low BOD-value, which can be discharged without further treatment. The RO retentate can be further treated by ED, followed occasionally by ion exchange, to yield a product with a composition (on a dry basis) of 98.5% lactose, 1% protein and 0.5% salts. The latter can be used in dietetic formulations or for various lactose products. Areas of application of lactose include production of pharmaceutical lactose (Booij 1985), fermentation to produce alcohol or lactic acid (Coton 1985), hydrolysis to produce glucose and galactose as sweetening agents (Kosaric and Asher 1983) and production of polyurethane foam (Hustad *et al.* 1970). Lactose may be crystallized from the UF permeate, but the economics of the process depends largely on the costs of removing salts by ED or ion exchange.

In this work the electrodialysis of lactose solutions with compositions similar to those of a permeate obtained by UF of sweet whey and a reconstituted UF-whey retentate has been studied. The UF retentate was supplied by ILAS (Reny Picot, Asturias), the largest whey processing plant in Spain.

MATERIALS AND METHODS

Experiments were carried out in a stackpack electrodialysis unit (Stantech, Hamburg, Germany). The ED-unit consisted of 10 cell pairs sandwiched between two electrode compartments (the stack can take up to 20 cell pairs).

The effective membrane area was 100 cm^2/membrane. The ion exchange membranes employed were for cation-exchange-SC-1 (transport number Na^+, 0.91 at 25C in 1 N NaCl) and for anion-exchange-SA-1 (transport number Cl^-, 0.93 determined at 25C in 0.5 N NaCl). The two types of membranes were separated either by a diluting or a concentrating spacer. The electrodes consisted of a stainless-steel cathode and a platinum-plated titanium anode.

The feed streams to the anode and cathode compartments and the concentrating and diluting streams were pumped by four centrifugal magnetically-coupled polypropylene pumps. The power supply assembly allowed either the voltage (0–40 V) or the current (0.025–5 A) to be adjusted.

A few elements were added to the commercial unit, namely two stainless-steel tanks (15 L), two constant temperature baths and two rotameters.

The ED-system was operated in a batch-recirculation manner. A constant voltage was applied in each run. The corresponding current densities varied following changes in overall conductivity.

After each run the membrane stack was cleaned-in-place using the following sequence of operations:

(1) Flushing with deionized water for 5 min
(2) Recirculation of a 1 wt% solution of NaOH for 20 min
(3) Rinsing with deionized water for 10 min
(4) Recirculation with a 0.35 wt% solution of HCl for 20 min and
(5) Rinsing with deionized water for 10 min

Feed Solutions

The following feed solutions were used in the ED-experiments:

Model Permeate. A simulated milk ultrafiltrated (SMUF) as indicated by Jennes and Koops (1962) was used. The total solids concentration of the solution was 10 wt%, similar to that of solutions fed to spray dryers.

Reconstituted UF-Whey Retentate (WPC). A powdered UF-whey retentate was dissolved in water to produce a synthetic UF-whey retentate containing 10 wt% solids and the following composition: protein (34.9 wt%), fat (5.0 wt%), lactose (50.3 wt%), moisture (4.0 wt%).

Concentrating and Electrode Washing Streams. The initial concentrating stream was a 6 g/L NaCl solution and the electrode washing was a 0.1 N Na_2SO_4 solution, acidified to pH $\approx$ 2 with H_2S0_4.

Analytical Methods

The samples were analyzed for pH, conductivity, ash, chlorides and the major cations using the following methods:

pH: By a pH-meter (Cole Palmer, Model 5986-62).
Conductivity: Conductivity-meter (Jenway, Model 4010).
Chlorides: By the Volhard method (Burns and Muraca 1960).
Cations: Concentrations of K^+, Na^+ and Ca^{2+} ions were determined by atomic emission spectroscopy (Philips spectrometer, Model PU 9100) at 766.5 nm (K^+), 589 nm (Na^+) and 422.7 nm (Ca^{2+}).
Ash: Weight after calcination at 550C (Spanish Food Industry Standards) (Casado 1991).

RESULTS AND DISCUSSION

Limiting Current

The transport of ions is proportional to the quantity of electricity that flows through the circuit. Hence the rate of transport of ions increases with the electric current. As the voltage applied across the membranes is raised, the current density increases linearly, up to a critical value, at which point there is a drop corresponding to a change in pH due to the dissociation of water. The limiting current density is important in the electrodialysis of whey. If the current density becomes excessive, the pH will decrease and membrane fouling will occur as a consequence of precipitation of proteins and salts at the surface of the membrane. The rate of mass transfer will then decrease and the stack will heat up.

Figure 1 shows a plot of the current density as a function of the voltage applied for the synthetic whey permeate solution at 18C. A limiting current, i_{lim}, of 25.2 mA/cm^2 is observed at a voltage of 32 V. The operating current density should be ca. 80% of the corresponding limiting value, in order to avoid membrane polarization effects.

Figure 2 shows limiting current density plots for electrodialysis of reconstituted concentrated whey at 20, 35 and 45C, for three different flow rates. The limiting current increases with both temperature and flow rate. However, for this feedstock it is advisable to operate below 20C in order to avoid microbial proliferation. Moreover, an increase in flow rate results in a larger pressure drop through the membrane stack, thereby leading to greater power requirements.

The limiting current is usually expressed as a function of the Reynolds number.

$$i_{lim} = \alpha \, Re^{\beta} \qquad (1)$$

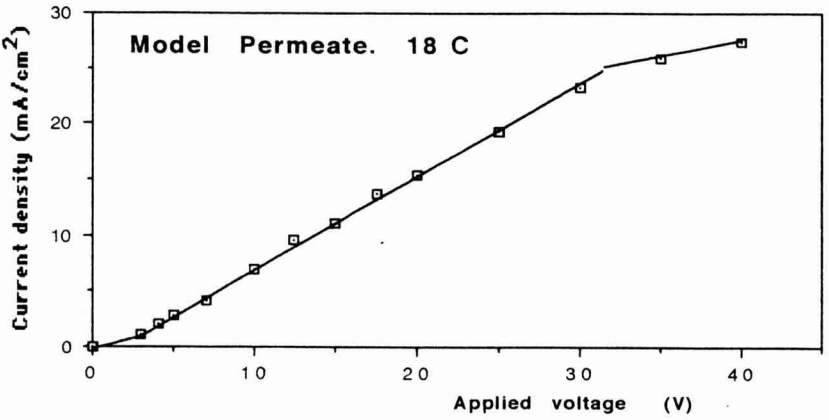

FIG. 1. CURRENT DENSITY VERSUS VOLTAGE APPLIED FOR ELECTRODIALYSIS OF A MODEL PERMEATE SOLUTION AT 18C

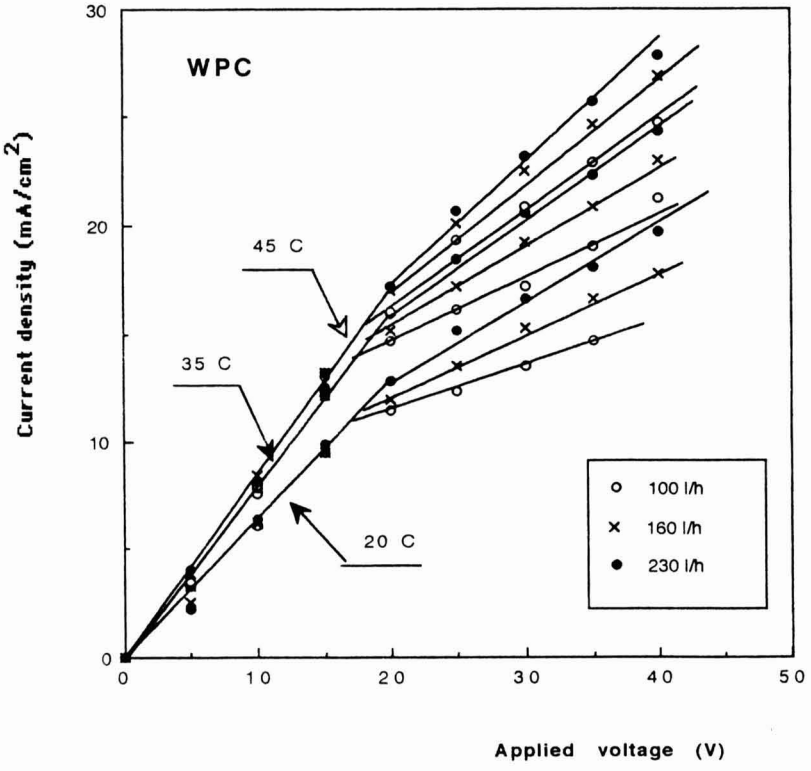

FIG. 2. CURRENT DENSITY VERSUS VOLTAGE APPLIED FOR ELECTRODIALYSIS OF WPC RETENTATE AT 20C, 35C AND 45C

On the basis of our experimental results the values of the parameters α and β are

$$20C \quad \alpha = 6.50 \quad \beta = 0.18 \tag{2}$$
$$35C \quad \alpha = 5.08 \quad \beta = 0.27 \tag{3}$$
$$45C \quad \alpha = 11.54 \quad \beta = 0.10 \tag{4}$$

for flow rates between 100 and 230 L/h (Re = 28 − 106).

Electrodialysis of reconstituted UF-whey concentrate was characterized by lower values of i_{lim} than for the lactose solution. This result can be explained by considering the following expression for i_{lim} (López-Leiva 1988).

$$i_{lim} = \frac{D}{\delta} F C_b \left[t_a^- - t^- \right] \tag{5}$$

The effective thickness of the boundary layer for mass transfer of lactose (δ) increases with the increasing protein content of the solution and increasing salt deposition on the membrane. An increase in operating temperature decreases the viscosity of the solution, leading to an increase in i_{lim}.

Electrodialysis of a Model Permeate

A lactose solution with a composition similar to that of a UF-whey permeate, as indicated previously, was demineralized by ED. Physical property measurements and composition analyses were carried out for the product streams from ED at 25 and 35C. Temperatures higher than 45C were avoided, since such operation would cause a decrease in the membrane life. Results are shown in Tables 1 and 2.

The conductivity of the solution (σ) is a suitable variable for following the demineralization process. The reduction in the conductivity of the product stream reaches 90% after 89 min when the process is run at 25C and after 64 min at 35C. The rate of removal of the various ions in the diluate follows the order $K^+ > Cl^- > Na^+ > Ca^{2+}$; the low value for Ca^{2+} is due to its larger ionic volume. This behavior has also been reported in the literature (Boer and Robbertsen 1981; Short and Doughty 1977).

If the rate of ash removal per unit area of membrane (kg/h m^2) is plotted as a function of conductivity in a log-log plot, the data follow a straight line at both 25 and 35C (see Fig. 3). The line for 35C lies below the line for 25C. The proximity of this temperature, 35C, to the maximum allowable temperature of membrane operation could explain this anomalous behavior. The maximum ash removal rate is reached between 25 and 30C.

TABLE 1.
PHYSICAL PROPERTIES AND IONIC CONCENTRATIONS (g/L) OF THE PRODUCT STREAMS FOR ELECTRODIALYSIS OF MODEL PERMEATE AT 25C, V=35 VOLTS

		Demineralized Stream						Concentrated Stream					
Time	I	pH	σ	Cl^-	Na^+	K^+	Ca^{2+}	pH	σ	Cl^-	Na^+	K^+	Ca^{2+}
min.	(A)		mS/cm			g/L			mS/cm			g/L	
0	3.20	5.1	8.8	2.38	1.04	1.14	0.78	7.1	10.3	3.04	3.88	0.89	0.27
10	2.80	4.9	6.2	1.56	0.75	0.75	0.61	6.3	13.6				
25	1.85	3.6	3.5	0.78	0.42	0.34	0.33	6.1	15.9				
40	1.24	3.1	2.1	0.32	0.18	0.11	0.18	5.7	18.0				
55	0.79	2.9	1.5	0.02	0.04	0.05	0.07	5.4	18.3	5.36	5.43	1.99	1.06

TABLE 2.
PHYSICAL PROPERTIES AND IONIC CONCENTRATIONS (g/L) OF THE PRODUCT STREAMS FOR ELECTRODIALYSIS OF MODEL PERMEATE AT 35C, V= 35 VOLTS

		Demineralized Stream						Concentrated Stream					
Time	I	pH	σ	Cl^-	Na^+	K^+	Ca^{2+}	pH	σ	Cl^-	Na^+	K^+	Ca^{2+}
min.	(A)		mS/cm			g/L			mS/cm			g/L	
0	2.89	2.7	10.2	2.54	0.97	1.14	0.75	6.6	9.4	1.96	2.33	0	0
5	2.80	2.7	8.5	2.05	0.89	0.98	0.71	5.7	11.2	2.27			
15	2.51	2.9	6.1	1.29	0.62	0.63	0.47	4.1	13.8	2.37			
20	2.26												
25	1.99	3.0	4.2	0.88	0.51	0.42	0.36	3.3	15.7	3.04	2.88	0.81	0.81
30	1.74												
35	1.50	3.0	2.9	0.36	0.41	0.26	0.26	3.1	17.1	3.35			
40	1.31												
50	0.99	2.9	1.7		0.24	0.12	0.15	3.0	18.1	4.26			
65	0.63	3.0	0.9	0.08	0.12	0.04	0.06	2.9	18.8	4.59			
75	0.55												
80	0.41	3.1	0.6	0.03	0.05	0.01	0.03	2.8	18.9	4.61	3.23	1.29	1.29

The data in Tables 1 to 5 show that model permeate is demineralized to reach a given final ash concentration more rapidly than the WPC solution. This is due to an inherently greater rate of ash removal as shown by the ion reduction data. The explanation for this phenomenon lies in the high proportion of Ca and phosphate bonded to the proteins in the WPC solution in spite of their high conductivity in solution; i.e., Ca and P are only slowly removed because their relative transport number in the membrane is lower than other ions. This is further illustrated in Fig. 3, which shows that the rate of demineralization for the Model Permeate is higher at a certain level conductivity. The data in Fig. 3 imply that scaling-up from pilot to large scale could be calculated on a membrane area basis.

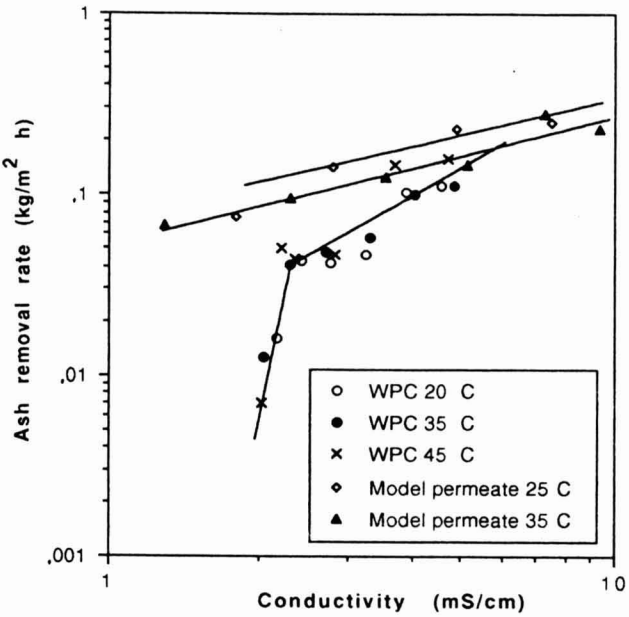

FIG. 3. ASH REMOVAL RATE VERSUS CONDUCTIVITY FOR ELECTRODIALYSIS OF MODEL PERMEATE AT 25C (◇) and 35C (▲) AND A WPC AT 20C (○), 35C (●) AND 45C (x)

Electrodialysis of a Reconstituted UF-Whey Retentate

Nine series of tests were carried out with a UF whey retentate from a whey treatment plant. Three different flow rates (100, 160 and 230 L/h) and three temperatures (20, 35 and 45C) were investigated. Values of physical properties and ionic (Cl^-, Na^+, K^+, Ca^{2+} and Mg^{2+}) concentrations determined as functions of time of ED are shown in Tables 3, 4, and 5.

The data shown in Tables 3–5 indicate that the pH decreases only slightly during the demineralization process. The fact that only a small change of pH is observed is attributable to operating conditions at currents that are always below 80% of the i_{lim} value. Inspection of the data also indicates that divalent ions (Ca^{2+} and Mg^{2+}) are removed more slowly than monovalent ions (Na^+ and K^+). This result is attributed to the lower mobilities of the divalent ions and their ability to form complexes with proteins. This hypothesis is also supported by the fact that the rate at which the conductivity of the demineralized solution decreases is slightly larger than that corresponding to the removal of ash. The ash content encompasses the calcium and phosphate ions, but when these ions are complexed with proteins, they make no contribution to the conductivity of the solution.

TABLE 3.
PHYSICAL PROPERTIES AND IONIC CONCENTRATIONS (g/L) OF THE DEMINERALIZED STREAM FOR ELECTRODIALYSIS OF WPC: T = 20C, V = 15 VOLTS

Flow rate of 100 l/h								
Time	I	pH	σ	Cl^-	Na^+	K^+	Ca^{2+}	Mg^{2+}
min.	(A)		mS/cm				g/L	
0	0.91	6.45	5.1	0.81	0.64	1.35	0.91	0.10
5	0.48	6.41	4.7	0.72				
15	0.39	6.39	4.3	0.61	0.61	1.14	0.85	0.09
25	0.35	6.37	4.0	0.51				
40	0.29	6.33	3.6	0.46	0.60	0.96	0.81	0.08
55	0.25	6.32	3.2	0.33				
70	0.23	6.29	3.1	0.31	0.55	0.74	0.72	0.07

Flow rate of 160 l/h								
Time	I	pH	σ	Cl^-	Na^+	K^+	Ca^{2+}	Mg^{2+}
min.	(A)		mS/cm				g/L	
0	0.85	6.49	5.1	0.98	0.51	1.11	0.74	0.19
5	0.57	6.49	4.5	0.74				
15	0.46	6.42	4.1	0.51	0.48	0.84	0.71	0.17
25	0.41	6.37	3.8	0.42				
40	0.33	6.38	3.4	0.33	0.45	0.71	0.63	0.16
55	0.28	6.37	2.9	0.17				
70	0.24	6.36	2.6	0.15	0.44	0.58	0.56	0.15

Flow rate of 230 l/h								
Time	I	pH	σ	Cl^-	Na^+	K^+	Ca^{2+}	Mg^{2+}
min.	(A)		mS/cm				g/L	
0	0.81	6.47	5.2	0.91	0.52	0.99	0.81	0.19
5	0.71	6.55	4.6	0.86	0.49	0.91	0.75	0.18
15	0.55	6.54	3.7	0.55				
25	0.44	6.53	3.2	0.34	0.46	0.71	0.68	0.16
40	0.34	6.51	2.7	0.24				
55	0.28	6.52	2.3	0.13	0.42	0.52	0.58	0.14
70	0.23	6.51	2.0	0.09	0.39	0.46	0.55	0.14

TABLE 4.
PHYSICAL PROPERTIES AND IONIC CONCENTRATIONS (g/L) OF THE DEMINERALIZED STREAM FOR ELECTRODIALYSIS OF WPC: T = 35C, V = 15 VOLTS

Flow rate of 100 l/h								
Time	I	pH	σ	Cl^-	Na^+	K^+	Ca^{2+}	Mg^{2+}
min.	(A)		mS/cm				g/L	
0	1.21	6.41	5.0	1.02	0.62	1.24	0.87	0.09
5	0.61	6.37	4.7	0.77				
15	0.47	6.34	4.2	0.69	0.59	1.05	0.82	0.09
25	0.41	6.32	3.7	0.59				
40	0.32	6.29	3.3	0.45	0.52	0.79	0.74	0.08
55								
70	0.24	6.21	2.6	0.21	0.5	0.62	0.64	0.07

Flow rate of 160 l/h								
Time	I	pH	σ	Cl^-	Na^+	K^+	Ca^{2+}	Mg^{2+}
min.	(A)		mS/cm				g/L	
0	1.16	6.48	5.1	0.79	0.67	1.24	0.93	0.10
5	0.69	6.48	4.4	0.69				
15	0.53	6.45	3.9	0.57	0.60	1.01	0.86	0.09
25	0.43	6.45	3.4	0.44				
40	0.34	6.45	2.9	0.30	0.52	0.74	0.77	0.08
55	0.29	6.4	2.5	0.21				
70	0.25	6.34	2.3	0.09	0.47	0.55	0.69	0.07

Flow rate of 230 l/h								
Time	I	pH	σ	Cl^-	Na^+	K^+	Ca^{2+}	Mg^{2+}
min.	(A)		mS/cm				g/L	
0	1.25	6.46	5.2	0.92	0.51	0.98	0.74	0.19
5	0.93	6.46	4.3	0.79	0.49	0.88	0.71	0.17
15	0.66	6.35	3.6	0.56				
25	0.51	6.26	3.1	0.35	0.44	0.67	0.62	0.16
40	0.38	6.14	2.5	0.25				
55	0.31	6.01	2.1	0.15	0.39	0.43	0.49	0.14
70	0.26	5.91	1.9	0.07	0.37	0.37	0.44	0.12

TABLE 5.
PHYSICAL PROPERTIES AND IONIC CONCENTRATIONS (g/L) OF THE DEMINERALIZED STREAM FOR ELECTRODIALYSIS OF WPC: FLOW RATE = 230 L/H, V = 20 VOLTS

Temperature of 20 (C)								
Time	I	pH	σ	Cl^-	Na^+	K^+	Ca^{2+}	Mg^{2+}
min.	(A)		mS/cm	g/L				
0	1.24	6.54	4.9	0.89	0.61	1.27	0.95	0.12
5	0.75	6.54	4.3	0.69				
15	0.59	6.53	3.5	0.40	0.57	0.98	0.87	0.11
25	0.49	6.51	3.1	0.36				
40	0.38	6.48	2.6	0.23	0.51	0.69	0.80	0.10
55	0.33	6.44	2.3	0.09				
70	0.24	6.37	2.0	0.06	0.45	0.51	0.67	0.08

Temperature of 35 (C)								
Time	I	pH	σ	Cl^-	Na^+	K^+	Ca^{2+}	Mg^{2+}
min.	(A)		mS/cm	(g/L)				
0	1.52	6.63	5.2	0.90	0.65	1.23	0.88	0.11
5	0.93	6.61	4.5	0.72				
15	0.69	6.60	3.7	0.39	0.59	0.87	0.82	0.10
25	0.52	6.56	3.1	0.27				
40	0.39	6.54	2.5	0.15	0.51	0.71	0.71	0.09
55	0.30	6.50	2.1	0.04				
70	0.25	6.45	1.9	0.04	0.46	0.37	0.64	0.08

Temperature of 45 (C)								
Time	I	pH	σ	Cl^-	Na^+	K^+	Ca^{2+}	Mg^{2+}
min.	(A)		mS/cm	g/L				
0	1.75	6.52	5.2	1.07	0.90	0.98	0.73	0.15
5	1.07	6.52	4.2	0.72				
15	0.66	6.54	3.2	0.37	0.70	0.71	0.62	0.13
25	0.51	6.62	2.6	0.24				
40	0.42	6.33	2.3	0.09	0.59	0.51	0.57	0.12
55	0.33	6.22	2.1	0.03				
70	0.26	6.39	1.8	0.02	0.43	0.33	0.48	0.11

The extent of ash removal is perhaps a more appropriate parameter for expressing the efficiency of ion depletion by ED. Figure 3 contains a plot of the rate of ash removal as a function of conductivity for the reconstituted retentate stream. The effects of temperature and feed flow rate through the ED stack are shown in Fig. 4.

Analysis of the experimental data indicates that the optimum demineralization conditions correspond to a temperature range of 35–45C and a feed flow rate of 230 l/h. These values agree well with values reported previously in the literature (Ahlgren 1972; Houldsworth 1980; Johnson *et al.* 1976).

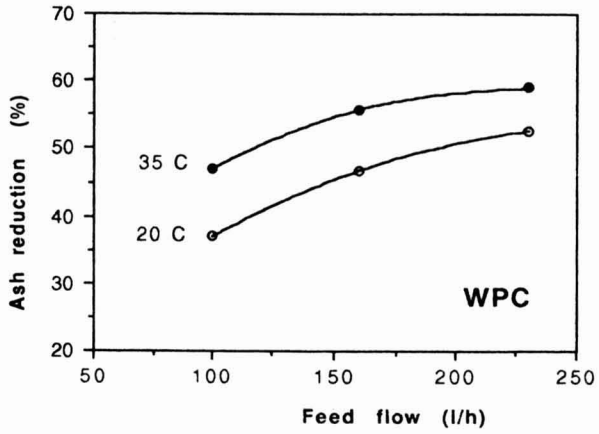

FIG. 4. ASH REDUCTION VERSUS FEED FLOW RATE DURING ED OF WPC AFTER 60 MIN OF OPERATION
T (C): (○) 20, (●) 35

A higher degree of demineralization implies a higher energy consumption and a higher electrical efficiency factor, τ, defined by:

$$\tau = \frac{100\ F\ V\ \Delta C}{n \int I\ dt} \tag{6}$$

where $\int I\ dt$ represents the total quantity of electrical charge transported by the cell-pair.

Average current efficiencies and power consumption data were obtained for the different runs. Data for an operation time of 60 min are shown in Table 6. The data on water transport from diluting to concentrating stream was 0.22 L/h m^2 at an average current of 0.4 A and 0.27 L/h m^2 at an average current of 0.5 A.

TABLE 6.
ELECTRICAL EFFICIENCY AND ENERGY CONSUMPPTION FOR ELECTRODIALYSIS OF WPC AFTER 60 MIN OF OPERATION

Temperature (C)	20	35	45
Electrical efficiency (%)	81.6	74.5	84.2
Energy consumption (kW-h/eq.removed) x 10^2	6.59	7.25	6.40
Ash removal (%)	54.0	55.2	64.2

CONCLUDING REMARKS

ED is a useful method for the demineralization of whey and UF-whey derivatives. The tests carried out with SC-1 and SA-1 ion-exchange membranes have shown the variation of the deashing rate and the analytical reduction of relevant ions. The analytical data for ion removal reported in this work are useful for the design and operation of an ED unit prior to the separation of individual proteins (i.e., α-lactalbumin, β-lactoglobulin and other proteins). The raw solutions used were a model permeate (reference solution) and a UF retentate (WPC) with approximately the same composition in individual ions.

SYMBOLS

C_b Bulk concentration, (Eq/L)
ΔC Change of concentration between the demineralized and feed streams (Eq/L)
D Diffusion coefficient for salt, (m^2/s)
F Faraday's constant, 96599 (A s/Eq)
I Electrical current, (A)
i_{lim} Limiting current density, (mA/cm^2)
n Number of cell-pairs in the stack
Re Reynolds number
t Time (min)
t^- Transport number of anion in bulk solution
t_a^- Transport number of anion in anionic membrane
V Volume of demineralized stream, (L)

Greek Letters

α Coefficient in Eq. (1)
β Coefficient in Eq. (1)
δ Boundary layer thickness, (m)
τ Electrical efficiency factor
σ Electrical conductivity, (mS/cm)

ACKNOWLEDGMENTS

The authors wish to thank Industrias Lácteas Asturianas (ILAS) from Navia and FICYT (Asturias, Spain), Instituto de Cooperación Iberoamericana (ICI, Spain) and CONICET (Argentina) and the Center for Dairy Research (Madison, WI) for supporting this work.

REFERENCES

AHLGREN, R.M. 1972. Electromembrane processing of cheese whey. In *Industrial Processing with Membranes*, (R.E. Lacey, and S. Loeb, eds.) pp. 71–82, Wiley-Interscience, New York.

BATCHELDER, B.T. 1987. Electrodialysis applications in whey processing. Bull. IDF, 212, 84–90.

BOER, R. and ROBBERTSEN, T. 1981. Electrodialysis and ion exchange processes: The case of milk whey. In *Progress in Food Engineering: Solid Extraction, Isolation and Purification. Texturization*, (C. Cantarelli and C. Peri, eds.). Proc. Eur. Symp. of the Food Working Party of the E.F.C.E. Kusnacht. Switzerland.

BOOIJ, C.J. 1985. Use of lactose in the pharmaceutical and chemical industry. J. Soc. Dairy Technol. *39*(4), 105–109.

BURNS, E.A. and MURACA, R.F. 1960. Determination of small amounts of chloride by Volhard titration. Evaluation of operator determinate end-point error. Anal. Chim. Acta *23*, 136–144.

CASADO, P. 1991. *Guía para el Análisis Químico de la Leche y los Derivados Lácteos*, pp. 196–198, Ed. Ayala, Madrid.

COTON, S.G. 1985. Whey resources and utilization. J. Soc. Dairy Technol. *38*(4), 97–100.

HOULDSWORTH, D.W. 1980. Demineralization of whey by means of ion exchange and electrodialysis. J. Soc. Dairy Technol. *33*(2), 45–51.

HUSTAD, G.O., RICHARDSON, T. and AMUNDSON, C.H. 1970. Polyurethane foams from dried whey. J. Dairy Sci. *53*(1), 18–24.

JENNES, R. and KOOPS, J. 1962. Preparation and properties of a salt solution which simulates milk ultrafiltrate. Neth. Milk Dairy J. *16*, 153–164.

JOHNSON, K.T., HILL, C.G. and AMUNDSON, C.H. 1976. Electrodialysis of raw whey and whey fractionated by reverse osmosis and ultrafiltration. J. Food Sci. *41*, 770–777.

KOSARIC, N. and ASHER, Y. J. 1983. The utilization of cheese whey and its components. Adv. Biochem. Eng. Biotechnol. *32*, 25–60.

LÓPEZ LEIVA, M.H. 1988. The use of electrodialysis in food processing. Part 1: Some theoretical concepts. Lebensm. Wiss. Technol. *21*, 119–125.

RYDER, D.N. 1980. Economic considerations of whey processing. J. Soc. Dairy Technol. *33*(2), 73–79.

SHORT, J.L. and DOUGHTY, R.K. 1977. Demineralization of deproteinated wheys by electrodialysis. N. Z. J. Dairy Sci. Technol. *12*, 156–159.

THE INFLUENCE OF pH ON THE KINETICS OF ACID HYDROLYSIS OF SUCROSE

A. PINHEIRO TORRES, F.A.R. OLIVEIRA[1], C.L.M. SILVA and S.P. FORTUNA

Escola Superior de Biotecnologia
R. Dr. António Bernardino de Almeida
P-4200 Porto, Portugal

Accepted for Publication August 3, 1993

ABSTRACT

Sucrose acid hydrolysis was studied as a potential chemical time-temperature integrator to use under pasteurization conditions. A nonisothermal method was used to determine the kinetic parameters of this reaction at different pH values in the range of 0.8 to 2.5 and covering the range of temperatures from 50 to 90C. The nonisothermal method was first validated with the classical two-step isothermal method at pH 2.5. Kinetic parameters showed to be highly collinear (correlation of 0.99), but it was concluded that the activation energy can be assumed independent of pH and equal to 99 kJ/mole with the preexponential factor being proportional to the H^+ concentration. Results are favorable for the future application of this system in the evaluation of pasteurization processes. Since the activation energy was found to be independent of the pH, this system is useful as a TTI for validation of mathematical models, but not so much for monitoring quality factors, except those with an equal activation energy.

INTRODUCTION

The main criterium to establish the efficacy of a thermal process is the microbial safety of the final product (Stumbo 1973) and therefore microbiological methods are commonly used for process assessment (Kessler 1988). In many cases, the heat applied for bacterial inactivation degrades desirable organoleptic and nutritive properties (Stumbo 1973). Studies on the associated destruction of nutrients and quality factors during thermal processing are referred by Lund (1975), Thompson (1982) and others. Mathematical procedures to predict reduction of microorganisms or nutrient destruction in thermal processing were developed (Ball and Olson 1957; Hayakawa and Ball 1969; Teixeira *et al.* 1969;

[1]Author to whom correspondence should be addressed.

Journal of Food Process Engineering **17** (1994) 191-208.

Stumbo 1973), but they all require as input the temperature history of the product. These data were collected for cans and other batch processes using heat penetration tests (Ball and Olson 1957).

Measuring the exact temperature distribution during a continuous thermal process by conventional methods offers obvious problems and therefore research is focusing on the development of alternative on-line methods to indicate the effects of continuous thermal processes on the kinetics of safety and quality factors (Berry *et al.* 1989; Weng 1991) or simply to validate experimentally temperature profiles in heat exchangers predicted by various mathematical models. For this first purpose, several chemical and biochemical indicators have been proposed in literature. Acid hydrolysis of sucrose was proposed by Lou (1977) and Adams *et al.* (1984) as a chemical indicator for can sterilization and for UHT processes, respectively.

However, acid hydrolysis of sucrose is also a potential chemical time temperature integrator (TTI) for lower temperature processes, that is, pasteurization. The rate of this reaction might be controlled to the desired sensitivity to pasteurization times and temperatures by selection of the right pH of the sucrose solution. Therefore, the dependence of kinetic parameters of sucrose acid hydrolysis on pH at pasteurization conditions has to be well known.

Hydrolysis of sucrose into its two monosaccharides, commonly called inversion of sucrose, can be catalyzed by acids, bases, salts or enzymes (Vukov 1965; Bender and Brubacher 1973). The mechanism of this reaction is well studied (Bender and Brubacher 1973; Whistler and Daniel 1985). Most research on this subject has been more commercially oriented in two different contexts: (1) the production of liquid sugar by various methods, as reviewed by Marignetti and Mantovani (1979/80), with emphasis on yield and not on the kinetics itself; and (2) the description of hydrolysis of sucrose at very low rates (low temperatures and high pH), to determine conditions of minimum inversion (Honig 1953; Meade 1963). An equation for determining rate constants for various temperatures (20–130C) and pH (1 to 6.5) was proposed by Vukov (1965), but was not experimentally verified.

To describe the effect of time and temperature on a first order reaction, two parameters are needed (Lund 1975): the rate constant at a reference temperature and the dependence of rate on temperature. In the system under study, the dependence of these parameters on pH also needs to be described. Available kinetic parameters of this reaction are limited and do not cover all ranges of pH and temperature of interest (Table 1). Reported kinetic data do not show a clear relation of these parameters with pH, and frequently published results seem contradictory.

The main objective of this work was the detailed description of the kinetics of sucrose acid hydrolysis at temperatures below 100C and pH below 2.5 for future use as a TTI in pasteurization processes. Reaction conditions were chosen

TABLE 1.
REPORTED KINETIC DATA FOR ACID HYDROLYSIS OF SUCROSE

Reference	pH	E_a (kJ/mol)	ln k_0 [a]	ΔT (C)	method	sucrose det.	acid
Adams et al.(1984)	2.50	106.3	31.78	60-100	isothermal	FPD	H_2SO_4
Sadeghi and Swartzel (1990)	2.5	94.6	27.91	110-140	"	Somogyi-Nelson	H_2SO_4
Sadeghi and Swartzel (1990)	2.5	46.0	15.80	"	EPM [c]	Somogyi-Nelson	H_2SO_4
Lou (1977)[a]	3.16	94.0	26.27	110-127	isothermal	Glucostat	HCl
Lou (1977)[a]	3.22	92.4	25.45	"	"	Glucostat	HCl
Lou (1977)[a]	3.30	99.4	27.16	"	"	Glucostat	HCl
Rhim et al. (1989b)	3.30	102.3	28.89	70-98	NI - LIT[d]	enzymatic	-
Rhim et al. (1989b)	3.30	106.0	30.47	60-98	"	enzymatic	-
Rhim et al. (1989b)	3.30	103.70	29.69	60-90	"	enzymatic	-
Lou (1977)[b]	3.40	133.9	36.31	110-127	isothermal	Glucostat	HCl

[a] k_0 in (min^{-1}) ; [b] Data taken from Rhim et al. (1989a) ; [c] equivalent point method ; [d] nonisothermal with linear increasing temperature

for compatibility with this future application, including the selection of the solvent and the acid catalyst.

THEORETICAL CONSIDERATIONS

Sucrose Hydrolysis

Sucrose hydrolysis gives two reducing monosaccharides according to the following reaction:

$$\text{Sucrose} + H_2O \longrightarrow \text{Glucose} + \text{Fructose} \quad (1)$$

This reaction, when catalyzed with acid and at constant pH and temperature, follows first order kinetics (Honig 1953; Meade 1963; Vukov 1965).

$$-\frac{dS}{dt} = k_T \times S \quad (2)$$

The observed reaction rate constant k_T increases with decreasing pH with an exponential dependence (Meade 1963; Vukov 1965). Bender and Brubacher (1973) studied the kinetics of acid hydrolysis of sucrose with a mechanistic approach and found the protonation of the sucrose molecule [Eq. (3)] to be the slowest, thus the rate-determining step, with an equilibrium constant K_{eq} limiting the formation of the intermediate compound [Eq. (4)].

$$S + H^+ \rightleftharpoons SH^+ \quad (3)$$

$$K_{eq} = \frac{SH^+}{S \times H^+} \quad (4)$$

The overall rate of disappearance of sucrose is therefore equal to the rate of disappearance of the intermediate rate limiting compound SH^+ (Bender and Brubacher 1973):

$$-\frac{dS}{dt} = k_{kin} \times SH^+ \quad (5)$$

By substitution of Eq. (4) in Eq. (5), the rate of disappearance of sucrose can be related with the sucrose concentration, and the observed rate constant in Eq. (2) is then proportional to the concentration of hydrogen ions by a constant k^* [Eq. (6)].

$$k_T = k_{kin} \times K_{eq} \times H^+ = k^* \times H^+ \tag{6}$$

The rate Eq. (2) can therefore be rewritten as Eq. (7), showing that sucrose hydrolysis may be described as a first order reaction both in terms of hydrogen ion and sucrose concentrations:

$$-\frac{dS}{dt} = k^* \times H^+ \times S \tag{7}$$

The temperature dependence of the observed rate constants follows the Arrhenius equation over a wide range of pH and temperatures (Vukov 1965; Lou 1977) and the activation energy is independent of temperature, as concluded by Ward (1986) from an analysis of data reported by various authors. Therefore:

$$k_T = k_0 \times \exp\left(-\frac{Ea}{RT}\right) \tag{8}$$

Vukov (1965) stated that Ea is independent of pH and assumed an average value of 108.5 kJ/mole $\pm$ 3.0, based on data he gathered in literature. However, more extensive literature review indicates values as different as 46.0 and 133.9 kJ/mole (Table 1).

If the equilibrium constant is assumed to follow an Arrhenius-type temperature dependence (Atkins 1982), and combining Eq. (6) and (8), it can be concluded that the preexponential constant is proportional to H^+ and the activation energy is independent of this catalyst:

$$k_0 = k_{0,kin} \times K_{0,eq} \times H^+ = k_0^* \times H^+ \tag{9}$$

$$Ea = Ea_{kin} + Ea_{eq} \tag{10}$$

This deduction supports the hypothesis of a pH independent activation energy suggested by Vukov (1965).

Nonisothermal Method

Kinetic studies are directed at the development of a mathematical model describing reaction rate as a function of all relevant variables that are in this case time, temperature and pH (or hydrogen ion concentration). Nonisothermal methods for kinetic parameter determination fit best the aim of this study, as they represent thermal treatments better than the classical isothermal two-step method. Some other advantages of these methods are that they can overcome the problem associated with thermal lag in kinetic studies and simplify the collection of data (Rhim *et al.* 1989b).

The classical isothermal methods for kinetic parameter determination are two-step methods, where rate constants k_T are obtained at different temperatures from a set of isothermal experiments, according to the following general equation:

$$\frac{dc}{dt} = - k_T c^n \tag{11}$$

The dependence of the rate constants on temperature is then obtained by fitting the data to the Arrhenius model (Eq. 8), giving the preexponential factor k_0 and the activation energy Ea.

The same parameters can be obtained from one experiment with changing temperature, where both concentration and temperature are recorded as function of time. This is the basis of nonisothermal methods, which are one-step methods. The rate equation for first-order kinetics (n = 1) and the Arrhenius equation combined give the following equation:

$$c_t = c_0 \exp\left\{-k_0 \int_0^t \exp\left(-\frac{Ea}{RT}\right) dt\right\} \tag{12}$$

A linear temperature increase (approximately) was used. In this case, the temperature evolves gradually with time and the process covers equal temperature ranges in equal intervals of time. In this case there is no analytical solution to the integral in Eq. (12) (Rhim *et al.* 1989b) and therefore the equation was solved numerically. Integral methods (Hill 1977; Hill and Grieger-Block 1980) were preferred to differential methods, as proposed by Nunes *et al.* (1991). Nonlinear least squares regression is preferable in this situation (Box *et al.* 1978). Rate of convergence can be improved and linear dependence of

parameters decreased with a substitution of variables, as proposed by Nelson (1983). A new variable (δ) is introduced, defined as:

$$\delta = \ln k_0 - \frac{E_a}{R}\beta \tag{13}$$

where β is the best weight of the temperature profile found for this case. In this situation β is:

$$\beta = \frac{1}{\mathbb{N}} \sum_{i=1}^{\mathbb{N}} \frac{1}{T_i} \tag{14}$$

where $\mathbb{N}$ is the number of temperatures T_i recorded during the experiment. The improvements obtained with this transformation have also been observed by Haralampu *et al.* (1985) for isothermal kinetic studies.

The final equation from which the theoretical concentrations of sucrose were calculated has the following form:

$$\ln c_t = \ln c_0 - \int_0^t \exp\left[\delta - \frac{Ea}{R}\left(\frac{1}{T(t)} - \beta\right)\right] dt \tag{15}$$

The optimization program to obtain the kinetic parameters (δ and Ea) of the reaction (Fig. 1) was written in FORTRAN 77 for running on a personal computer IBM (model 55 SX). The optimization procedure was a nonlinear least squares regression using the Simplex method (Holzman 1980). The objective function was the sum of squares of the residuals between logarithms of predicted and experimental sucrose concentrations, as follows:

$$\text{o.f.} = \Sigma(\ln c_{teo} - \ln c_{exp})^2 \text{ (minimum)} \tag{16}$$

The predicted concentrations were calculated at each time by Eq. (15). Restrictions to the Simplex were based on the physical consistency of critical parameters (concentrations and kinetic parameters) and were imposed as suggested by Nedler and Mead (1965). A typical concentration curve is shown in Fig. 2.

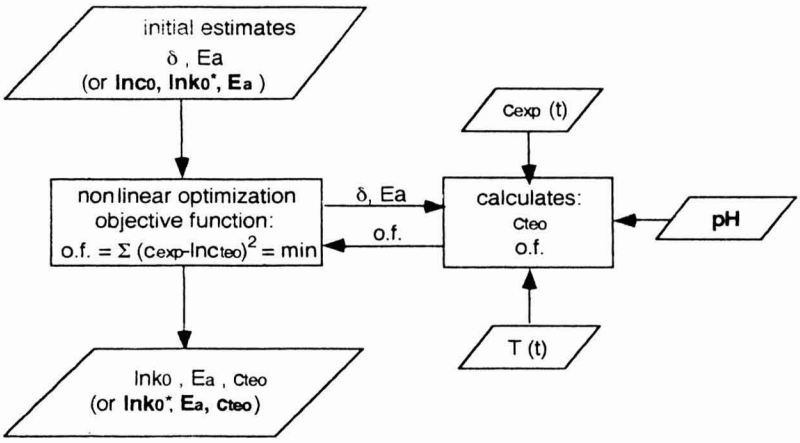

FIG. 1. FLOW DIAGRAM OF THE COMPUTER PROGRAM

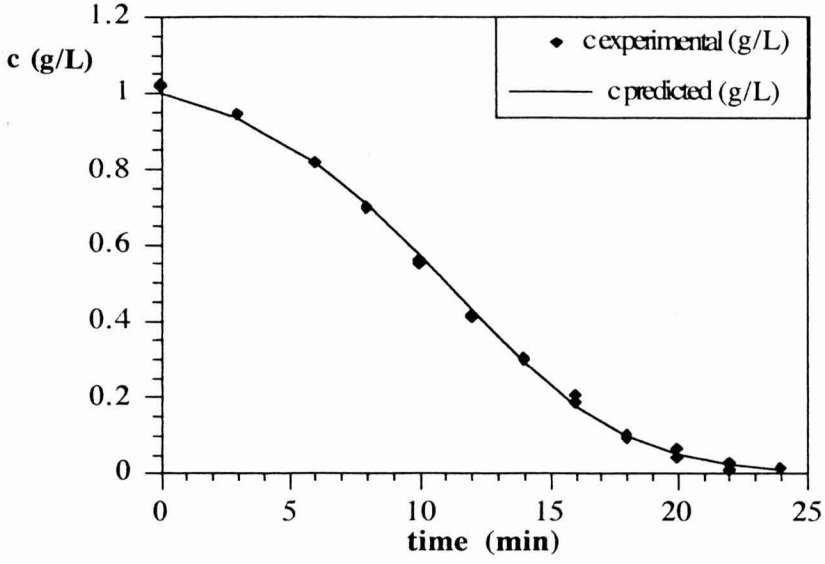

FIG. 2. EXPERIMENTAL AND PREDICTED SUCROSE CONCENTRATIONS AT pH 1.5 UNDER NONISOTHERMAL CONDITIONS

MATERIALS AND METHODS

Nitric acid was chosen as catalyst based on the following criteria: (1) it was a strong monoprotic acid, (2) it would be inert towards stainless steel of a processing unit at the concentrations used, and (3) it had a good pH stability with time. Tap water was used as solvent, as it would be more convenient for future applications, namely for using in a pilot plant or industrial equipment, where large amounts of solution are necessary. Available tap water had quite constant properties along the year and the reaction in the available tap water gave results with errors in the order of magnitude of demineralized water.

Solutions of nitric acid (Merck) were prepared at pH from 0.8 to 2.5 and standardized by automatic titration against a standard 0.10 M NaOH solution (high performance titration laboratory TitraLab, from Radiometer Copenhagen). Solutions of sucrose (food grade) at 1.0 g/L were prepared from each corresponding acid solution. This concentration was chosen to give final samples for analysis in the range of maximum sensitivity of the analytical method and of the measuring equipment. It was experimentally verified that no significant change in the pH occurred during an experiment.

The sugar solutions were put into 15 duplicate 1.2 × 10 cm stoppered test tubes, which were small enough to avoid a significant thermal lag (maximum verified: 60 s). The tubes were immersed in a thermostatically controlled water bath with reciprocating motion (Shaking Water Bath SW-21C from Julabo). Temperature was increased linearly from 50 to 90C (Fig. 3) during the time required to achieve 90% reduction of the disaccharide. The sample temperature was monitored with two thermocouples dipped in additional test tubes and was registered at appropriate time intervals. At 15 predetermined time intervals, tubes in duplicate were removed and plunged into cooling water at 5–10C.

The nonreducing disaccharide concentration was determined by measuring the increase in reducing monosaccharides in the sample, that are the only hydrolysis products. The reducing sugars content was quantified by spectrophotometric dosage at 540 nm (UV/VIS spectrometer UNICAM 8625) by the DNS method as described by Oliveira (1988), which is valid for concentrations between 0.1 and 1 g/L. For each experiment, a calibration curve was made with standard glucose solutions [D(+)-Glucose anhydrous for biochemistry, Merck]. Disaccharide concentration at time t was then obtained by difference of reducing sugar concentration after total hydrolysis and reducing sugar concentration at the same time t.

RESULTS AND DISCUSSION

The acid hydrolysis of sucrose was confirmed to be a first order reaction (see Fig. 4) and the rate constant to follow an Arrhenius dependence on temperature (see Fig. 5) in the range of experimental conditions covered.

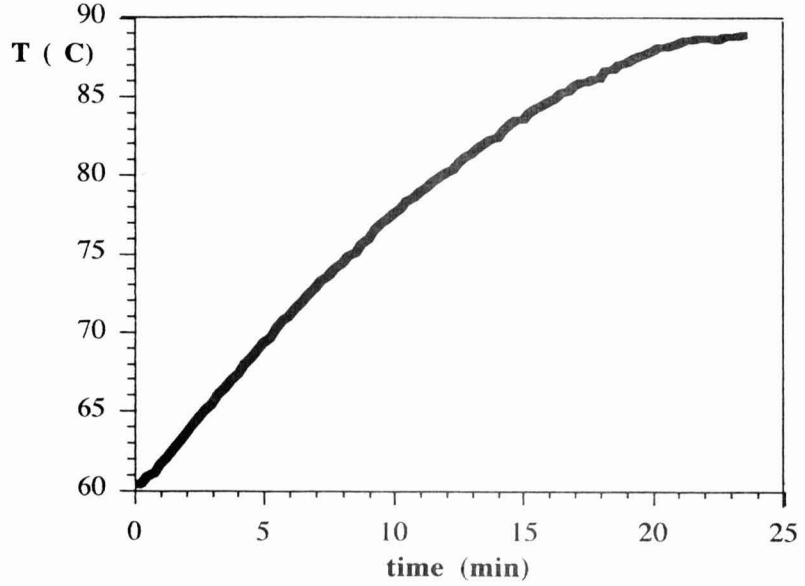

FIG. 3. TYPICAL TEMPERATURE HISTORY FOR THE NONISOTHERMAL METHOD (pH 1.5)

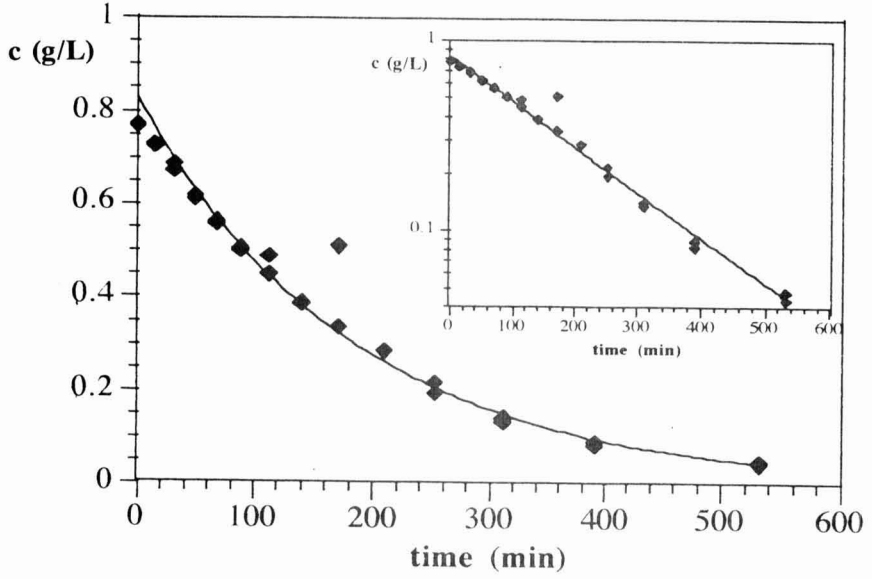

FIG. 4. ACID HYDROLYSIS OF SUCROSE AT 70C (pH 2.5)

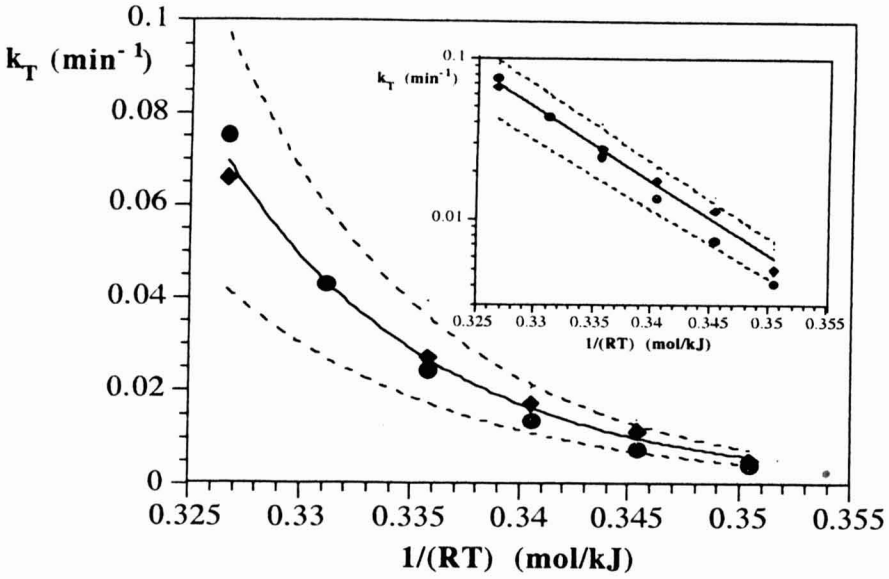

FIG. 5. RATE CONSTANTS AT pH 2.5
Diamonds represent isothermal data, circles represent nonisothermal data and the dotted line represents the 95% confidence interval for the isothermal method.

Validation of the Nonisothermal Method

The nonisothermal method was validated at pH 2.5, by comparison with results obtained with the classical isothermal method. This pH was chosen because published results at other pH values within the range of temperature/pH of interest to this study were scarce. For this validation 6 isothermal runs were carried out at different temperatures, from 70 to 95C. The parameters were obtained by the classical two-step approach. In all regressions, the procedure described by Bard (1974), based on the covariance matrix of the estimates, was used for calculating both the correlation factors and the confidence intervals for the parameters. The procedure is only exactly valid for linear regressions, but it has been suggested as a good approximation for nonlinear regressions and is widely used for this situation (Bard 1974; Seber and Wild 1989). The isothermal method showed an increase of the 95% confidence interval of the rate constants with temperature (Fig. 5). The rate constants obtained with the nonisothermal method fall within this confidence interval, thus showing that the two methods provide consistent results.

Dependence of Kinetic Parameters on pH

Using the nonisothermal method the values of Ea and ln k_0 were determined for different pH values from 0.8 to 2.5. The results are plotted on Fig. 6 and 7, respectively. The 95% confidence intervals for each experiment are marked with vertical lines. It can be noted that these intervals have a considerable magnitude. The points show a high scatter as well and a clear relation between the kinetic parameters and pH is not evident. Particularly, it is impossible to conclude that ln k_0 varies linearly with pH, while Ea is independent of pH, as the theory suggests. Due to the significant scattering of the results, it is not possible either to suggest another model that can accurately predict the sucrose concentration variation at all pH values.

It is well known that the Ea and ln k_0 values are highly collinear (Haralampu *et al.* 1985). In this case this has been confirmed by the calculated statistical correlation between both parameters, which was larger than 0.99. This means that for a given set of data there is a very large number of pairs of ln k_0 and Ea that predict equally well the variation of the rate constant with time. That is, although the plotted values correspond to the minimum residual for a given pH, there is a high number of other Ea/ln k_0 combinations that are statistically similar, with a 95% probability.

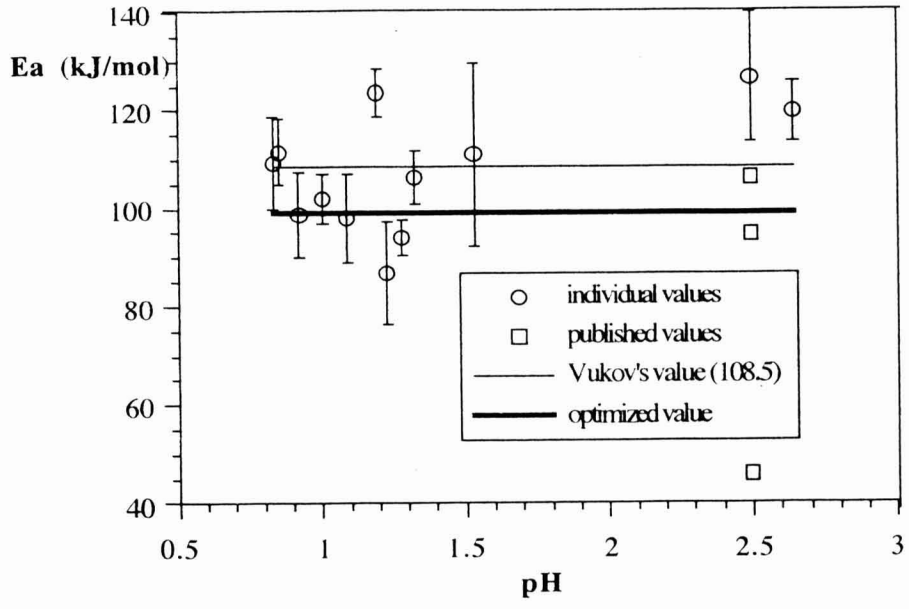

FIG. 6. DEPENDENCE OF THE ACTIVATION ENERGY ON pH

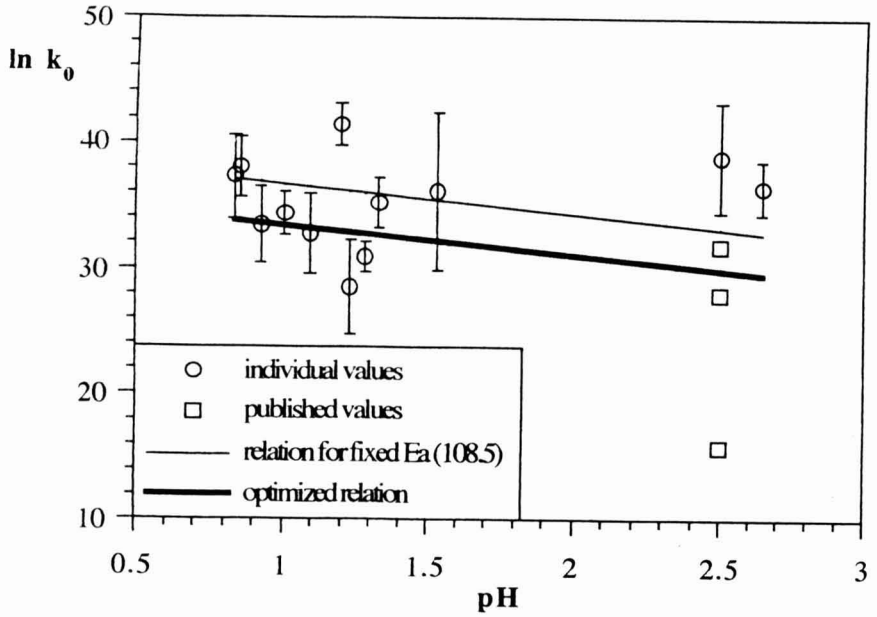

FIG. 7. DEPENDENCE OF THE PREEXPONENTIAL FACTOR ON pH

Therefore, a different analysis is required. Combining Eq. (9) with Eq. (12), a more general relation between concentration and time can be obtained:

$$\ln c_t = \ln c_0 - H^+ \int_0^t \exp\left[\ln k_0^* - \frac{Ea}{R\,T(t)}\right] dt \qquad (17)$$

A nonlinear regression based on this equation was then applied to all experimental data obtained, instead of analyzing each pH set of data separately. The objective function was again the sum of the residuals of the logarithms of sucrose concentration but the parameters considered were c_0, $\ln k_0^*$ and Ea (the differences in the computer program flow diagram are represented in bold in Fig. 1). The estimated parameters and corresponding 95% confidence intervals were:

c_0	=	1.01 ± 0.01 g/L
$\ln k_0^*$	=	35.6 ± 0.5 (k_0^* in L/min/mole)
Ea	=	99 ± 2 kJ/mole

It should be noted that this procedure does not decrease the collinearity problems between both parameters. Its advantages come from the fact that it is statistically more correct: since a one-time only regression is carried out, there is no propagation of error from one correlation to another.

These values are also shown in Fig. 6 and 7 (thickest line). The 95% confidence intervals are not represented because of their very small magnitude. The activation energy is lower than the one suggested by Vukov (1965) but lies well within the expected range. Figure 7 also shows the dependence of ln k_0 on pH using the value of Ea suggested by Vukov (1965): 108.5 kJ/mole. This shows that if a constant Ea value is assumed, then the relationship found for ln k_0 as a function of pH is the one predicted theoretically. Obviously, Vukov's Ea leads to higher residuals, if applied to our data.

Figure 8 shows the predicted variation of concentration with time, at different pH values, using the individual values of ln k_0 and Ea obtained at each pH and the Ea and ln k_0 values obtained with Eq. (17). It can be observed that the two predicted curves are quite similar.

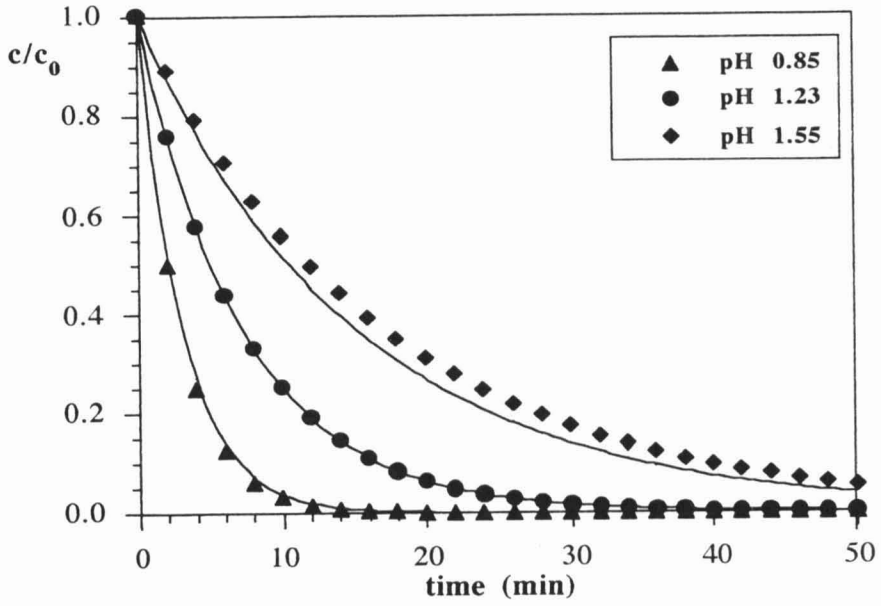

FIG. 8. PREDICTED CONCENTRATION PROFILES AT 70C
The points were generated with kinetic parameters obtained for each pH. The lines were obtained with Ea = 99 kJ/mole and $k_0 = \exp(35.6) \times H^+$ in min^{-1}.

CONCLUSIONS

The isothermal and the nonisothermal method produced consistent results, proving that nonisothermal methods can be used instead of the conventional isothermal ones, having the advantage of reducing time and reagent requirements. Furthermore, in this case the system is tested under conditions similar to the ones it is going to be used for (TTI).

Ea and k_0 values are highly collinear, making the selection of their determination procedure very important. An appropriate analysis allows to conclude that the activation energy of the sucrose acid hydrolysis can be assumed independent of both temperature and pH, while the preexponential factor varies linearly with hydrogen ion concentration, as follows:

$$k_0 = 2.77 \times 10^{15} \times H^+ \tag{18}$$

This behavior has a theoretical support and was validated experimentally by the good fits between such model and experimental results.

Controlling the pH, one can control the rate of the hydrolysis process. For a given temperature a pH can be selected so that after a required time period the variation in the sucrose concentration allows for an accurate determination. Table 2 shows the pH values required to obtain a 90% reduction in the sucrose concentration for different combinations of time/temperature, usual in pasteurization. It can also be noted that the activation energy of this reaction is similar to the activation energy of some quality degradation changes, as Adams *et al.* (1984) also referred. It is however important to note that this system is only applicable as a TTI for factors exhibiting exactly the same activation energy (Weng 1991). Therefore, its application is far more interesting for experimental verification of mathematical models than for assessing quality changes, where its use is rather restricted, since quality factors can have energy activation as different as 30 and 170 kJ/mole (Lund 1975). It is also very important to note that this reaction should not be used to assess microorganism inactivation, unlike suggested by Lou (1977).

TABLE 2.
ESTIMATED pH VALUES REQUIRED FOR A 90% REDUCTION OF SUCROSE (ACID HYDROLYSIS) AT DIFFERENT PROCESSING CONDITIONS

Product	Processing conditions	estimated pH for hydrolysis
acid products (4.0-4.3)	93.3 C - 5 min	1.74
acid products (4.3-4.5)	93.3 C - 10 min	2.04
dairy products	62-65 C - 30 min	1.21-1.35
tomato paste	105 C - 3 min	1.89

ACKNOWLEDGMENTS

The authors acknowledge Junta Nacional de Investigação Científica e Tecnológica (JNICT) and the CEC (AAIR Program) for financial support.

NOMENCLATURE

c	Concentration (g/L)
c_0	Initial concentration (g/L)
Ea	Activation energy (J/mole)
H^+	Hydrogen ion concentration (mole/L)
k_T	Observed kinetic rate constant at temperature T (min^{-1})
k_0	Preexponential factor (min^{-1})
k^*	Constant, as defined in Eq. (6) (L/min/mole)
k_0^*	Constant, as defined in Eq. (9) (L/min/mole)
k_{kin}	Rate constant, as defined in Eq. (5) (min^{-1})
K_{eq}	Equilibrium constant, as defined in Eq. (4) (L/mole)
n	Order of reaction
N	Number of temperatures recorded during an experiment
o.f.	Objective function, as defined in Eq. (16)
R	Universal gas law constant (= 8.314 J/mole/K)
S	Sucrose concentration (mole/L)
SH^+	Protonated sucrose concentration (mole/L)
t	Time (min)
T	Temperature (K)
TTI	Time-temperature integrator
β	Weight of inverse of temperatures, as defined in Eq. (14) (K^{-1})
δ	Parameter, as defined in Eq. (13)

Subscripts:

exp	Experimental
teo	Theoretical
t	At time t

REFERENCES

ADAMS, J.P., SIMUNOVIC, J. and SMITH, K.L. 1984. Temperature histories in a UHT indirect heat exchanger. J. Food Sci. *49*, 273.

ATKINS, P.W. 1982. *Chimie Physique*, Vol. 1, 2nd Ed., pp. 311–349, Lavoisier, Paris.

BALL, C.O. and OLSON, F.C.W. 1957. *Sterilization in Food Technology*, pp. 195–248, McGraw Hill Book Co., New York.

BARD, Y. 1974. *Nonlinear Parameter Estimation*, Academic Press, New York.

BENDER, M.L. and BRUBACHER, L.J. 1973. *Catalysis and Enzyme Action*, pp. 40–44, McGraw Hill, New York.

BERRY, M.F., SINGH, R.K. and NELSON, P.E. 1989. Kinetics of methylmethionine sulfonium in buffer solutions for estimating thermal treatment of liquid foods. J. Food Processing Preservation *13*, 475–488.

BOX, G.E.P., HUNTER, W.G. and HUNTER, J.S. 1978. *Statistics for Experimenters*, pp. 453–509, John Wiley & Sons, New York.

BRUNNER, R.L. 1964. Determination of reducing value. In *Methods in Carbohydrate Chemistry*, Vol. IV, Chap. 19, Academic Press, New York.

HARALAMPU, S.G., SAGUI, I. and KAREL, M. 1985. Estimation of Arrhenius model parameters using three least squares methods. J. Food Processing Preservation *9*, 129–143.

HAYAKAWA, K. and BALL, C.O. 1969. Theoretical formulae for temperatures in cans of solid food and for evaluation of various heat processes. Can. Inst. Food Technol. J. *2*, 167.

HILL JR., C.G. 1977. *An Introduction to Chemical Engineering Kinetics and Reactor Design*, pp. 24–75, John Wiley & Sons, New York.

HILL JR., C.G. and GRIEGER-BLOCK, R.A. 1980. Kinetic data: generation, interpretation and use. Food Technol. *34*(2), 56.

HOLZMAN, A. (1980). *Mathematical Programming for Operations Researchers and Computer Scientists*, Marcel Dekker, New York.

HONIG, P. 1953. *Principles of Sugar Technology*, Vol. 1, pp. 1–17, 447–449, Elsevier Publishing Co., New York.

KESSLER, H.G. 1988. *Lebensmittel- und Bioverfahrenstechnik - Molkereitechnologie*, pp.136–141, Verlag A. Kessler, Munich.

LOU, W.C. 1977. Disaccharide hydrolysis as a predictive measurement for the efficacy of heat sterilization in canned foods, Ph.D. thesis, Univ. of Massachusetts.

LUND, D.B. 1975. Effects of heat processing on nutrients. In *Nutritional Evaluation of Food Processing*, 2nd Ed., (R.S. Harris and E. Karmas, eds.) Chap. 9, Van Nostrand Reinhold/AVI, New York.

MARIGNETTI, N. and MANTOVANI, G. 1979/80. Liquid sugar. Sugar Technol. Rev. *7*, 3–47.

MEADE, G.P. 1963. *Cane Sugar Handbook*, 9th Ed., John Wiley & Sons, London.

NEDLER, J.A. and MEAD, R. 1965. A Simplex method for function minimization. Comput. J. *7*, 308–313.

NELSON, R.R. 1983. Stability prediction using the Arrhenius model. Computer Prog. Biomed. *16*, 55–60.

NUNES, R.V., RHIM, J.W. and SWARTZEL, K.R. 1991. Kinetic parameter evaluation with linearly increasing temperature profiles: integral methods. J. Food Sci. *56*(5), 1433.

OLIVEIRA, F.A.R. 1988. Mass transfer analysis for the leaching of water soluble components from food, pp. 146–148, Ph.D. thesis, Univ. Leeds, UK.

RHIM, J.W., NUNES, R.V., JONES, V.A. and SWARTZEL, K.R. 1989a. Appearance of a kinetic compensation effect in the acid catalysed hydrolysis of disaccharides: a research note. J. Food Sci. *54*(1), 222.

RHIM, J.W., NUNES, R.V., JONES, V.A. and SWARTZEL, K.R. 1989b. Determination of kinetic parameters using linear increasing temperature. J. Food Sci. *54*(2), 446.

SADEGHI, F. and SWARTZEL, K.R. 1990. Generating kinetic data for use in design and evaluation of high temperature food processing systems. J. Food Sci. *55*(3), 851.

SEBER, G.A.F. AND WILD, C.J. 1989. *Nonlinear Regression*, John Wiley & Sons, New York.

STUMBO, C.R. 1973. *Thermobacteriology in Food Processing*, 2nd Ed., Academic Press, New York.

TEIXEIRA, A.A., DIXON, J.R., ZAHRADNIK, J.W. and ZINSMEISTER, G.E. 1969. Computer optimization of nutrient retention in thermal processing of conduction heated foods. Food Technol. *23*, 677.

THOMPSON, D.R. 1982. The challenge in predicting nutrient changes during food processing. Food Technol. *36*(2), 97–108, 115.

VUKOV, K. 1965. Kinetic aspects of sugar hydrolysis. Int. Sugar J. *67*, 172–175.

WARD, J.R. 1985. Temperature dependence of the activation enthalpy for sucrose hydrolysis. Int. J. Chem. Kinetics *17*(1), 11–15.

WENG, Z. 1991. A time-temperature integrator for thermal processing of foods: a case study on immobilized peroxidase, pp. 1–15, Ph.D. thesis, Kuleuven, Belgium.

WRISTLER, R.L. and DANIEL, J.R. 1985. Carbohydrates. In *Food Chemistry*, 2nd Ed. (O.R. Fennema, ed.), Chap. 3, Marcel Dekker, New York.

DETERMINATION OF CONVECTIVE HEAT TRANSFER COEFFICIENT BETWEEN FLUID AND CUBIC PARTICLES IN CONTINUOUS TUBE FLOW USING NONINVASIVE EXPERIMENTAL TECHNIQUES[1]

KHALED B. ZITOUN and SUDHIR K. SASTRY[2]

The Ohio State University
Department of Agricultural Engineering
590 Woody Hayes Drive
Columbus, OH 43210

Accepted for Publication September 14, 1993

ABSTRACT

Convective heat transfer coefficients (h_{fp}) between fluids and cubic particles in continuous flow were investigated with respect to flow rate, viscosity, particle size, and radial location using noninvasive methods: (1) liquid crystal color change, and (2) measurements of relative velocity via flow visualization (for verification of liquid crystal results). All tests were conducted using sodium carboxymethyl cellulose (CMC) as the carrier fluid. Results indicate that h_{fp} increases with decreasing particle size, increasing flow rates and (as expected) decreasing viscosity. Radial location affects h_{fp} values: changing the particle position from the center to the bottom of the tube increases the convective heat transfer coefficient. Comparison between the methods indicates good agreement, providing a means of verification for the liquid crystal method.

INTRODUCTION

Optimal process design for aseptic processing of particulates requires good estimates of heat transfer parameters, including the convective heat transfer coefficient at the fluid to particle interface. Previous work has included studies on immobilized particles (Chandarana *et al.* 1990; Zuritz *et al.* 1990; Chang and

[1]Salaries and research support provided by state and federal funds appropriated to the Ohio Agricultural Research and Development Center, The Ohio State University. References to commercial products and trade names are made with the understanding that no discrimination and no endorsement by The Ohio State University is implied.
[2]Corresponding author.

Journal of Food Process Engineering **17** (1994) 209-228. *All Rights Reserved.*

Toledo 1989; Awuah *et al.* 1991), and for free particles (Sastry *et al.* 1990; Heppell 1985; Mwangi *et al.* 1992).

Sastry (1992), discussed different methods that could be used to determine fluid-to-particle heat transfer coefficient. Advantages and limitations were discussed for each approach and examined critically. The eight approaches cited by the author were: (1) stationary particle methods (Chandarana *et al.* 1990), (2) microbiological methods and history indicator (Heppell 1985), (3) moving thermocouple (Sastry *et al.* 1989), (4) liquid crystal methods (Stoforos *et al.* 1989; Balasubramaniam 1993), (5) melting point indicator (Mwangi *et al.* 1992), (6) relative velocity methods (Balasubramaniam 1993), (7) transmitter methods (Lesho and Hogrefe 1989), and (8) liquid temperature calorimetry (Sastry 1992). Many of these methods were considered useful to cross-validate and complement one another, but none of them was considered applicable to all conditions. More recent work from this laboratory (Balasubramaniam and Sastry 1994) has found that under laminar flow conditions, the effect of particle-to-pipe dimension ratio was not clear cut; this was attributed to variation in particle trajectories (which were not controlled).

Zitoun and Sastry (1994) determined convective heat transfer coefficients for cubic particles in non-Newtonian carrier fluids in laminar flow using the moving thermocouple approach of Sastry *et al.* (1990). Results indicated increasing heat transfer coefficients with increasing flow rate, decreasing viscosity and decreasing particle-to-tube dimension ratio. The results indicated that the dimension ratio effect was the opposite of that observed by Sastry *et al.* (1990) under turbulent flow conditions. The differences were attributed to the mixed and highly turbulent flow regime in the earlier study, which resulted in the dominance of "channeling" or "Bernoulli" type effects under turbulent flow. However, the study of Zitoun and Sastry (1994) did not involve control of particle trajectories. A better understanding of trends in h_{fp} would be achieved if parameters such as radial location were controlled, dictating the use of suitable noninvasive techniques. The studies of Stoforos *et al.* (1989) and Balasubramaniam (1993) indicated the feasibility of using liquid crystal temperature sensors; and Balasubramaniam (1993) also included a flow visualization technique (relative velocity method) that could be used for cross validation with other methods. Accordingly this research work emphasizes the determination of the convective heat transfer coefficient for moving cubic particles in holding tubes as affected by particle size, fluid flow rate, viscosity, and radial location; using liquid crystal sensors as the primary measurement technique; and using relative velocity measurement for cross validation. It was recognized that the relative velocity technique is dependent on existing correlations, and its use was therefore considered limited to that of verifying whether the data from other methods were consistent with observed flow patterns.

MATERIALS AND METHODS

All studies were conducted at 3 flow rates, 3 particle sizes, 3 viscosities of carrier fluid, and 2 radial locations, and were replicated 6 times. A summary of experimental conditions is presented in Table 1. Sodium carboxymethyl cellulose (CMC) was used as the carrier fluid in all studies. The measurement of temperatures upstream and downstream of the test section (diameter of 5.08×10^{-2}m and length of 1.5 m) were controlled using two thermocouples (Fig. 1). The temperature was constant at 45C $\pm$ 0.5C.

Liquid Crystal Method

Experimental Procedure. The experimental procedure involved introduction of a liquid crystal-coated transducer particle into an entry port upstream of the test section (Fig. 1), and videotaping of its color changes along the test section. Radial location was controlled in the initial sets of experiments using a specially constructed metallic screen tunnel (Fig. 2) that permitted precise radial entry points for transducers while minimizing interference with the rest of the flow field. Due to matched densities with the fluid and since the test duration was too short for radial migration effects to occur, particles introduced at a given radial location continued at that location through the tube length. After some use, it was observed that the tunnel caused scratching of the liquid crystal layer; hence its use was discontinued for the rest of the liquid crystal runs, although it was still used for the relative velocity method. Radial location was controlled by the trial and error procedure by pushing the particle to the estimated radial location providing a controlled initial impetus at the introduction port. The actual radial location was then determined after the fact by viewing the videotape. A large number of videotaped test runs were screened to select six replications at each of the radial locations. Only a fraction of the test runs could be used by this approach.

TABLE 1.
EXPERIMENTAL CONDITIONS

Variables	Values		
Flow rate (m^3/s)	2.52×10^{-4}	3.76×10^{-4}	5.05×10^{-4}
Particle size (cm)	1.176	1.595	1.994
CMC concentration %	0.2	0.4	0.8
Radial location	center		bottom

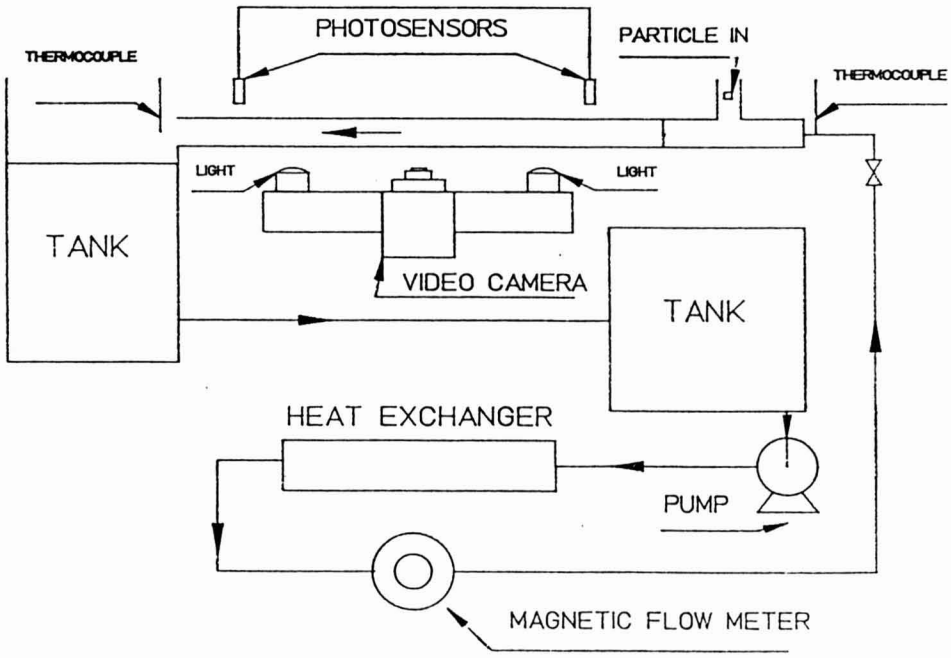

FIG. 1. SCHEMATIC DIAGRAM OF EXPERIMENTAL SETUP

A calibration run was conducted at each test condition by videotaping the color changes of a liquid crystal coated particle while attached to a thermocouple wire. The video images were analyzed to determine time-temperature data. The hue (h) was related to temperature by the following equation:

$$T(C) = 0.287132\, h + 2.863041 \tag{1}$$

All analyses were carried out using image analysis software (Image-Pro, Media Cybernetics Inc., Silver Spring, MD). Values of h_{fp} were found by using the Newton's law of heating and cooling (for Bi < 0.1) since the transducers used were of high thermal conductivity.

$$\ln \frac{(T-T_\infty)}{(T_i-T_\infty)} = -\frac{h_{fp}\, A}{MC_p}\, t \tag{2}$$

By plotting ln $(T - T_\infty)$ versus time, h_{fp} was determined from the slope of the curve, as: slope $= -(h_{fp}\, A)/M\, C_p$, and the intercept $=$ ln $(T_i - T_\infty)$.

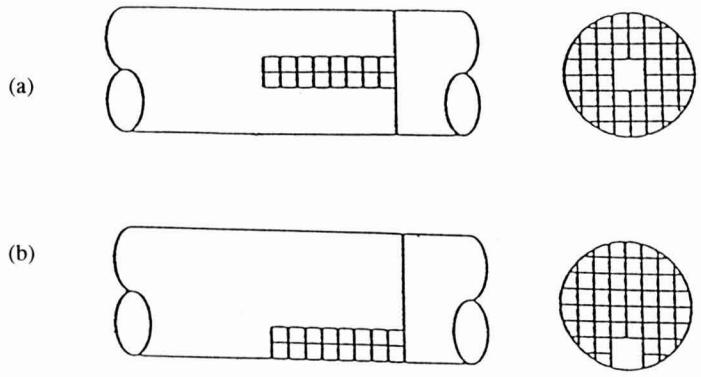

FIG. 2. METALLIC SCREEN TUNNEL (a) FOR CENTER RADIAL LOCATION; (b) USED FOR BOTTOM RADIAL INTRODUCTION

Particle Details. Hollow particles were made from aluminum sheet metal. To obtain the appropriate density to simulate food particles, sheets of specific thickness were used (Table 2). After cutting the sheet to the desired dimensions (1.994, 1.595 and 1.176 for large, medium and small sizes, respectively) the six sides of the cube were assembled.

Coating Technique. The technique to coat particles with liquid crystals required the following steps. Liquid crystal slurry was prepared by mixing one part of liquid crystal with three to four parts of the binder. A hollow cubic aluminum transducer particle was coated with water soluble black paint using an air brush. After the particles dried, liquid crystal was applied using an air brush, and then air dried. The dimensions and physical properties of the metal transducer particles are presented in Table 2. The slight difference in apparent density was less than 0.05%.

TABLE 2.
DIMENSIONS AND PROPERTIES OF METAL TRANSDUCER PARTICLES USED IN THE LIQUID CRYSTAL METHOD

Material	Side (m)	Thickness (m)	Density Kg/m^3	Specific heat KJ/Kg C
Aluminum	0.01176	0.001524	1078.74	0.94
Aluminum	0.01595	0.001207	1078.86	0.94
Aluminum	0.01994	0.000787	1078.83	0.94

Relative Velocity Method

Experimental Procedure. Neutrally buoyant transducer particles (properties in Table 3) were introduced into carrier fluid (CMC solutions; rheological properties determined as described later) and videotaped during their passage.

Fluid velocities were visualized using finely ground polystyrene tracers in the flow. Particle-fluid relative velocities were determined upon video replay by determining the time elapsed (measured by digital timer accurate to 1/60 s) for the particle and tracers to move a specified distance (determined by a grid placed on the tube) at the same radial location (details are presented in Fig. 3). For example, from Fig. 3, the velocity of the particle between times t_1 and t_3 was determined from the distance traversed (based on the number of equidistant grid points) divided by the elapsed time ($t_3 - t_1$). During this same time interval, the tracer traversed a straight line trajectory before and after passing the particle, plus a curvilinear path in the vicinity of the particle. These distances were determined by estimating tracer coordinates over successive frames of the videotape, and divided by elapsed time to yield the tracer velocity. The relative velocity between fluid and particle was then determined as the difference between particle and tracer velocities.

The screen tunnel (Fig. 2) as described under the liquid crystal method, was used to introduce particles at precise radial locations. The relative velocity versus radial location was determined in three dimensions, by using a mirror above the holding tube at an angle of 45.

Relative velocity data were used, along with product rheological properties, to determine h_{fp} values. This approach is easier for spherical particles (Balasubramaniam and Sastry 1994) where several dimensionless correlations (e.g., Ranz and Marshall 1952) are readily available for the unbounded flow case. In the present situation, no relationships were found for cubic particles. As a result, it was decided to use the available relations for spheres as approximations, while recognizing the inaccuracy inherent in the assumption. The approach

TABLE 3.
DIMENSIONS AND DENSITIES OF TRANSDUCER PARTICLES
USED IN THE RELATIVE VELOCITY METHOD

Material	length (m)	Material density (Kg/m^3)	Apparent density (Kg/m^3)
Polystyrene	0.01994	1078.45	1078.66
Polystyrene	0.01595	1078.45	1078.11
Polystyrene	0.01176	1078.45	1078.54

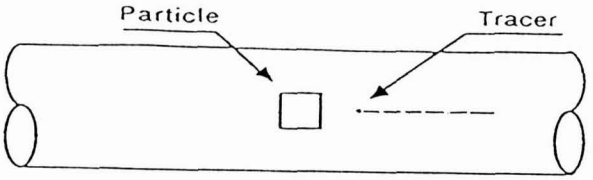

(a) at time t_1

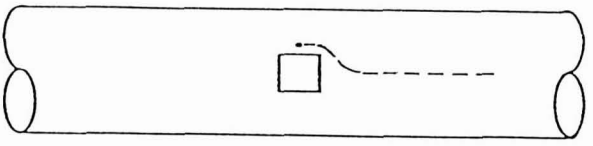

(b) at time t_2

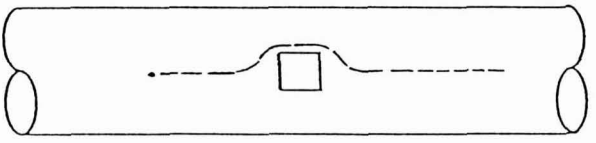

(c) at time t_3

FIG. 3. CRITERIA FOR CHOICE OF TRACER ($t_1 < t_2 < t_3$)
(a) A tracer moving at the same radial location as the axis of the particle; (b) a tracer moving over the transducer particle; (c) a tracer overtaking the transducer particle.

was considered appropriate, because the major purpose of the relative velocity method is not to accurately measure heat transfer coefficients *per se*, but rather to verify whether results of heat transfer methods are reasonable and consistent with the relative velocity data. Three empirical correlations were used, which apply for forced convection heat transfer between a fluid at constant temperature flowing past a single spherical particle; these were the equations of Ranz and Marshall (1952):

$$Nu = 2.0+0.6\ Re_{gs}^{0.5}\ Pr_{gs}^{0.33} \tag{3}$$

Kramers (1947):

$$Nu = 2.0+1.3\ Pr_{gs}^{0.15}+0.66\ Pr_{gs}^{0.31}\ Re_{gs}^{0.5} \tag{4}$$

and Whitaker (1972):

$$Nu = 2+(0.4\ Re_{gs}^{0.5}+0.06\ Re_{gs}^{2/3})\ Pr_{gs}^{0.4}\ (\mu/\mu_s)^{0.25} \tag{5}$$

The heat transfer coefficient h_{fp} was determined from the Nusselt number:

$$Nu = \frac{h_{fp} L_p}{k_f} \tag{6}$$

where L_p is the characteristic length of the cube. A number of choices of characteristic length were considered. For example, Chang and Toledo (1989) have used L_p equal to the diameter of a sphere having the same surface area as the actual cubic particle. The values of h_{fp} in this study were determined using a characteristic length L_p, different from those mentioned in many studies in the literature (Sparrow and Stretton 1985; King 1932; Lienhard 1973), and corresponded to an equivalent diameter of the cubic particle having the same volume as a sphere ($L_p = 2\ S\ (3/4\pi)^{1/3}$). This definition of L_p was considered appropriate to our study, since it keeps the density of the particle constant.

Physical Properties of Fluid. The non-Newtonian fluids used were aqueous solutions of sodium carboxymethyl cellulose (CMC). CMC solutions were prepared by adding the appropriate amount of CMC powder to water; the powder was slowly dispersed into the tank and stirred with an electric mixer. Then, the appropriate amount of sugar was added to match the density of the particle. Before the test the solution was transferred to the system and recirculated with venting to ensure the absence of air bubbles in the system.

The rheological properties were determined by using a coaxial cylinder viscometer (Rheomat Model 115, Contraves Industrial Division, Cincinnati, OH) and measuring shear stress (τ) and shear rate ($\dot{\gamma}$). The measurements were conducted before and after test to determine if significant shear breakdown effects occurred.

Results were analyzed based on the Ostwald-de-Waele power law model:

$$\tau = K\ \dot{\gamma}^n \tag{7}$$

A regression program (Systat 1989, Systat Inc., Evanston, IL) was used to determine K and n. The constants K, n obtained to fit the experimental data were statistically found with a correlation coefficient that ranged from 0.978 to

1. The rheological properties of the two fluid carriers used in the two different methods are presented in Table 4. The density of fluid with different concentrations of CMC and the quantity of sugar added to water in order to match the density of particles are summarized in Table 5.

The specific heat and the thermal conductivity of CMC were predicted from the following expressions (Heldman and Singh 1981):

$$C_{pf} = 1.675 + 0.025\ (\textit{Water content},\ \%) \tag{8}$$

$$k_f = [326.575 + 1.0412\ T - 0.00337\ T^2]\ [0.796 + 0.009346\ (\textit{Water content},\ \%)]\ 10^{-3} \tag{9}$$

TABLE 4.
RHEOLOGICAL PROPERTIES OF THE FLUID CARRIERS

	L.C.M. 45°C		R.V.M.	
% CMC	K	n	K	n
0.2	0.068	0.747	0.137[a]	0.709[a]
0.4	0.244	0.662	0.512[b]	0.611[b]
0.8	0.422	0.659	1.181[c]	0.527[c]

L.C.M.: Fluid carrier for the liquid crystal method.
R.V.M.: Fluid carrier for the relative velocity method.
a: At 31C
b: At 31.8C
c: At 32.4C

TABLE 5.
DENSITY OF THE FLUID WITH DIFFERENT CONCENTRATIONS OF CMC

Temperature C	% CMC	% Sugar	Density (Kg/m^3)
31	0.2	19.63	1078.32
31.8	0.4	19.78	1078.21
32.4	0.8	19.81	1078.05
45	0.2	21.24	1077.98
45	0.4	20.34	1078.43
45	0.8	20.34	1078.97

RESULTS AND DISCUSSION

Liquid Crystal Method

Generalized Reynolds and Prandtl numbers are presented in Table 6; since Re_g is less than 1400, the flow regime is laminar. Table 7 presents the values of h_{fp} as affected by flow rate, radial location and the size of particles. The average values of h_{fp} were calculated based on 6 replications, and the standard deviation ranged from 22 to 120 W/m^2K. By investigating the effect of the flow rate on the convective heat transfer coefficients, it was found that h_{fp} increased with increasing flow rate ($p<0.05$) and increased as the particle radial location changed from center to bottom ($p<0.05$; only 5 values out of 54 did not satisfy $p<0.05$, but they satisfied $p<0.1$; these readings were also from the highest viscosity condition for which the greatest h_{fp} variation occurred). Values of h_{fp} were found to decrease with increasing CMC concentration in the solution ($p<0.05$). For particle to tube size ratio, h_{fp} values increased when the particle size decreased ($p<0.05$). The above observation is similar to the result obtained using moving thermocouple methods (Zitoun and Sastry 1994), but there is an apparent inconsistency with the results obtained by Sastry *et al.* (1990). The principal reason for the difference is the flow regime: laminar in the present instance; fully developed turbulence in the earlier study. When fully developed turbulence occurs, the fluid is radially well mixed due to eddies, and the principal source of relative velocities would appear to be the "Bernoulli" or "channeling" effect, where the particle acts as an obstruction, and the fluid accelerates through the gap between particle and tube wall. This effect also occurs in laminar flow and has been noted by Balasubramaniam and Sastry (1994), but the effect is restricted primarily to those streamlines that move faster than the particle. In laminar flow, only the faster streamlines distort shape to

TABLE 6.
GENERALIZED REYNOLDS AND PRANDTL NUMBERS USED FOR LIQUID CRYSTAL METHOD

	%CMC					
	0.2		0.4		0.8	
$Q\ 10^{-4}$ m^3/s	Re_g	Pr_g	Re_g	Pr_g	Re_g	Pr_g
2.25	200.3	220.8	70.6	626.8	41.2	1075.2
3.76	333.0	199.3	121.4	546.5	70.9	936.3
5.05	477.5	185.3	178.5	495.9	104.3	848.8

TABLE 7.
FLUID-TO-PARTICLE HEAT TRANSFER COEFFICIENTS VALUES AT VARIOUS FLOW RATES, PARTICLE SIZES, AND CMC CONCENTRATIONS AT 45C, AS DETERMINED BY THE LIQUID CRYSTAL METHOD

		h_{fp} (w/m^2 K)		
Q 10^{-4} m^3/s	S.R.L.	% CMC 0.2	0.4	0.8
2.52	lb	551.0	401.5	313.0
2.52	lc	495.6	369.7	268.5
2.52	mb	611.7	449.7	418.9
2.52	mc	553.5	407.4	363.0
2.52	sb	636.9	526.2	482.5
2.52	sc	598.8	467.6	402.4
3.76	lb	653.7	544.4	461.0
3.76	lc	613.7	500.5	409.1
3.76	mb	665.0	569.1	467.0
3.76	mc	643.7	506.5	393.2
3.76	sb	803.7	671.5	594.1
3.76	sc	754.0	629.5	491.0
5.05	lb	739.5	656.0	506.4
5.05	lc	686.7	619.5	463.2
5.05	mb	781.2	706.9	589.4
5.05	mc	737.5	653.8	526.3
5.05	sb	928.7	821.5	639.6
5.05	sc	887.0	740.5	553.2

S.R.L.:Size and radial location.
l, m, s:size of particles; b, c: radial locations.
lb: Large bottom; lc: Large center;
mb: Medium bottom; mc: Medium center;
sb: Small bottom; sc: Small center.

move past the particle; thus the particle size effect in restricting the flow path is not as pronounced in laminar as in turbulent flow.

The effect of radial location appears to be due partially to lack of rotation of centrally located particles. The particles at the tube bottom were exposed to fluid velocity gradients, which caused them to rotate, increasing their heat transfer coefficient. Further insights were obtained by the relative velocity study (see discussion under relative velocity method). Due to the fact that Fourier numbers were greater than 0.2 and Biot numbers found in this set of experiments (see

TABLE 8.
VALUES OF BIOT NUMBERS FOR EACH h_{fp} VALUE CORRESPONDING TO A SPECIFIC FLOW RATE, PARTICLE SIZE, CONCENTRATION OF CMC, AND RADIAL LOCATION FOR THE LIQUID CRYSTAL METHOD

$Qx10^{-4}$ m^3/s	% CMC	$Biot_l$	$Biot_m$	$Biot_s$
2.52	0.2	0.038	0.027	0.055
2.52	0.4	0.027	0.020	0.045
2.52	0.8	0.021	0.019	0.042
2.52	0.2	0.034	0.025	0.052
2.52	0.4	0.025	0.018	0.040
2.52	0.8	0.018	0.016	0.035
3.76	0.2	0.045	0.030	0.069
3.76	0.4	0.037	0.025	0.058
3.76	0.8	0.031	0.021	0.051
3.76	0.2	0.042	0.029	0.065
3.76	0.4	0.034	0.023	0.054
3.76	0.8	0.028	0.017	0.042
5.05	0.2	0.050	0.035	0.080
5.05	0.4	0.045	0.032	0.071
5.05	0.8	0.035	0.026	0.055
5.05	0.2	0.047	0.033	0.076
5.05	0.4	0.042	0.029	0.068
5.05	0.8	0.032	0.023	0.048

l: Large
m: Medium
s: Small

Table 8) are small (<0.1), the use of the lumped capacitance method is justified.

Dimensionless correlations were developed to relate Nusselt number (Nu) to generalized tube Reynolds (Re_g) and Prandtl (Pr_g) numbers, ratio of particle characteristic length and diameter of the tube (L_p/D), and ratio of the radial location of the axis of particle to the radius of the tube ($R - r/R$). Multiple regression analysis after logarithmic linearization yielded the following equation:

$$Nu = 2 + 8.4703\ Re_g^{0.553}\ Pr_g^{0.2716} \left(\frac{L_p}{D}\right)^{0.6272} \left(\frac{R-r}{R}\right)^{-0.1142} \qquad r^2=0.949 \qquad (10)$$

Figure 4 shows a rearranged form of Eq. (10) with Nusselt number found experimentally and predicted (solid line). The high r^2 values indicate that much of the variability in previous results can be explained by the effects of radial location. In all cases, heat transfer coefficients were higher than expected from zero relative velocity.

Relative Velocity Method

Values of generalized Reynolds and Prandtl numbers are presented in Table 9, showing that the regime is clearly laminar. The results of the relative velocities and their corresponding heat transfer coefficients using the Ranz and Marshall relation for 0.2%, 0.4% and 0.8% CMC are presented in Fig. 5, 6 and 7, respectively. The value of relative velocity V_r represents the average value of three different relative velocities of the same particle size and the same radial location. Statistical analysis indicated that the standard deviation ranged from 4.5% to 19.3% of the mean. The value of the liquid to particle heat transfer coefficients increased with increasing flow rates and with decreasing

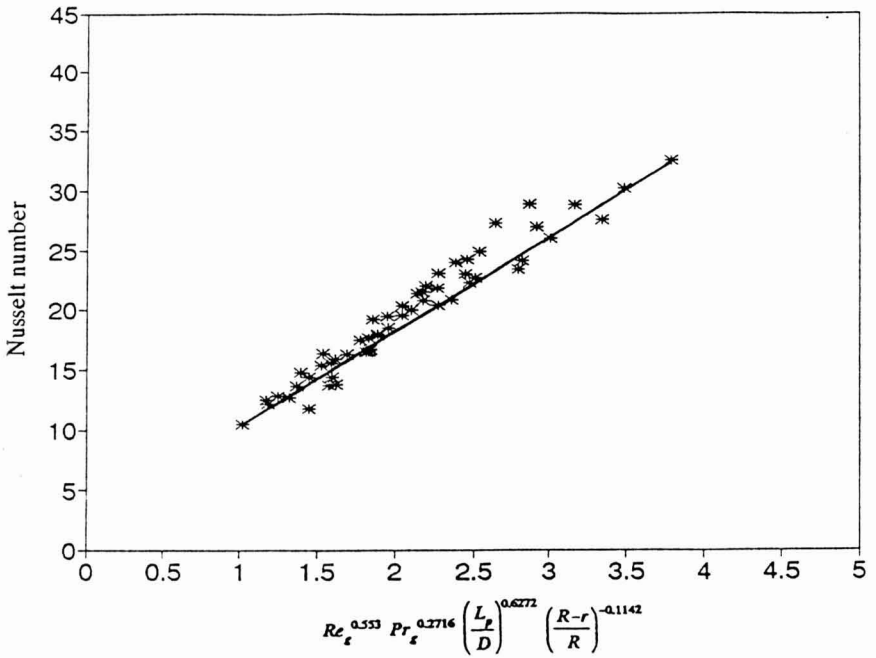

FIG. 4. CORRELATION BETWEEN EXPERIMENTAL AND PREDICTED NUSSELT NUMBER

TABLE 9.
GENERALIZED REYNOLDS AND PRANDTL NUMBERS USED FOR THE RELATIVE VELOCITY METHOD

	%CMC					
	0.2		0.4		0.8	
Q 10^{-4} m^3/s	Re_g	Pr_g	Re_g	Pr_g	Re_g	Pr_g
2.52	110.4	413.6	38.7	1176.9	21.2	2146.3
3.76	186.4	367.5	68.0	1005.1	38.5	1771.7
5.05	270.2	338.0	101.4	898.7	58.9	1546.3

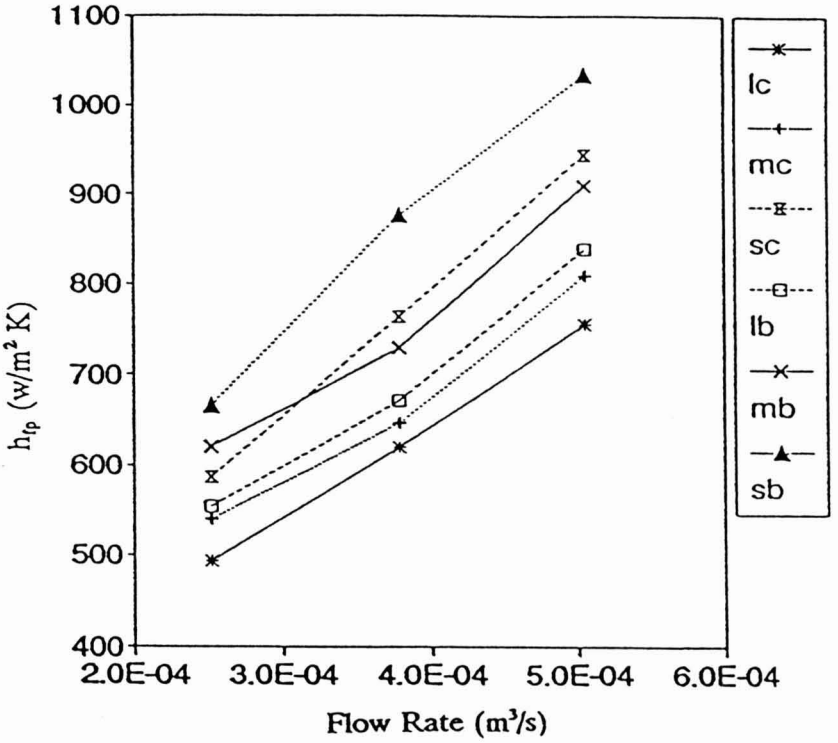

FIG. 5. PLOT OF HEAT TRANSFER COEFFICIENT h_{fp} AS INFLUENCED BY FLOW RATE, PARTICLE SIZE, AND RADIAL LOCATION AT 0.2% CMC CONCENTRATION FOR THE RELATIVE VELOCITY METHOD (RANZ AND MARSHALL RELATION)

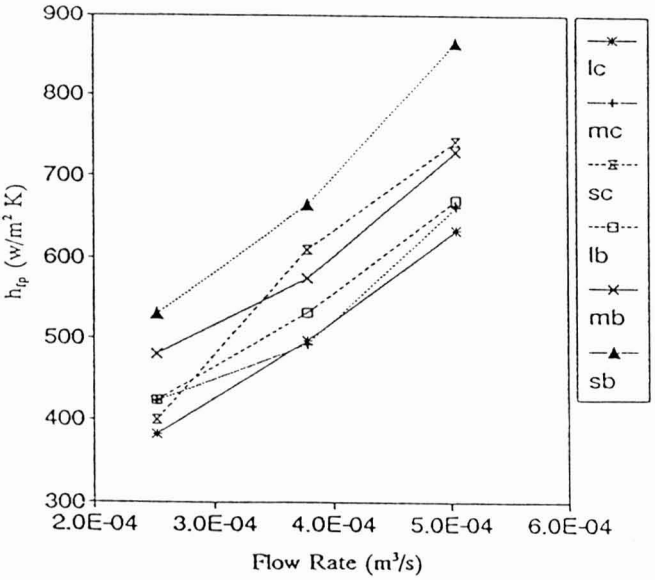

FIG. 6. PLOT OF HEAT TRANSFER COEFFICIENT h_{fp} AS INFLUENCED BY FLOW RATE, PARTICLE SIZE, AND RADIAL LOCATION AT 0.4% CMC CONCENTRATION FOR THE RELATIVE VELOCITY METHOD (RANZ AND MARSHALL RELATION)

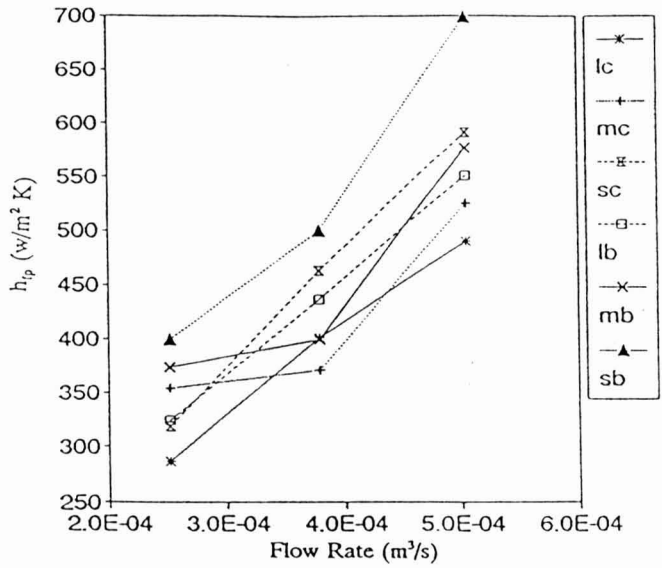

FIG. 7. PLOT OF HEAT TRANSFER COEFFICIENT h_{fp} AS INFLUENCED BY FLOW RATE, PARTICLE SIZE, AND RADIAL LOCATION AT 0.8% CMC FOR THE RELATIVE VELOCITY METHOD (RANZ AND MARSHALL RELATION)

size of particles with 0.05 level of significance, and decreased with increasing viscosity as expected with 0.05 level of significance. Values of h_{fp} at the bottom were higher than those at the center ($p < 0.05$) because of the higher values of relative velocities obtained at the bottom than those at the center (only 13 out of 162 data values did not satisfy the level of significance $p<0.05$, but they satisfied $p<0.1$; this was observed for high viscosity condition, for which higher standard deviations occurred). The values of h_{fp} determined have the same trend with h_{fp} values obtained using Kramers and Whitaker relations. These results are not only fully consistent with the findings of the liquid crystal method, but are also in good quantitative agreement, providing an extra measure of validation for the liquid crystal results.

The flow visualization studies yield further insight into the bottom-to-center difference observed in the liquid crystal studies. When the particle moves at the bottom the fluid surrounding the bottom of particle is moving slower than fluid at the center, which moves at a faster velocity. This particle experiences a significant velocity gradient over its surface, and may either rotate (thereby increasing fluid disturbance and h_{fp}) or slide against the wall tube thereby decreasing the particle velocity (increasing *relative* velocity) and h_{fp}.

A significant increase occurred in the relative velocity ($p<0.01$) between the low flow rate (2.52×10^{-4} m^3/s) at the bottom and at the center compared to that of a higher flow rate (5.05×10^{-4} m^3/s). This shows that the flow field around the particle has a great impact on the fluid to particle heat transfer coefficient. The ability of the surrounding fluid to continuously supply the particle with hot fluid affects the magnitude of h_{fp}.

The values of relative velocity found in the present study are higher than those presented by Sastry *et al.* (1990), and were in all cases, different from zero. For their case, the relative velocity was measured by determining particle velocities directly and using average fluid velocities. Their results show moderate agreement for low particle size and low flow rates, but underprediction at higher values of particle size. In the present study, the flow visualization experiments enabled us to more accurately determine the relative velocity, which explains the differences with the method cited previously. The difference can be explained by the fact that the local velocity of fluid in the vicinity of a particle is different from the average fluid velocity.

The values of h_{fp} decreased with increasing particle size, exactly as observed in the liquid crystal method. Axially located particles generally did not rotate significantly, because the shear field about them was symmetric, resulting in no net moment about the particles. The particles in this case moved at high velocities and adjacent streamlines moved by them slowly; i.e., low relative velocities. The streamlines immediately surrounding the particles were distorted, but the distortions further away from the particle (close to the wall) were slight;

indicating that the far flow field had little effect on the particle (i.e., wall effects were slight in this laminar flow situation).

By contrast, the particles at the bottom were subjected to a wide variation in flow conditions. For particles that slid (rather than rolled) along the bottom, the side closest to the tube wall was in contact with slow-moving fluid, while the side closest to the axis was exposed to fast moving streamlines that accelerated by it in the "Bernoulli" manner. Rolling particles were exposed to more complex and disturbed fluid patterns. These visualization results provide further insight into the liquid crystal observations and provide a measure of verification for these results. They also help explain differences between these results and previous results for turbulent flow.

CONCLUSIONS

Fluid-to-particle convective heat transfer coefficient (h_{fp}) increased with increasing flow rate, decreasing viscosity and decreasing particle size in both methods; also the same results were obtained when the radial location was changed from the center to the bottom. Results of the relative velocity method help provide some verification and insight into the trends observed by the liquid crystal method. Effects of particle-to-tube dimension ratio in this study differed from that of previous studies; this appears to be due to the different flow regime (laminar in this study, turbulent in the others).

For the liquid crystal method the values of h_{fp} (individual replications) ranged from 270 to 930 W/m^2K. The relative velocity method yielded higher convective heat transfer coefficient h_{fp} than those of liquid crystal. The values of h_{fp} ranged from 287 to 1277 W/m^2K depending on correlations used. The h_{fp} values from the relative velocity method are only approximate, since they depend on correlations developed for spherical particles, but the general agreement in the range of values indicates some consistency in the methods.

The results indicate that disturbance of the flow field occurs in the vicinity of particles in continuous flow, and that the disturbance depends on the radial location as well as particle size. It is the *local* velocity field that influences h_{fp}, and the results are different for laminar and turbulent flows. Heat transfer coefficient values measured were higher than expected from zero fluid-particle relative velocity.

NOMENCLATURE

A	Surface area of the particle, m^2
C_p	Specific heat of the particle, J/KgC

D	Diameter of the tube, m
h_{fp}	Fluid-to-particle heat transfer coefficients, W\m^{2}K
h	Hue
K	Consistency coefficient, Pa s^n
k	Thermal conductivity W/mC
L_p	Characteristic length, m
M	Mass of the particle, Kg
n	Flow behavior index, dimensionless
r	Radial coordinate of center of particle (m)
R	Radius of the tube, m
S	Side of the cube, m
t	Time, s
T	Temperature, C
V	Velocity, m/s
V_r	Relative velocity, m/s

Dimensionless Numbers

Bi	Biot number = $h_{fp}L_p/2k_p$
Fo	Fourier number = $\alpha t/L_p^2$
Nu	Nusselt number [defined in Eq. (6)]
Pr_g	Generalized Prandtl number = $2^{n-3}K\{(3n+1)/n\}^nC_{pf}D^{1-n}/k_fV^{1-n}$
Re_g	Generalized Reynolds number = $V^{2-n}D^n\rho/[2^{n-3}K\{(3n+1)/n\}^n]$

Greek Letters

α	Thermal diffusivity, m^2/s
μ	Viscosity (Pa s)
ρ	Density, Kg/m^3
τ	Shear rate, Pa
$\dot{\gamma}$	Shear rate, s^{-1}

Subscripts

f	Fluid
i	Initial
p	Particle
s	Slip (corresponding to relative velocity between fluid and particle), or surface, in Whitaker correlation
∞	Free stream conditions

REFERENCES

AWUAH, G.B., RAMASWAMY, H.S., SIMPSON, B.K., PANNU, K. and SMITH, J.K. 1991. Fluid to particle surface heat transfer coefficients associated with carboxymethyl cellulose solutions. ASAE paper # 916601. Amer. Soc. Agr. Eng., St. Joseph, MI.

BALASUBRAMANIAM, V.M. 1993. Liquid-to-particle convective heat transfer in aseptic processing systems. Ph.D. Dissertation, The Ohio State University, Columbus.

BALASUBRAMANIAM, V.M. and SASTRY, S.K. 1994. Liquid-to-particle convective heat transfer in a non-Newtonian carrier medium during continuous tube flow. J. Food Eng. (In Press).

CHANDARANA, D.I., GAVIN, A. and WHEATON, W.F. 1990. Particle/fluid interface heat transfer under UHT conditions at low particle/fluid relative velocities. J. Food Process Engineering *13*(3), 191–206.

CHANG, S.Y. and TOLEDO, R.T. 1989. Heat transfer and simulated sterilization of particulate solids in a continuously flowing system. J. Food Sci. *54*(4), 1017–1023, 1030.

HELDMAN, D.R. and SINGH, R.P. 1981. *Food Process Engineering*, Van Nostrand Reinhold/AVI, New York.

HEPPELL, N.J. 1985. Measurement of the liquid-solid heat transfer coefficient during continuous sterilization of liquids containing solids. Presented at the 4th Int. Cong. Eng. Food, Edmonton, Alberta, Canada, July 7–10.

KING, W.J. 1932. The basic laws and data of heat transmission III. Mech. Eng. *54*, 347–353. Cited in Sparrow, E.M. and Stretton, A.J. 1985. Natural convection from variously oriented cubes and from other bodies of unity aspect ratio. Int. J. Heat Mass Transfer *24*(4), 741–752.

KRAMERS, H. 1946. Heat transfer from spheres to flowing media. Physica, *12*, 61. Cited in Zenz, F.A. and Othmer, D.F. 1960. *Fluidization and Fluid Particle Systems*, Treinhold Publ. Corp., New York.

LESHO, J.C. and HOGREFE, A.F. 1989. Indigestible size continuously transmitting temperature monitoring pill. U.S. Pat. No. 4, 844, 076.

LIENHARD, J.H. 1973. On the commonality of equations for natural convection from immersed bodies. Int. J. Heat Mass Transfer *16*, 2121–2123. Cited in Sparrow, E.M. and Stretton, A.J. 1985. Natural convection from variously oriented cubes and from other bodies of unity aspect ratio. Int. J. Heat Mass Transfer *28*(4), 741–752.

MWANGI, J.M., DATTA, A.K. and RIZVI, S.H. 1992. Heat transfer in aseptic processing of particulate foods. In *Advances in Aseptic Processing Technologies*, (R.K. Singh and P.E. Nelson, eds.) pp. 73–103, Elsevier Applied Science Publishers, New York.

RANZ, W.E. and MARSHALL, W.R., Jr. 1952. Evaporation from drop. Chem. Eng. Progress *48*, 141. Cited in Incropera, F.P. and De Witt, D.F. 1990. *Introduction to Heat Transfer*, John Wiley & Sons, New York.

SASTRY, S.K. 1992. Liquid to particle heat transfer coefficient in aseptic processing. In *Advances in Aseptic Processing Technologies*, (R.K. Singh and P.E. Nelson, eds.) pp. 63–72, Elsevier Applied Science Publishers, New York.

SASTRY, S.K., HESKITT, B.F. and BLAISDELL, J.L. 1989. Convective heat transfer at particle-liquid interface in aseptic processing systems. Food Technol. *43*(3), 132–136, 143.

SASTRY, S.K., LIMA, M., BRIM, J., BRUNN, T. and HESKITT B.F. 1990. Liquid to particle heat transfer during continuous tube, flow: Influence of flow rate and particle to tube diameter ratio. J. Food Process Engineering *13*, 239–253.

SPARROW, E.M. and STRETTON, A.J. 1985. Natural convection from variously oriented cubes and from other bodies of unity aspect ratio. Int. J. Heat Mass Transfer *28*(4), 741–752.

STOFOROS, N.G., PARK, K.L. and MERSON, R.L. 1989. Heat transfer in particulate foods during aseptic processing. Abstract no. 545, presented at the 1989 IFT Annual Meeting, Chicago, IL, June 25–29, 1989.

WHITAKER, S. 1972. Forced convection heat transfer correlations for flow in pipes, past flat plates, single cylinders, single spheres, and for flow in packed beds tube bundles. AIChe J. *18*, 361–371.

ZITOUN, K.B. and SASTRY, S.K. 1994. Determination of convective heat transfer coefficient between fluid and cubic particle in continuous tube flow using the moving thermocouple method. J. Food Process Engineering *17*(2), 229–241.

ZURITZ, C.A., McCOY, S.C. and SASTRY, S.K. 1990. Convective heat transfer coefficients for irregular particles immersed in non-Newtonian fluid during tube flow. J. Food Eng. *11*, 159–174.

CONVECTIVE HEAT TRANSFER COEFFICIENT FOR CUBIC PARTICLES IN CONTINUOUS TUBE FLOW USING THE MOVING THERMOCOUPLE METHOD[1]

KHALED B. ZITOUN and SUDHIR K. SASTRY[2]

The Ohio State University
Department of Agricultural Engineering
590 Woody Hayes Drive
Columbus, OH 43210

Accepted for Publication September 14, 1993

ABSTRACT

The convective heat transfer coefficient, h_{fp}, between fluid and cubic particles was investigated with respect to flow rate, viscosity, and particle to tube dimension ratio using a moving thermocouple method. This study was conducted for a single particle. The determined values of h_{fp} ranged from 199 W/m^2C and 749 W/m^2C. Results indicate that an increase in viscosity or dimension ratio decreased h_{fp} values. In contrast, an increase in flow rate increased values of h_{fp}. The effect of particle to tube dimension ratio was the opposite of those in previous studies by this method and appears to be due to differences in flow regime (laminar in this study, as compared to fully developed turbulence in previous work). A dimensionless correlation developed to relate Nusselt number to generalized Reynolds and Prandtl numbers, ratio of particle characteristic length and diameter of the tube, had an r^2 value of 0.94.

INTRODUCTION

A major concern in aseptic processing of liquids containing particulates is commercial sterility. Since low-acid foods can support the growth of *Clostridium Botulinum (C. Bot.)*, the thermal process design requires consideration of the possibility that *C. Bot.* may be present at the slowest heating locations of individual food particles. The application of aseptic thermal processing of foods

[1] Salaries and research support provided by State and Federal Funds appropriated to the Ohio Agricultural Research and Development Center, The Ohio State University. References to commercial products and trade names are made with the understanding that no discrimination and no endorsement by The Ohio State University is implied.

[2] Corresponding author.

Journal of Food Process Engineering **17** (1994) 229-241.

containing particulates involves consideration of a variety of factors that affect the process. The overall challenge in the processing of low acid foods is to provide maximum nutrient retention while maintaining microbiological safety of the final product. In recent years, there has been a considerable growth of interest, research, and development in applying this technology to the processing of low acid foods containing particulates.

Heat transfer data are important in the design of thermal process schedules. Successful process filing with the U.S. Food and Drug Administration requires documented understanding of process heat transfer. Lack of such heat transfer information still limits significant commercial realization of aseptic technology for particulates.

Some of the previous research on measurement of the liquid-particle heat transfer coefficient (h_{fp}) has dealt with stationary particles (Chang and Toledo 1989; Zuritz *et al.* 1990; Awuah *et al.* 1991; Chandarana *et al.* 1990). Some studies have been conducted for free particles (Heppell 1985; Stoforos *et al.* 1989; Sastry 1989,1990; Mwangi *et al.* 1992).

The goal of the present study was to measure fluid-to-particle convective heat transfer coefficients, h_{fp}, for cubic particles in continuous flow in a non-Newtonian carrier using the moving thermocouple method of Sastry *et al.* (1990). The variables studied were flow rate, particle to tube dimension ratio, and rheological properties of carrier fluid.

THEORY

In the case where the surface resistance to heat transfer is large compared to the internal resistance, the associated Biot numbers (Eq. 1) are then very small ($Bi = h_{fp}L_p/k < 0.1$); e.g., for high thermal conductivity materials like aluminum), and the heat transfer coefficient can be determined using a lumped capacity analysis (Incropera and De Witt 1990).

From an energy balance, the Newtonian law of heating and cooling is obtained:

$$\ln \frac{(T-T_\infty)}{(T_i-T_\infty)} = -\frac{h_{fp}\, A}{MC_p}\, t \qquad (1)$$

If T_∞ is constant by plotting ln $(T-T_\infty)$ versus time, we can determine h_{fp} from the slope of the curve.

Thus, the value of h_{fp} can be determined if particle and fluid temperature histories can be determined in some manner. Fluid temperature measurement is trivial, but noninvasive particle temperature measurement is not easy. Thermocouple measurements can be made, if the sensor moves with the particle and does not affect its rate of travel.

MATERIALS AND METHODS

Experimental Procedure

This study involved introduction of a hollow cubic metal transducer particle (initially at close to 0C) into a moving fluid stream, and measurement of its temperature (T) and that of the fluid (T_∞, maintained at 45 $\pm$ 1C) during motion within the fluid (Sastry *et al.* 1990). A 36 gauge copper-constantan thermocouple wire was attached to the transducer from the upstream end located on the inside wall of particle. Unlike the previous study (Sastry *et al.* 1990), the thermocouple was fed from the upstream rather than the downstream end, since the former was easier to accomplish with high-viscosity fluids. In order to keep the method applicable to tube flow, the velocity was maintained the same as that of a free particle (as determined from preliminary experiments). Heat transfer coefficients were calculated by the procedure detailed above.

The velocity of the free particle was determined by using two photoelectric sensors located at either end of the test section (Fig. 1). The first one was moved a sufficient distance downstream of the introduction port to avoid initial acceleration of the particle. As the particle passed the first sensor, a timer was activated and the residence time in the test section was measured. When the particle passed the second sensor, the clock was stopped and the velocity was calculated. For each flow rate, the velocity of free particles was calculated in order to collect baseline data.

Sample Details

The dimensions and physical properties of the metal transducer particles needed in the calculations are presented in Table 1. The wall thickness of particle was designed to ensure that its density was similar to that of real food particle. Density (ρ) of each particle was determined in the laboratory and specific heat was calculated, taking into account the mass and specific heat of the solder (lead). In order to match the density between the liquid and the particle, the density of the fluid was adjusted by adding sugar to make the particle neutrally buoyant.

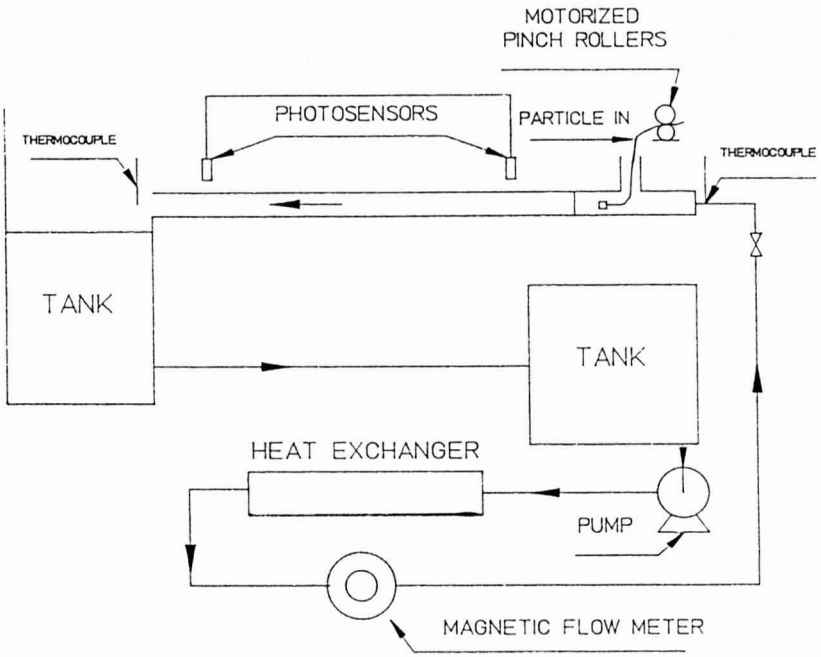

FIG. 1. SCHEMATIC DIAGRAM OF EXPERIMENTAL SETUP USED FOR THE MOVING THERMOCOUPLE METHOD

TABLE 1.
DIMENSIONS AND PROPERTIES OF METAL TRANSDUCER PARTICLES

Material	L_p (m)	Thickness of material (m)	Apparent Density Kg/m^3	Specific heat KJ/Kg C
Aluminum	0.00588	0.001524	1078.52	0.8483
Aluminum	0.007975	0.001207	1078.71	0.9063
Aluminum	0.009970	0.000787	1078.77	0.9176

Rheological Properties of Fluid

The non-Newtonian fluids used were aqueous solutions of sodium carboxymethylcellulose (CMC), prepared by adding the appropriate amount of CMC powder to water, dispersing it slowly in the tank and then stirring with an electric mixer. After that, the appropriate amount of sugar was added to match the density of the particle. Before the test, the solution was transferred to the system and recirculated with venting to ensure absence of air bubbles in the system.

Rheological properties were determined by measuring shear stress (τ) and shear rate ($\dot{\gamma}$) using a coaxial cylinder viscometer (Rheomat Model 115; Contraves Industrial Division, Cincinnati, OH). The measurements were conducted before and after each test to determine if significant shear breakdown effects occurred.

Results were analyzed based on the Ostwald-de-Waele power law model (Brodkey 1967):

$$\tau = K \dot{\gamma}^n \tag{2}$$

A general nonlinear regression package (Systat 1989; Systat Inc., Evanston, IL) was used to determine K and n. The experimental data were statistically found to possess correlation coefficients that ranged from 0.978 to 1, showing good fit of the experimental data. The rheological properties of the fluid carriers are presented in Table 2. The density of fluid with different concentrations of CMC and the quantity of sugar added to water in order to match the density of particles are summarized in Table 3. Each concentration had a different viscosity, but all of them had the same density approximately in order to match the density of particles.

TABLE 2.
RHEOLOGICAL PROPERTIES OF THE FLUID CARRIERS

%CMC	K (Pa s^n)	n
0.2	0.063	0.752
0.4	0.239	0.663
0.8	0.439	0.651

TABLE 3.
DENSITY OF THE FLUID WITH DIFFERENT CONCENTRATIONS OF CMC

Temperature C	% CMC	% Sugar	Density (Kg/m^3)
45	0.2	21.24	1077.98
45	0.4	20.34	1078.43
45	0.8	20.34	1078.97

RESULTS AND DISCUSSION

Table 4 presents the values of generalized Reynolds and Prandtl numbers in this study. The flow regime can be seen to be laminar.

The results of the mean convective heat transfer coefficients h_{fp} determined using Eq. (1) and the method described thereafter are presented in Table 5. Average values of h_{fp} presented were calculated based on 6 replications. Standard deviation of the h_{fp} found in this study ranged between 33.6 and 57.9 W/m^2K. The correlation coefficients obtained ranged from 0.894 to 0.997, which reflects a good fit for most experimental conditions. Situations involving lower correlation coefficients probably reflect conditions of time varying h_{fp} values, which may occur of particle radial location changes during the experiment.

The effect of flow rates, particle sizes, and CMC concentrations are given in Table 5. The values of h_{fp} increased with increasing flow rates (statistically significant, $p<0.05$), and decreased with increasing viscosity of the fluid ($p<0.05$) and increasing particle size ($p<0.05$). Plots of heat transfer coefficient h_{fp} versus flow rate presented in Fig. 2, 3, and 4 show the increase of h_{fp} with increasing flow rate in the three different sizes of particles. In spite

TABLE 4.
GENERALIZED REYNOLDS AND PRANDTL NUMBERS USED FOR MOVING THERMOCOUPLE METHOD

	%CMC					
	0.2		0.4		0.8	
Q $m^3/s \times 10^4$	Re_g	Pr_g	Re_g	Pr_g	Re_g	Pr_g
2.52	213.3	207.4	71.9	615.7	40.5	1094.0
3.79	353.8	187.5	123.6	537.0	69.9	949.7
5.05	506.6	174.6	181.6	487.4	103.1	859.0

TABLE 5.
FLUID TO PARTICLE HEAT TRANSFER COEFFICIENT VALUES AT VARIOUS FLOW RATES, PARTICLE SIZES, AND CMC CONCENTRATIONS FOR MOVING THERMOCOUPLE METHOD

		% CMC		
		0.2	0.4	0.8
Q $m^3/s \times 10^4$	Size	h_{fp}	($W/m^{2o}K$)	
2.52	l	340.6	283.2	198.9
2.52	m	435.5	337.8	254.2
2.52	s	497.4	398.2	329.4
3.76	l	462.6	429.5	316.5
3.76	m	540.4	464.3	346.2
3.76	s	617.6	486.4	409.6
5.05	l	583.2	491.7	378.6
5.05	m	634.6	527.7	413.5
5.05	s	749.4	615.2	466.3

l: Large particle.
m: Medium particle.
s: Small particle.

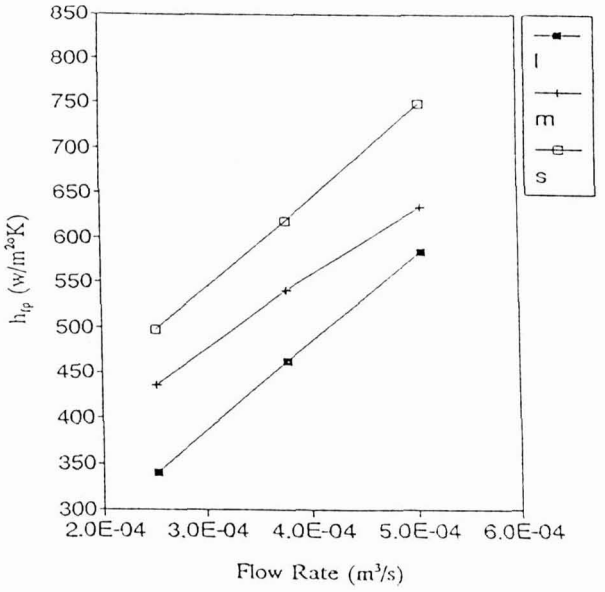

FIG. 2. PLOT OF HEAT TRANSFER COEFFICIENT h_{fp} AS INFLUENCED BY FLUID FLOW RATE AND PARTICLE SIZE AT 0.2% CMC

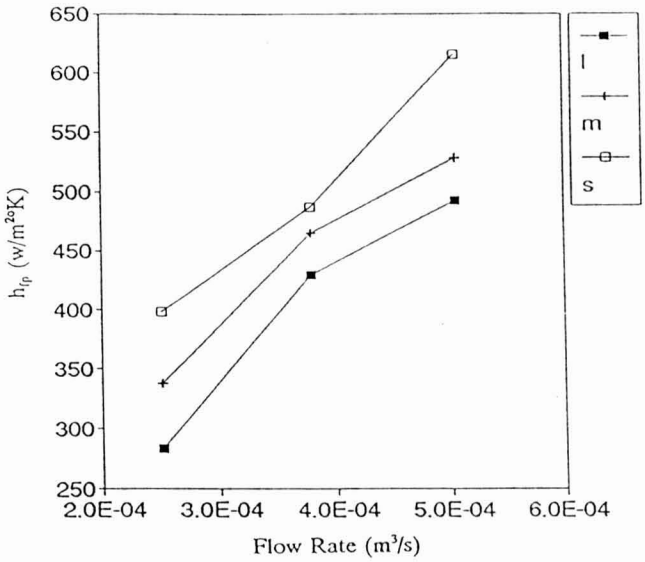

FIG. 3. PLOT OF HEAT TRANSFER COEFFICIENT h_{fp} AS INFLUENCED BY FLUID FLOW RATE AND PARTICLE SIZE AT 0.4% CMC

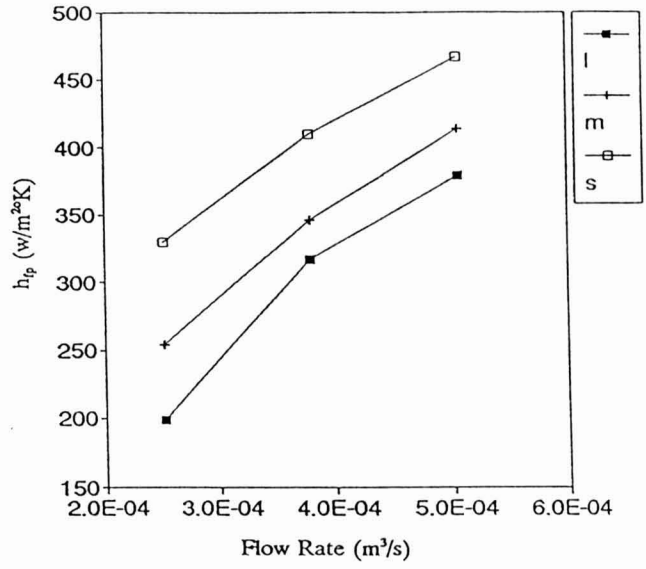

FIG. 4. PLOT OF HEAT TRANSFER COEFFICIENT h_{fp} AS INFLUENCED BY FLUID FLOW RATE AND PARTICLE SIZE AT 0.8% CMC

of the neutral buoyancy between particle and fluid, the variations between replications may be explained by the particle trajectory due to the interfering effects of the thermocouple wire and the curling tendency of the thermocouple.

The trends in h_{fp} with flow rate and rheological properties are as expected; however, the effect of particle dimension to pipe diameter ratio is the opposite of that observed by Sastry *et al.* (1990). The explanation may lie in the flow regimes under consideration. The study of Sastry *et al.* (1990) was conducted under turbulent flow conditions, where the velocity profile is (on average) relatively flat compared to laminar flow. Additionally, turbulent eddies would ensure the presence of a highly disturbed flow field adjacent to the particle regardless of radial location. Under turbulent conditions, the primary factor affecting relative velocity would appear to be the "Bernoulli effect", in which the particle behaves as an obstruction to fast moving fluid elements, which then accelerate through the gap between the particle and the wall. Larger particles would form narrower gaps, resulting in larger fluid-particle relative velocities and h_{fp} values.

Under the present (laminar) flow conditions, the *local* conditions around the particle have greater effects. An examination of the Ranz and Marshall (1952) equation reveals that h_{fp} would be expected to vary as $L_p^{-0.5}$, indicating that for unbounded flows, h_{fp} should *decrease* with particle size. In laminar flow, it appears that only those streamlines close to the particle dictate the heat transfer coeffient; and the particle-eddy-wall interactions of turbulent flow are relatively less important. Further flow visualization studies (Balasubramaniam and Sastry 1992; Zitoun 1992) have shown that in laminar flow the velocity field about the particle follows streamlines; different radial locations have different velocities, indicating the importance of local conditions on heat transfer.

In this method, the trajectories of the particle cannot be controlled because of the thermocouple attached; therefore, the determination of heat transfer coefficient, h_{fp}, with radial location as a parameter was not possible. This limitation has also been noted by Balasubramaniam and Sastry (1992), a study which yielded inconclusive results on particle size effects. During the experimentation, the velocities of particle attached with thermocouple accurately duplicated the free-particle velocities. Because of restriction of particle rotation, h_{fp} could be higher than the values obtained by this method. Biot numbers determined using the values of thermal conductivity of the particle (k) and the heat transfer coefficient (h_{fp}) are ranged between 0.0046 and 0.005. Fourier numbers (Fo) were also higher than 5.5. Therefore, these values justify the use of the lumped transient method described in heat transfer equation and solution section with an error less than 0.7% (Ramaswamy *et al.* 1982). Table 6 summarizes the values of Biot and Fourier numbers for each h_{fp} corresponding to each flow rate, particle size and CMC concentration.

Dimensionless correlations were developed to relate Nusselt number (Nu) to generalized tube Reynolds (Re_g), Prandtl (Pr_g) numbers, and ratio of particle characteristic length and diameter of the tube (L_p/D). Multiple regression analysis (SAS) after logarithmic linearization of the equation was made, yielding the following equation, with $r^2 = 0.94$:

$$Nu = 2 + 0.685\ Re_g^{0.7023}\ Pr_g^{0.0.3925} \left(\frac{L_p}{D}\right)^{0.5314} \tag{3}$$

In the above relation, the form used is similar to that for spheres, where the limiting case of conductive heat transfer corresponds to a Nusselt number of 2. This is not strictly true for cubes; however this correlation is intended for estimation in the range of conditions of the present experiment. Figure 5 shows a rearranged form of Eq. 3 versus Nusselt number found experimentally and predicted (solid line).

TABLE 6.
VALUES OF BIOT AND FOURIER NUMBERS FOR EACH HEAT TRANSFER COEFFICIENT (h_{fp}) CORRESPONDING TO A SPECIFIC FLOW RATE, PARTICLE SIZE AND CONCENTRATION OF CMC

Q m^3/s x 10^4	% CMC	$Biot_l$ x 10	Fo_l	$Biot_m$ x 10	Fo_m	$Biot_s$ x 10	Fo_s
2.52	0.2	0.030	5.5	0.030	8.6	0.022	20.0
2.52	0.4	0.024	6.5	0.023	11.0	0.018	26.9
2.52	0.8	0.017	6.3	0.017	11.5	0.015	27.5
3.76	0.2	0.040	9.1	0.037	14.8	0.027	36.7
3.76	0.4	0.037	9.3	0.032	15.2	0.022	36.5
3.76	0.8	0.027	9.8	0.024	16.1	0.018	38.7
5.05	0.2	0.050	11.4	0.043	18.8	0.033	45.6
5.05	0.4	0.042	12.2	0.036	19.7	0.027	49.1
5.05	0.8	0.033	13.1	0.028	21.7	0.021	51.8

l: Large particle.
m: Medium particle.
s: Small particle.

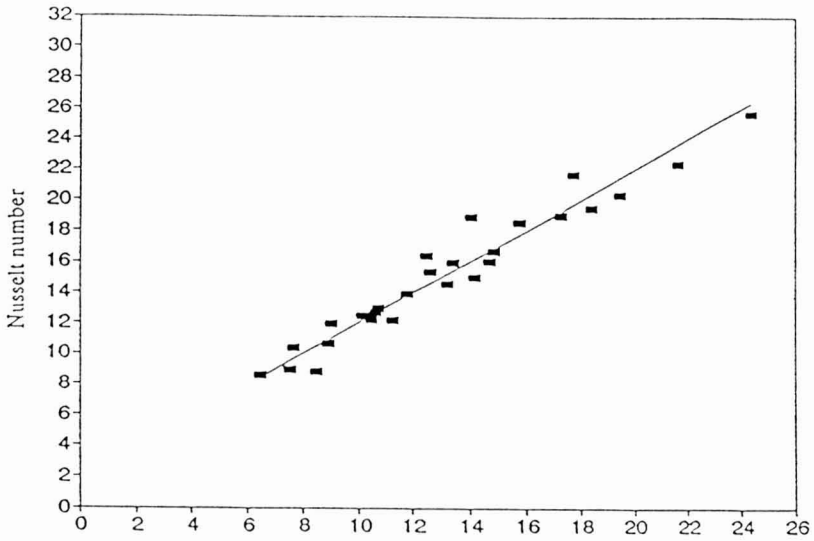

FIG. 5. CORRELATION BETWEEN EXPERIMENTAL AND PREDICTED NUSSELT NUMBER

CONCLUSIONS

The average values of heat transfer coefficient h_{fp} ranged from 198.9 W/m^2C to 749.3 W/m^2C. Data on h_{fp} versus flow rate showed an increase of h_{fp} with increasing flow rate, decreasing with increasing the viscosity and particle size. The effect of particle to tube dimension ratio seems to be different from that of previous studies, and is likely due to differences in flow regime between studies. Since particle trajectories could not be controlled in this method, the effect of particle radial location could not be studied. Further studies using multiple particles would be useful to determine particle interactions in holding tubes.

NOMENCLATURE

A Surface area of the particle, m^2
C_p Specific heat of the particle, J/KgC
D Diameter of the tube, m
h_{fp} Fluid-to-particle heat transfer coefficients, W/m^2K
K Consistency coefficient

k_f Thermal conductivity of fluid, W/mC
k_p Thermal conductivity of particle, W/mC
L_p Characteristic length, m
M Mass of the particle, Kg
n Flow behavior index, dimensionless
Q Flow rate (m^3/s)
t Time, s
T Temperature, C
V Velocity, m/s

Dimensionless Numbers

Bi Biot number = $h_{fp}L_p/k_p$
Fo Fourier number = $\alpha t/L_p^2$
Nu Nusselt number = $h_{fp}a/k_f$
Pr_g Generalized Prandtl number = $2^{n-3}K\{(3n+1)/n\}^nC_pD^{1-n}/k_fV^{1-n}$
Re_g Generalized Reynolds number = $V^{2-n}D^n\rho_f/[2^{n-3}K\{(3n+1)/n\}^n]$

Greek Letters

α Thermal diffusivity, m^2/s
ρ Density, Kg/m^3
τ Shear stress, Pa
$\dot{\gamma}$ Shear rate, s^{-1}

Subscripts

f Fluid
i Initial
p Particle
∞ Free stream conditions

REFERENCES

AWUAH, G.B., RAMASWAMY, H.S., SIMPSON, B.K., PANNU, K. and SMITH, J.K. 1991. Fluid to particle surface heat transfer coefficients associated with carboxymethyl cellulose solutions. ASAE paper # 916601. American Society of Agr. Engs., St. Joseph, MI.

BALASUBRAMANIAM, V.M. and SASTRY, S.K. 1994. Liquid-to-particle convective heat transfer in a non-Newtonian carrier medium during continuous tube flow. J. Food Eng. (In Press).

BRODKEY, R.S. 1967. *The Phenomena of Fluid Motions*. Addison-Wesley Series in Chemical Engineering. Addison Wesley, Reading, MA.

CHANDARANA, D.I., GAVIN, A. and WHEATON, W.F. 1990. Particle/fluid interface heat transfer under UHT conditions at low particle/fluid relative velocities. J. Food Process Engineering *13*(3), 191–206.

CHANG, S.Y. and TOLEDO, R.T. 1989. Heat transfer and simulated sterilization of particulate solids in a continuously flowing system. J. Food Sci. *54*(4), 1017–1023, 1030.

CRC. 1972. *Handbook of Chemistry and Physics*, 53rd. Ed., The Chemical Rubber Co., Cleveland, OH.

HEISLER, M.P. 1947. Temperature charts for induction and constant temperature heating. Trans. ASME *69*, 227–232.

HEPPELL, N.J. 1985. Measurement of the liquid-solid heat transfer coefficient during continuous sterilization of liquids containing solids. Presented July 7–10, at the 4th Int. Cong. Eng. Food, Edmonton, Alberta, Canada.

INCROPERA, F.P. and DE WITT, D.F. 1990. *Introduction to Heat Transfer*, John Wiley & Sons, New York.

MWANGI, J.M., DATTA, A.K. and RIZVI, S.H. 1992. Heat transfer in aseptic processing of particulate foods. In *Advances in Aseptic Processing Technologies*, (R.K. Singh and P.E. Nelson, eds.) pp. 73–103, Elsevier App. Sci., New York.

RAMASWAMY, H.S., LO, K.V. and TUNG, M.A. 1982. Simplified equations for transient temperatures in convective foods with convective heat transfer at the surface. J. Food Sci. *47*(6), 2042–2047.

SASTRY, S.K., HESKITT, B.F. and BLAISDELL, J.L. 1989. Convective heat transfer at particle-liquid interface in aseptic processing systems. Food Technol. *43*(3), 132–136, 143.

SASTRY, S.K., LIMA, M., BRIM, J., BRUNN, T. and HESKITT B.F. 1990. Liquid-to-particle heat transfer during continuous tube, flow: Influence of flow rate and particle to tube diameter ratio. J. Food Process Engineering *13*(3), 239–253.

STOFOROS, N.G., PARK, K.L. and MERSON, R. L. 1989. Heat transfer in particulate foods during aseptic processing. Abstract no. 545, Presented June 25–29 at the 1989 IFT Annual Meeting, Chicago, IL.

ZITOUN, K.B. 1992. Convective heat transfer coefficients between fluid and cubic particles in continuous tube flow. M.S. Thesis, The Ohio State University, Columbus, OH.

ZURITZ, C.A., McCOY, S.C. and SASTRY, S.K. 1990. Convective heat transfer coefficients for irregular particles immersed in non-Newtonian fluid during tube flow. J. Food Eng. *11*, 159–174.

FNP PUBLICATIONS IN FOOD SCIENCE AND NUTRITION

Journals

JOURNAL OF FOOD LIPIDS, F. Shahidi
JOURNAL OF RAPID METHODS AND AUTOMATION IN MICROBIOLOGY, D.Y.C. Fung and M.C. Goldschmidt
JOURNAL OF MUSCLE FOODS, N.G. Marriott and G.J. Flick, Jr.
JOURNAL OF SENSORY STUDIES, M.C. Gacula, Jr.
JOURNAL OF FOODSERVICE SYSTEMS, C.A. Sawyer
JOURNAL OF FOOD BIOCHEMISTRY, J.R. Whitaker, N.F. Haard and H. Swaisgood
JOURNAL OF FOOD PROCESS ENGINEERING, D.R. Heldman and R.P. Singh
JOURNAL OF FOOD PROCESSING AND PRESERVATION, D.B. Lund
JOURNAL OF FOOD QUALITY, J.J. Powers
JOURNAL OF FOOD SAFETY, T.J. Montville
JOURNAL OF TEXTURE STUDIES, M.C. Bourne

Books

MEAT PRESERVATION: PREVENTING LOSSES AND ASSURING SAFETY, R.G. Cassens
S.C. PRESCOTT, M.I.T. DEAN AND PIONEER FOOD TECHNOLOGIST, S.A. Goldblith
FOOD CONCEPTS AND PRODUCTS: JUST-IN-TIME DEVELOPMENT, H.R. Moskowitz
MICROWAVE FOODS: NEW PRODUCT DEVELOPMENT, R.V. Decareau
DESIGN AND ANALYSIS OF SENSORY OPTIMIZATION, M.C. Gacula, Jr.
NUTRIENT ADDITIONS TO FOOD, J.C. Bauernfeind and P.A. Lachance
NITRITE-CURED MEAT, R.G. Cassens
POTENTIAL FOR NUTRITIONAL MODULATION OF AGING, D.K. Ingram *et al.*
CONTROLLED/MODIFIED ATMOSPHERE/VACUUM PACKAGING OF FOODS, A.L. Brody
NUTRITIONAL STATUS ASSESSMENT OF THE INDIVIDUAL, G.E. Livingston
QUALITY ASSURANCE OF FOODS, J.E. Stauffer
THE SCIENCE OF MEAT AND MEAT PRODUCTS, 3RD ED., J.F. Price and B.S. Schweigert
HANDBOOK OF FOOD COLORANT PATENTS, F.J. Francis
ROLE OF CHEMISTRY IN THE QUALITY OF PROCESSED FOODS, O.R. Fennema, W.H. Chang and C.Y. Lii
NEW DIRECTIONS FOR PRODUCT TESTING OF FOODS, H.R. Moskowitz
PRODUCT TESTING AND SENSORY EVALUATION OF FOODS, H.R. Moskowitz
ENVIRONMENTAL ASPECTS OF CANCER: ROLE OF MACRO AND MICRO COMPONENTS OF FOODS, E.L. Wynder *et al.*
FOOD PRODUCT DEVELOPMENT IN IMPLEMENTING DIETARY GUIDELINES, G.E. Livingston, R.J. Moshy, and C.M. Chang
SHELF-LIFE DATING OF FOODS, T.P. Labuza
ANTINUTRIENTS AND NATURAL TOXICANTS IN FOOD, R.L. Ory
UTILIZATION OF PROTEIN RESOURCES, D.W. Stanley *et al.*
VITAMIN B_6: METABOLISM AND ROLE IN GROWTH, G.P. Tryfiates
POSTHARVEST BIOLOGY AND BIOTECHNOLOGY, H.O. Hultin and M. Milner

Newsletters

MICROWAVES AND FOOD, R.V. Decareau
FOOD INDUSTRY REPORT, G.C. Melson
FOOD, NUTRITION AND HEALTH, P.A. Lachance and M.C. Fisher
FOOD PACKAGING AND LABELING, S. Sacharow

GUIDE FOR AUTHORS

Typewritten manuscripts in triplicate should be submitted to the editorial office. The typing should be double-spaced throughout with one-inch margins on all sides.

Page one should contain: the title, which should be concise and informative; the complete name(s) of the author(s); affiliation of the author(s); a running title of 40 characters or less; and the name and mail address to whom correspondence should be sent.

Page two should contain an abstract of not more than 150 words. This abstract should be intelligible by itself.

The main text should begin on page three and will ordinarily have the following arrangement:

Introduction: This should be brief and state the reason for the work in relation to the field. It should indicate what new contribution is made by the work described.

Materials and Methods: Enough information should be provided to allow other investigators to repeat the work. Avoid repeating the details of procedures that have already been published elsewhere.

Results: The results should be presented as concisely as possible. Do not use tables *and* figures for presentation of the same data.

Discussion: The discussion section should be used for the interpretation of results. The results should not be repeated.

In some cases it might be desirable to combine results and discussion sections.

References: References should be given in the text by the surname of the authors and the year. *Et al.* should be used in the text when there are more than two authors. All authors should be given in the Reference section. In the Reference section the references should be listed alphabetically. See below for style to be used.

RIZVI, S.S.H. 1986. Thermodynamic properties of foods in dehydration. In *Engineering Properties of Foods*, (M.A. Rao and S.S.H. Rizvi, eds.) pp. 133–214, Marcel Dekker, New York.

MICHAELS, S.L. 1989. Crossflow microfilters ins and outs. Chem. Eng. *96*, 84–91.

LABUZA, T.P. 1982. *Shelf-Life Dating of Foods*, pp. 66–120, Food & Nutrition Press, Trumbull, CT.

Journal abbreviations should follow those used in *Chemical Abstracts*. Responsibility for the accuracy of citations rests entirely with the author(s). References to papers in press should indicate the name of the journal and should only be used for papers that have been accepted for publication. Submitted papers should be referred to by such terms as "unpublished observations" or "private communication." However, these last should be used only when absolutely necessary.

Tables should be numbered consecutively with Arabic numerals. The title of the table should appear as below:

TABLE 1.
ACTIVITY OF POTATO ACYL-HYDROLASES ON NEUTRAL LIPIDS, GALACTOLIPIDS AND PHOSPHOLIPIDS

Description of experimental work or explanation of symbols should go below the table proper. Type tables neatly and correctly as tables are considered art and are not typeset. Single-space tables.

Figures should be listed in order in the text using Arabic numbers. Figure legends should be typed on a separate page. Figures and tables should be intelligible without reference to the text. Authors should indicate where the tables and figures should be placed in the text. Photographs must be supplied as glossy black and white prints. Line diagrams should be drawn with black waterproof ink on white paper or board. The lettering should be of such a size that it is easily legible after reduction. Each diagram and photographshould be clearly labeled on the reverse side with the name(s) of author(s), and title of paper. When not obvious, each photograph and diagram should be labeled on the back to show the top of the photograph or diagram.

Acknowledgments: Acknowledgments should be listed on a separate page.

Short notes will be published where the information is deemed sufficiently important to warrant rapid publication. The format for short papers may be similar to that for regular papers but more concisely written. Short notes may be of a less general nature and written principally for specialists in the particular area with which the manuscript is dealing. Manuscripts that do not meet the requirement of importance and necessity for rapid publication will, after notification of the author(s), be treated as regular papers. Regular papers my be very short.

Standard nomenclature as used in the engineering literature should be followed. Avoid laboratory jargon. If abbreviations or trade names are used, define the material or compound the first time that it is mentioned.

EDITORIAL OFFICE: DR. D.R. HELDMAN, COEDITOR, *Journal of Food Process Engineering*, Food Science/Engineering Unit, University of Missouri-Columbia, 235 Agricultural/Engineering Bldg., Columbia, MO 65211 USA; or DR. R.P. SINGH, COEDITOR, *Journal of Food Process Engineering*, University of California, Davis, Department of Agricultural Engineering, Davis, CA 95616 USA.

CONTENTS